



UNIVERSIDADE D  
COIMBRA

Rafael Paulo Silveira

**ORGANELLE-TARGETED  
RADIOCONJUGATES FOR AUGER THERAPY  
OF PROSTATE CANCER**

**Dissertação no âmbito do Mestrado em Biologia Celular e  
Molecular orientada pelo/a Professor Doutor Paulo Jorge Gouveia  
Simões Da Silva Oliveira e pela Professora Doutora Ana  
Margarida Malaquias Pires Urbano apresentada à Faculdade de  
Ciências e Tecnologia da Universidade de Coimbra, Departamento  
de Ciências da Vida**

Julho de 2022





FACULDADE DE  
CIÊNCIAS E TECNOLOGIA  
UNIVERSIDADE DE  
**COIMBRA**

Master in Cellular and Molecular Biology

# Organelle-targeted radioconjugates for Auger therapy of prostate cancer

Rafael Paulo Silveira

Ana M. Urbano

Paulo J. Oliveira

Coimbra, Julho 2022



*“One day, in retrospect, the years of struggle will strike you as the most beautiful”*

– Sigmund Freud



This work was performed at the Center for Neuroscience and Cell Biology, UC Biotech Building, Biocant Park, University of Coimbra, Portugal, in MitoXT group under the supervision of Prof. Dr. Paulo J Oliveira (CNC, University of Coimbra) and Prof. Dr. Ana M. Urbano (Department of Life Sciences, University of Coimbra).

## Funding

This work was supported by the European Regional Development (ERDF), through the COMPETE2020 – Operational Programme for Competitiveness and Internalization and Portuguese national funds via FCT -Fundação para a Ciência e a Tecnologia, under project PTDC/MED-QUI/1554/2020



UNIÃO EUROPEIA

Fundo Europeu  
de Desenvolvimento Regional



1 2



9 0

FACULDADE DE  
CIÊNCIAS E TECNOLOGIA  
UNIVERSIDADE DE  
COIMBRA



## Acknowledgements

Ao longo desta epata tive o apoio e o suporte de diversas pessoas. Um ano longo que me permitiu crescer a todos os níveis.

Ao Doutor Paulo Oliveira agradeço a oportunidade de realizar esta tese, pela disponibilidade, pelos ensinamentos a nível científico, pela compreensão e pelo apoio oferecido ao longo do ano. Agradeço também à Doutora Ana Urbano, por toda a ajuda e disponibilidade demonstrada.

À Doutora Sandra Mota por tudo o que me ensinou, pela paciência, pela constante motivação e por toda a ajuda prestada.

Agradeço igualmente a todos os membros do MitoXT Group, pela ajuda, pela partilha de conhecimento e pela boa disposição diária.

À minha família, à minha mãe, ao meu pai e à minha irmã agradeço por tudo, pela preocupação, pelo apoio, pelos conselhos e por fazerem tudo o que esta ao seu alcance para me ajudar.

À Maria agradeço por estar presente em todos os momentos, pela motivação constante e por me apoiar nesta etapa.

Aos meus amigos de longa data, Dylan, Hugo e Rafael agradeço pelo suporte, pelas conversas aos fins de semana, por me ouvirem falar da tese e por me apoiarem desde sempre.

Aos meus amigos Bernardo, Leandro e Diana agradeço pela amizade, pelo apoio, pela diversão, pelos jantares e pelas conversas.



## Abstract

Prostate cancer (PCa) remains a major public health problem since it is one of the most diagnosed cancer in men worldwide and one of the leading causes of cancer-related deaths. Thus, there is a huge demand for novel diagnostic and therapeutic strategies. Recently, targeted radionuclide therapy (TRT) has emerged as an efficient tool for cancer treatment. TRT strategies deliver ionizing radiation to tumors in a targeted manner, reducing off-target damage. In PCa, targeting prostate-specific membrane antigen (PSMA), which is overexpressed in prostatic cancer, has shown enormous potential.

TRT using Auger electrons (AE) has shown greater potential to treat small size cancers and metastases, because of their high level of cytotoxicity to tumor cells, high linear energy transfer (LET) and short-range biological effectiveness. Moreover, organelles such as mitochondria are emerging as potential targets for radiotherapy-based therapies. Therefore, the AugerTher project aims to study dual-targeted metal complexes based on AE-emitting radionuclides carrying a PSMA ligand (PSMA<sub>617</sub>) for selective uptake by PCa cells, and pharmacophores with a well-recognized affinity for the nucleus or the mitochondria. By initiating the targeting of mitochondria, this project expects to change the radiation biology paradigm, which sustains that the biological effects of radiation are associated to nuclear damage.

In the present study, we assessed the effects of PSMA<sub>617</sub> alone and <sup>nat</sup>In-DOTAGA-AO on the viability and cellular metabolism of PCa, using four *in vitro* cell models (cell lines PNT2, LNCaP, PC3-FLU and PC3-PIP). Our findings suggests that the PSMA<sub>617</sub> alone did not induce toxicity to the cells, but was accompanied by small alterations in mitochondrial and glycolytic functions, regardless the cell phenotype (normal or cancerous). Interestingly, we found that cells that do not express PSMA were more sensitive to PSMA<sub>617</sub>. Moreover, the alterations observed, although non-significant, suggest that treatment with PSMA<sub>617</sub> in cells expressing PSMA may lead to the internalization of PSMA protein leading to a decrease in cell metabolism which at long-term can lead to cell proliferation and migration inhibition. On the other hand, all the cells internalized the cold-surrogate <sup>nat</sup>In-DOTAGA-AO within the nucleus and

mitochondria which leads to alterations in mitochondrial and glycolytic function, mitochondrial membrane potential (MMP), and mitochondrial ROS production. Moreover, although  $^{nat}In$ -DOTAGA-AO did not induce cytotoxicity in our *in vitro* models, it seems to revert the cancerous phenotype.

Therefore, this study represents an important preliminary work for a major project, and supports the development of AE-emitting radiocomplexes functionalized with targeting ligands such as PSMA<sub>617</sub> and mitochondria-directed ligand to target specific PCa cells' organelles.

**Keywords:** Cancer theragnostics; Radiopharmaceuticals; Mitochondria; Metabolism

## Resumo

O cancro da próstata continua a ser um dos maiores problemas de saúde pública sendo um dos cancros mais diagnosticados em homens a nível mundial e é uma das principais causas de morte relacionada ao cancro. Assim, a procura de novas estratégias diagnósticas e terapêuticas é elevada. Recentemente, a terapia com radionuclídeo direcionado (TRT) tem surgido como uma eficiente ferramenta para o tratamento de cancro. As estratégias de TRT direcionam radiação ionizante para os tumores, reduzindo assim danos para além do alvo. O Antígeno de Membrana Específico da Próstata (PSMA) que tem elevada expressão no cancro da próstata, em PCa o seu direcionamento tem mostrado um enorme potencial, tanto para diagnóstico, como para tratamento.

A utilização de eletrões Auger (AE) em TRT tem demonstrado uma grande potencial para tratar cancros e metástases de pequenas dimensões devido ao seu elevado nível de citotoxicidade em células tumorais, à alta transferência linear de energia (LET) e à eficácia biológica de curto alcance. Além disto, os organelos e as biomoléculas como a mitocôndria tem surgindo como potenciais alvos para terapias à base de radioterapia. Portanto, o projeto AugerTher tem como objetivo estudar complexos metálicos de direcionamento duplo baseados em radionuclídeos que emitam AE cuja estrutura é funcionalizada com um ligante PSMA (PSMA<sub>617</sub>) de modo que a que este complexo seja capturado seletivamente por as células PCa, e pretende ainda estudar os utilizar moléculas com alta afinidade com o núcleo e a mitocôndria para alvejar especificamente esses organelos. Assim, este projeto espera mudar o paradigma da biologia da radiação, que sustenta que os efeitos biológicos da radiação estão associados ao dano nuclear.

Neste estudo, nós avaliamos o efeito biológico do tratamento com PSMA<sub>617</sub> isolado e de <sup>nat</sup>In-DOTAGA-AO tanto na viabilidade das células, bem como no seu metabolismo celular, utilizando quatro modelos *in vitro* (PNT2, LNCaP, PC3-FLU and PC3-PIP). Os nossos resultados sugerem que a resposta das células a PSMA<sub>617</sub> isoladamente não induz toxicidade celular, mas ocorrem pequenas alterações na função mitocondrial e glicolítica, independentemente do fenótipo celular (normal ou cancerígena). Curiosamente, os resultados sugerem que as células que não expressam PSMA são mais

sensíveis ao PSMA<sub>617</sub>. Além disto, os resultados, embora não significativos, sugerem que o tratamento com PSMA<sub>617</sub> em células que expressam PSMA pode levar à internalização da proteína contribuindo para a diminuição do metabolismo celular que a longo prazo pode levar à diminuição da proliferação celular e inibição da migração. Por outro lado, todas as células internalizaram o composto frio <sup>nat</sup>In-DOTAGA-AO tanto no núcleo como na mitocôndria, levando a alterações das funções mitocondrial e glicolítica, do potencial de membrana mitocondrial (MMP) e da produção de ROS a nível mitocondrial. Para além disto, apesar do <sup>nat</sup>In-DOTAGA-AO não induzir citotoxicidade nos modelos *in vitro* estudados, as células cancerígenas parecem mudar o seu comportamento, tornando-se mais semelhantes às células normais da próstata (PNT2)

Portanto, este estudo representa um importante trabalho preliminar para um projeto maior, apoiando o desenvolvimento de radiocomplexos emissores de AE direcionados às células alvo através do ligando PSMA<sub>617</sub> e funcionalizados com grupos de direcionamento para organelos, nomeadamente as mitocôndrias.

**Palavras-chave:** Cancro da próstata; Radiofármacos; Mitocôndria; Metabolismo

## List of Acronyms and Abbreviations

<b>AA</b>	Antimycin A
<b>ADP</b>	Adenosine diphosphate
<b>AMP</b>	Adenosine monophosphate
<b>AO</b>	Acridine orange
<b>APS</b>	Ammonium persulfate
<b>ATP</b>	Adenosine triphosphate
<b>AUC</b>	Area under curve
<b>BCA</b>	Bicinchoninic acid
<b>BSA</b>	Bovine serum albumin
<b>DNA</b>	Deoxyribonucleic acid
<b>DRP1</b>	Dynamin-related protein-1
<b>ECAR</b>	Extracellular acidification rate
<b>EDTA</b>	Ethylenediaminetetraacetic acid
<b>ETC</b>	Electron transport chain
<b>FADH<sub>2</sub></b>	Flavin adenine dinucleotide
<b>FBS</b>	Fetal bovine serum
<b>FCCP</b>	Carbonyl cyanide-4-(trifluoromethoxy)phenylhydrazone
<b>FIS1</b>	Fission protein 1
<b>GPx</b>	Glutathione peroxidase
<b>GR</b>	Glutathione reductase
<b>GSH</b>	Reduced glutathione
<b>HRP</b>	Horseradish peroxidase
<b>KEAP1</b>	Kelch-like ECH-associated protein 1
<b>MFN1</b>	Mitofusin 1
<b>MFN2</b>	Mitofusin 2
<b>MMP</b>	Mitochondrial membrane potential
<b>mtDNA</b>	Mitochondrial DNA
<b>mtROS</b>	Mitochondrial reactive oxygen species
<b>NADH</b>	Nicotinamide adenine nucleotide (reduced form)
<b>NADPH</b>	Nicotinamide adenine nucleotide phosphate (reduced form)
<b>OCR</b>	Oxygen consumption rate
<b>OPA1</b>	Optic atrophy-1
<b>OXPHOS</b>	Oxidative phosphorylation
<b>PBS</b>	Phosphate-buffered saline
<b>PGC-1<math>\alpha</math></b>	Peroxisome proliferator-activated receptor gamma coactivator 1 $\alpha$
<b>PINK1</b>	PTEN-induced kinase 1
<b>PLL</b>	Poly-L-lysine
<b>PMSF</b>	Phenylmethanesulfonyl fluoride
<b>PVDF</b>	Polyvinylidene difluoride
<b>ROS</b>	Reactive oxygen species
<b>SOD</b>	Superoxide dismutase
<b>SDS</b>	Sodium dodecyl sulphate

<b>SDS-Page</b>	Sodium dodecyl sulphate ??
<b>SEM</b>	Standard error of mean
<b>SRB</b>	Sulforhodamine B
<b>TBS-T</b>	Tris-buffered saline tween
<b>TCA</b>	Trichloroacetic acid
<b>TEMED</b>	N, N,N',N'-tetramethylethylenediamide
<b>TMRM</b>	Tetramethylrhodamine methyl ester
<b>TPP<sup>+</sup></b>	Triphenylphosphonium cation
<b>2-DG</b>	2-Deoxy-glucose

## List of Content

Acknowledgement.....	V
Abstract.....	VII
Resumo.....	IX
List of Acronyms and Abbreviations.....	XI
List of Content.....	XIII
Figures Index.....	XVII
Tables Index.....	XIX
1. Introduction.....	1
1.1 Prostate cancer: incidence, mortality, diagnosis, staging and current treatment options.....	1
1.2 Radiation therapy: general mechanism of action and available modalities.....	3
1.3 Targeted radionuclide therapy.....	7
1.3.1 $\beta$ -emitting radionuclides.....	9
1.3.2 $\alpha$ -emitting radionuclides.....	9
1.3.3 AE-emitting radionuclides.....	10
1.4 Targeting strategies.....	11
1.4.1 Prostate-specific membrane antigen.....	12
1.4.2 Subcellular targeting of targeted radionuclide therapy.....	13
1.5 Mitochondria and cancer.....	14
1.5.1 Mitochondrial dynamics.....	15
1.5.2. Cell death.....	18
1.5.3. Mitochondrial DNA and ionizing radiation effects.....	19
1.6 Objectives.....	20
2 Material and Methods.....	21
2.1 Novel compounds.....	21
2.2 Cell culture.....	21
2.3 Preparation of total cell extracts.....	22
2.4 Western blotting.....	23
2.5 Resazurin assay.....	24

2.6	Sulforhodamine B assay.....	25
2.7	Real-time cell metabolic analysis.....	25
2.8	Evaluation of <sup>nat</sup> In-DOTAGA-AO internalization and localization.....	29
2.9	Assessment of mitochondrial membrane potential.....	30
2.10	Measurement of mitochondrial superoxide levels.....	30
2.11	Statistical analysis.....	31
3	Results.....	32
3.1	Cell lines characterization: PSMA expression levels.....	32
3.2	Effect of PSMA <sub>617</sub> compound in cell viability and metabolism.....	34
3.2.1	PSMA <sub>617</sub> did not induce cell mass or metabolic activity alterations.....	34
3.2.2	Long-term PSMA <sub>617</sub> exposure affect mitochondrial respiration of PCa cells.....	36
3.2.3	Short- and long-term exposure to PSMA <sub>617</sub> increases the glycolytic function of normal prostate PNT2 cells.....	40
3.2.4	Exposure to PSMA <sub>617</sub> has no effect on PC3-PIP cells but induce an energetic switch in PC3-FLU cells.....	42
3.2.5	PSMA <sub>617</sub> treatment did not induce alterations on the glycolytic function of PC3-FLU and PC3-PIP cells.....	45
3.3	Effects of <sup>nat</sup> In-DOTAGA-AO compound in cell viability and metabolism.....	49
3.3.1	<sup>nat</sup> In-DOTAGA-AO internalizes and co-localizes with the nucleus and mitochondria.....	49
3.3.2	<sup>nat</sup> In-DOTAGA-AO did not induce cell mass or metabolic activity alterations.....	51
3.3.3	<sup>nat</sup> In-DOTAGA-AO increases the glycolytic function of PNT2 cells.....	58
3.3.4	Short-term <sup>nat</sup> In-DOTAGA-AO treatment increased basal and ATP production-linked respiration of PC3-FLU cells while long-term exposure to 50 μM <sup>nat</sup> In-DOTAGA-AO decreases mitochondrial function of cells overexpressing PSMA..	60
3.3.5	Long-term <sup>nat</sup> In-DOTAGA-AO treatment increases PC3-FLU cells glycolytic reserve.....	63
3.3.6	<sup>nat</sup> In-DOTAGA-AO decreases the mitochondrial membrane potential of PNT2 cells while it increases the mitochondrial membrane potential of PC3-PIP cells.....	66

3.3.7 $^{nat}In$ -DOTAGA-AO treatment increased mitochondrial reactive oxygen species levels in LNCaP cells.....	68
4 Discussion.....	71
5 Conclusion and future perspectives.....	83
6 References.....	85



## Images index

<b>Figure 1.</b> Representation of different features of radionuclides emitting $\beta$ -particles, $\alpha$ -particles, and AE.....	17
<b>Figure 2.</b> Chemical structure of the compounds under investigation in this study. ....	21
<b>Figure 3.</b> Seahorse XF profile and respective parameters of the performed.....	26
<b>Figure 4.</b> Characterization of the cell lines: expression of PSMA in PNT2, LNCaP, PC3-FLU and PC3-PIP .....	33
<b>Figure 5.</b> Cytotoxic effect of PSMA <sub>617</sub> on PNT2, LNCaP, PC3-FLU and PC3-PIP cells.. ....	35
<b>Figure 6.</b> Impact of short-term exposure to PSMA <sub>617</sub> on mitochondrial oxygen consumption of PNT2 and LNCaP cells.....	38
<b>Figure 7.</b> Impact of long-term exposure to PSMA <sub>617</sub> on mitochondrial oxygen consumption of PNT2 and LNCaP cells.....	40
<b>Figure 8.</b> Impact of short-term exposure to PSMA <sub>617</sub> on glycolytic function of PNT2 and LNCaP cells. ....	41
<b>Figure 9.</b> Impact of long-term exposure to PSMA <sub>617</sub> on glycolytic function of PNT2 and LNCaP cells.. ....	42
<b>Figure 10.</b> Impact of short-term exposure to PSMA <sub>617</sub> on mitochondrial oxygen consumption of PC3-FLU and PC3-PIP cells.....	45
<b>Figure 11.</b> Impact of long-term exposure to PSMA <sub>617</sub> on mitochondrial oxygen consumption of PC3-FLU and PC3-PIP cells.....	47
<b>Figure 12.</b> Impact of short-term exposure to PSMA <sub>617</sub> on glycolytic function of PC3-FLU and PC3-PIP cells .....	47
<b>Figure 13.</b> Impact of long-term exposure to PSMA <sub>617</sub> on glycolytic function of PC3-FLU and PC3-PIP cells.....	48
<b>Figure 14.</b> <sup>nat</sup> In-DOTAGA-AO internalization and co-localization within the nucleus and mitochondria.....	50
<b>Figure 15.</b> Cytotoxic effect of <sup>nat</sup> In-DOTAGA-AO on PNT2, LNCaP, PC3-FLU and PC3-PIP cells .....	52
<b>Figure 16.</b> Impact of short-term exposure to <sup>nat</sup> In-DOTAGA-AO on mitochondrial oxygen consumption of PNT2 and LNCaP cells.....	56

<b>Figure 17.</b> Impact of long-term exposure to <sup>nat</sup> In-DOTAGA-AO on mitochondrial oxygen consumption of PNT2 and LNCaP cells.....	58
<b>Figure 18.</b> Impact of short-term exposure to <sup>nat</sup> In-DOTAGA-AO on glycolytic function of PNT2 and LNCaP cells.....	59
<b>Figure 19.</b> Impact of long-term exposure to <sup>nat</sup> In-DOTAGA-AO on glycolytic function of PNT2 and LNCaP cells.....	60
<b>Figure 20.</b> Impact of short-term exposure to <sup>nat</sup> In-DOTAGA-AO on mitochondrial oxygen consumption of PC3-FLU and PC3-PIP cell. ....	63
<b>Figure 21.</b> Impact of long-term exposure to <sup>nat</sup> In-DOTAGA-AO on mitochondrial oxygen consumption of PC3-FLU and PC3-PIP cells.....	65
<b>Figure 22.</b> Impact of short-term exposure to <sup>nat</sup> In-DOTAGA-AO on glycolytic function of PC3-FLU and PC3-PIP cells.....	65
<b>Figure 23.</b> Impact of short-term exposure to <sup>nat</sup> In-DOTAGA-AO on glycolytic function of PC3-FLU and PC3-PIP cells.....	66
<b>Figure 24.</b> Impact of <sup>nat</sup> In-DOTAGA-AO treatment on mitochondrial network area and mitochondrial membrane potential.....	68
<b>Figure 25.</b> Impact of <sup>nat</sup> In-DOTAGA-AO treatment on mitochondrial superoxide anion production on PNT2 and LNCaP cells. ....	69
<b>Figure 26.</b> Impact of <sup>nat</sup> In-DOTAGA-AO treatment on mitochondrial superoxide anion production on PC3-FLU and PC3-PIP cells. ....	70

## Tables index

**Table 1.** Antibodies used in western blotting analysis..... 24

**Table 2.** Key parameters of mitochondrial respiration and formulas used in their evaluation when performing the Agilent Seahorse XF Cell Mito Stress Test..... 27

**Table 3.** Key parameters of glycolytic function and respective formulas used in their evaluation when performing the Agilent Seahorse XF Cell *Glycolytic* Stress Test..... 28



# 1. Introduction

## 1.1. Prostate cancer: incidence, mortality, diagnosis, staging and current treatment options

Prostate cancer (PCa) is a major public health problem worldwide (Carlsson et al. 2020). With 1.4 million estimated new cases and more than 375,000 deaths in 2020, PCa is the second most incident cancer in men and the fifth most mortal. More specifically, the estimated PCa diagnosed cases represent 14.1% of all new cancer cases in male individuals and 7.3% in both males and females. Regarding mortality, PCa deaths represent 6.8% and 3.8% of all cancer-related deaths, considering males and both sexes, respectively. The patterns of incidence and mortality vary by region, with the highest incidence rates registered in Northern and Western Europe, with an incidence ratio of 83.4 and 77.6 per 100,000 men, respectively, while the Caribbean region and Middle Africa present the highest mortality rates, with 27.9 and 24.8 per 100,000 men (GLOBOCAN, Sung et al. 2021). So far, little is known about the etiology of the disease, and the established risk factors are aging, family history, and certain genetic mutations (e.g., BRCA1 and BRCA2). Patterns of incidence and mortality across the world are likely modulated by lifestyle and environmental factors, since smoking, excess body weight, and nutritional imbalance might increase the risk of PCa incidence (Rebbeck et al. 2013). Of note, the development and access to the health system also contribute to differences in the international incidence and mortality patterns. In high-income countries, rates of incidence are higher, due to greater diagnosis and monitoring of the disease. However, despite the higher incidence rate, there is a lower mortality rate, reflecting earlier screening and more advanced treatment. In poor-income countries, limited access to the health system, as well as the unavailability of more sophisticated diagnostic and treatment tools, are reflected in low incidence rate and higher mortality rates (Tsodikov et al. 2017; Jemal et al. 2020).

Prostate malignant transformation is a multistep process that initiates as prostatic intraepithelial neoplasia and is followed by localized prostate cancer, advanced prostate adenocarcinoma with local invasion and, finally, metastatic PCa (Wang G et al. 2018). An early-stage PCa is considered a localized tumor without identifiable metastases (Sebesta

et al. 2017; Litwin et al. 2017; Janiczek et al. 2017), and an advanced-stage PCa includes patients diagnosed with recurrent tumors or with identifiable metastases distant from the primary tumor, most frequently in the lymph nodes or bones (Litwin et al. 2017; Janiczek et al. 2017).

A determinant factor in the mortality rate is diagnosis as an early diagnosis is crucial to improve survival outcome. There are several PCa screening modalities, including digital rectal examination (DRE), trans-rectal ultrasound (TRUS), assessment of serum prostate-specific antigen (PSA) blood levels (also known as the PSA test), and histopathological or cytological examination of specimens from the gland (Surasi et al. 2020). These techniques vary in terms of sensitivity and capacity to detect PCa at different stages of the disease. For instance, although the PSA test is widely used for PCa screening, successfully detecting malignant disease at all stages, it has poor specificity, with only 30% to 40% of positive results confirmed by biopsy analysis (Uno H. et al. 2021). The PSA test assesses PSA levels in the blood which, are standardized for a certain age range, but the variation of PSA levels can change due to factors other than cancer, namely due to urine infection. Sometimes, false positives continue to be monitored over the years, namely by performing DRE and TRUS at regular intervals, which is associated with increasing pain and suffering for the patients, who may suffer from infections and hematuria. There may also create psychological distress associated with fear of a diagnosis confirmation (Dudith et al. 2021). To increase accuracy, diagnosis is often made using a combination of screening modalities (Popa et al. 2017).

Proper staging of PCa is also essential to establishing the most appropriate patient-specific treatment (Bouchelouche et al. 2010). In 1974, Gleason and Mellinger defined a grading system, which came to be known as the Gleason grading system, based on histological patterns of prostate adenocarcinoma (Gleason and Mellinger 1974). This grading system which has been refined over the years, is the most used grading system. It allows the sorting of patients into a five-grade stratification scheme according to the results of the screening trials. More specifically, clinicians consider PSA blood levels and the Tumor, Node, Metastasis (TNM) staging of the cancer, the latter assessing the size of the tumor and how far it has grown. Grade 1 (Gleason score  $\leq 6$ ) corresponds to the less aggressive tumor, with cells looking similar to normal prostate cells, and is

expectable to grow slowly. Grade 5 (Gleason score 9 or 10) is the most aggressive stage, with cells looking very abnormal, and is a cancer likely to grow quickly. Between these extreme grades, there are three grades with  $6 < \text{Gleason score} < 9$ . Available treatments for PCa include surgery, radiation therapy, standard chemotherapy (also known as traditional chemotherapy), immunotherapy, and androgen deprivation therapy. For early-stage PCa, active surveillance is often recommended, as these tumors are unlikely to grow quickly, but radiation therapy or radical prostatectomy may be considered. In advanced-stage PCa, the initial treatment options are prostatectomy and radiation therapy combined with different approaches of androgen deprivation therapy or immunotherapy and chemotherapy, if the initial options failure. (Bekelman et al. 2018; Chen et al. 2016). As can be appreciated, radiation therapy is an option to manage all PCa stages, either as monotherapy or combined with the other available treatments. Unfortunately, despite the available treatment options, advanced stages of the disease are still associated with high mortality. Thus, innovative treatments are clearly needed (Czerwinska et al. 2020).

## **1.2. Radiation therapy: general mechanism of action and available modalities**

Radiation therapy (also called radiotherapy) has been part of the multidisciplinary management of PCa for a long time, sparing patients the adverse effects of surgical intervention. This therapy uses high-energy particles or waves, such as x-rays, gamma rays, electron beams, or protons, to damage and eliminate malignant cells. The emitted particles have enough energy to ionize (i.e., induce gain or loss of electrons) atoms and molecules and, as such, are described as ionizing radiation (IR). Direct interaction of IR with cell structures and biomolecules, most notably DNA, induces chemical and biological changes that ultimately lead to cellular dysfunction and often death. In addition, IR exposure promotes the radiolysis of water, generating the hydroxyl radical ( $\cdot\text{OH}$ ) and hydrogen radical ( $\text{H}\cdot$ ). These radical species promote a cascade of reactions that produces superoxide ( $\text{O}_2^{\cdot-}$ ), hydrogen peroxide ( $\text{H}_2\text{O}_2$ ), and other secondary reactive oxygen species (ROS) (Filomeni et al. 2015; Plante 2021). In addition, IR stimulates the activity of inducible nitric oxide synthases (NOS), resulting in nitric oxide

( $\cdot\text{NO}$ ) production. Even though  $\cdot\text{NO}$  is inactive towards most cellular constituents, it reacts with  $\text{O}_2\cdot^-$ , generating the peroxynitrite anion ( $\text{ONOO}^-$ ). This highly reactive radical interacts with several species producing other reactive nitrogen species (RNS), namely peroxynitrous acid ( $\text{ONOOH}$ ), nitrogen dioxide ( $\text{NO}_2\cdot$ ), and dinitrogen trioxide ( $\text{N}_2\text{O}_3$ ), (Verigos et al. 2020; Zhao et al. 2021). Besides exogenous ROS/RNS, there are endogenous ROS/RNS sources, including the mitochondrial electron transport chain (ETC) (Zhao et al. 2019; Cheng et al. 2021), NADPH oxidase (NOX) and NOS. Although, at certain levels, ROS and RNS may play a role in cell signaling pathways crucial for maintaining cell homeostasis, exacerbate levels of reactive species imbalance the cellular redox status, resulting in several deleterious effects within cells (Plante 2021; Zhao et al. 2021). Specifically, ROS and RNS induce damage to proteins, fatty acids, and nucleotides, compromising the normal function of cellular organelles such as nucleus, mitochondria, cell membrane and lysosomes (Yang et al. 2021; Lei et al. 2020).

Cumulative ROS/RNS within cells damage nucleic acids, enhancing genomic instability because of deleterious alterations to bases and sugars, DNA strand cross-linking, single- and double-strand breaks (SSBs/DSBs), and DNA clustering (Ragunathan et al. 2020; Zhao et al 2021; Srinivas et al. 2019). DNA strand breaks occur randomly in the DNA backbone by  $\text{O}_2\cdot^-$  direct interaction and through activation of nucleic acid-binding enzymes. Those interactions include depurination and depyrimidinizations of DNA bases, such as the oxidation of deoxyguanosine (dG) to 8-hydroxyguanine (8-oxodG), one of the major products of DNA oxidation, and a well-known DNA damage hallmark (Srinivas et al. 2019). Upon DNA insult, cells immediately trigger intrinsic mechanisms of defense, the DNA damage response (DDR), activating an extensive protein network. Briefly, the damage site is recognized by the protein kinase ataxia telangiectasia mutated (ATM) and other sensor proteins, and through activation of the ATM/p53 pathway, the cell undergoes apoptosis or cell cycle arrest (Ku et al. 2019; Srinivas et al. 2019).

Lipids are another class of biomolecules targeted by IR. Radiation induces extensive damage to the lipid bilayer of biological membranes, through lipid peroxidation, in particular the peroxidation of polyunsaturated fatty acids (PUFAs). Subsequently, there is an increase in membrane permeability and disruption of ion gradients, compromising

all processes dependent on cell membrane integrity (Su et al. 2019; Bai et al. 2019). The oxidative degradation of lipids generates peroxy radicals, such as lipid hydroperoxides (LOOH) and PUFA fragments (malondialdehyde (MDA), acrolein, and 4-hydroxy-2-nonenal (HNE)). In turn, increased levels of peroxy radicals disrupt the cellular redox status, compromising several intracellular processes (Tsikas 2017; Kajarabille et al. 2019).

As briefly mentioned before IR-generated ROS/RNS also target proteins, modulating protein expression, inducing post-translation modifications (PTMs), and altering protein activity (Niforou K et al. 2014). Protein expression is mainly modulated by IR-induced epigenetic modifications (DNA methylation, histone methylation and acetylation) that change the gene expression pattern. (McDonagh 2017). PTMs induced by IR include oxidation, carbonylation, phosphorylation, acetylation, and glycosylation. Those modifications promote conformational changes, affecting protein structure and function, which subsequently alter protein interaction and protein trafficking resulting in deep impact on numerous signaling pathways and cellular processes (Niforou et al. 2014; McDonagh 2017).

As reported, cells are very susceptible to ROS and RNS and the damage sustained can be lethal to the cell. Therefore, cells have a complex defense system against excessive ROS/RNS levels, which is quickly activated upon IR exposure. This system includes a network of ROS/RNS-scavenging molecules and detoxifying enzymes that neutralize free radicals (Einor et al. 2016; Slimen et al. 2014). This detoxification is mainly carried out by superoxide dismutases (SODs), with an important contribution from several catalases activity such as peroxiredoxins (Prx) and glutathione peroxidases (GPxs). In addition, other scavenging molecules including glutathione (GSH), ascorbate (vitamin C), melatonin, lipoic acid, ubiquinone (coenzyme Q10), and vitamin E, play a crucial role in maintaining cellular redox status (Slimen et al. 2014). In response to IR-induced increased levels of oxidative stress, cells quickly modulate the expression of antioxidant enzymes through the activation of transcriptional factors such as nuclear factor (erythroid-derived 2)-like 2 and nuclear factor kappa-light-chain-enhancer of activated B cells (NF- $\kappa$ B) (Slimen et al. 2014).

Taking it in consideration, it is mandatory to ensure a balanced oxidative stress status, and therapies based on radiation need to ensure an accurate energy dosimetry to minimize the extremely deleterious effects of IR. The two classic modalities of radiation therapy available are external beam radiation therapy (EBRT) and brachytherapy (BT) (internal radiation) (Podder et al. 2018). In EBRT, the prostate gland is irradiated from outside the body with high-energy beams, such as X-ray, photons or protons which are generated by a linear accelerator. The major challenge associated with this modality is to spare the neighbouring healthy tissue from the radiation, ultimately preventing severe adverse effects, including urinary, bowel and sexual dysfunction, as well as secondary cancers (Brawley et al. 2018; Lumen et al. 2013). BT allows the delivery of localized high doses of radiation to small volumes, ensuring high cytotoxicity to damaged tissues, while sparing healthy tissue (Hannoun-Lèvi et al. 2017; Zaorsky et al. 2017). There are different BT approaches available, including the low-dose-rate (LDR) BT, in which a radioactive seed implanted into the prostate gland delivers a steady dose of radiation over the organ, during a period that might vary from hours to days to months or even permanently. This modality is usually used as monotherapy to manage low-risk disease patients and the most common radioisotopes used are iodine-125 ( $^{125}\text{I}$ ), palladium-103 ( $^{103}\text{Pd}$ ) and cesium-131 ( $^{131}\text{Cs}$ ) (Dutta S et al. 2018; Butler et al. 2016). Another BT approach is the high-dose-rate (HDR) modality, which involves delivering radiation in short bursts through thin tubes that are temporarily inserted into the prostate gland (Hannoun-Lèvi et al. 2017; Crook J et al. 2020). As monotherapy, BT and EBRT are mostly used to manage early-stage PCa with localized tumor. For advanced states of the disease, EBRT and BT are usually used in combination or combined with androgen deprivation therapy (Gay et al. 2018).

In addition to these main radiation therapy modalities, over time new radiation-based therapies have been studied (Gay et al. 2018). With the advancement of technology, these novel modalities take advantage of high-quality imaging tools, robotic assistance, and better delivery systems (Podder et al. 2018) for both cancer screening and treatment. Over the last years, one of the novel emerging approaches is the targeted radionuclide therapy (TRT) (Filippi et al. 2020).

### 1.3. Targeted radionuclide therapy

TRT is a theragnostic modality based on the use of a radioactive nucleus attached to a targeting vector to deliver cytotoxic doses of ionizing radiation to cancer cells (Gill et al. 2017) for both cancer imaging and treatment purposes (Filippi et al. 2020; Hindie et al. 2018). A key aspect of this modality is the use of specific ligands that interact with target biomolecules present in a diseased tissue (Filippi et al. 2020). This feature ensures the deposition of large amounts of energy in a narrow location, allowing it to reach the malignant cells and avoid damaging the surrounding healthy tissue (Sapienza et al. 2019). The cytotoxic effect is guaranteed by energetic emissions whose magnitude depends on the radionuclide, which can emit  $\alpha$ -particles,  $\beta$ -particles, or Auger electrons (AE) (Figure 1) (Czerwinska et al. 2020; Gill et al. 2017). The emitted energy originates from decaying radioactive atoms, each of which has its own features, namely chemistry, half-life, decay properties, tissue range, and availability (Czerwinska et al. 2020).

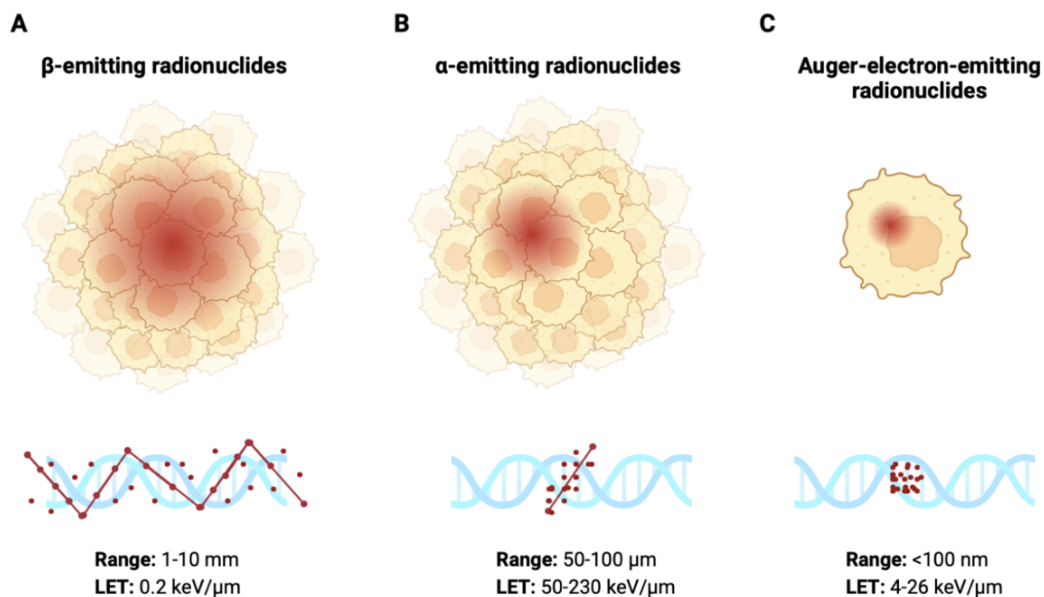


**Figure 1.** Representation of different features of radionuclides emitting  $\beta$ -particles,  $\alpha$ -particles, and AE, including tissue-penetration, LET and density of ionizing events. (A)  $\beta$ -emitting radionuclides. (B)  $\alpha$ -emitting radionuclides. (C) AE-emitting radionuclides. Figure 1 was created with BioRender. LET, linear energy transfer.

### 1.3.1. $\beta$ -emitting radionuclides

$\beta$ -emitting radionuclides generate  $\beta$ -particles during the decayment of the nucleus, which variable energy. In general,  $\beta$ -particles have a relatively long range (1–10 mm) and low linear energy transfer (LET) (0.2keV/ $\mu$ m) (Czerwinska et al. 2020). Consequently, this energy penetrates large masses of tissue and can hit not only large tumors but also their neighbouring healthy tissue (Czerwinska et al. 2020; Sadremomtaz et al. 2019). The cytotoxic effect of the  $\beta$ -particles is associated with water radiolysis, resulting in SSBs or DSBs (Tafreshi et al. 2019). The  $\beta$ -emitting radionuclides, iodine-131 ( $^{131}\text{I}$ ), copper-67 ( $^{67}\text{Cu}$ ), lutetium-177 ( $^{177}\text{Lu}$ ), and yttrium-90 ( $^{90}\text{Y}$ ) are the most investigated for the diagnostic and treatment of cancer, including PCa (Sadremomtaz et al. 2019). Westcott et al. describe the development and US Food and Drug Administration (FDA) approval of two commercially available  $^{90}\text{Y}$  attached to two different types of microspheres that ensure the selective radionuclide targeting (Westcott et al. 2016). According to Dash et al. 2014, and Das et al. 2015,  $^{177}\text{Lu}$  is a  $\beta$ -emitting radionuclide with enormous potential in nuclear medicine theragnostic, as it has a long half-life ensuring a diagnostic imaging advantage. This property has already been studied *in vivo*, with successful clinical tracking long after its administration (Dash et al. 2014; Das et al. 2015).

### 1.3.2. $\alpha$ -emitting radionuclides

Radiotherapy based on  $\alpha$ -emitting radionuclides is an interesting alternative to radiotherapy based on  $\beta$ -particles emitters (Marcu et al. 2018).  $\alpha$ -Particles are  $^4\text{He}$  nuclei, which have a larger size than other subatomic particles emitted from decaying radionuclides. Due to its size, its whole generated energy is deposited in a small area as these particles have a low penetrance capacity (50–100  $\mu$ m) (Parker et al. 2018). The radioactive nuclei decaying generates daughter nuclei that are often themselves  $\alpha$ -emitters leading to a decay cascade which contributes significantly to a greater energy deposition (Czerwinska et al. 2020; Parker et al. 2018). This high LET radiation (50–230keV/ $\mu$ m) has therefore a huge potential to handle small tumors, micro-metastases, and for the treatment of hematological malignancies (Marcu et al. 2018; Jurcic et al.

2019). These  $\alpha$ -particle agents interact directly with DNA macromolecules inducing lethal DNA DSB ensuring a high relative biological effectiveness. So far, several  $\alpha$ -emitting radionuclides approaches have been studied, with different radioisotopes, including astatine-211 ( $^{211}\text{At}$ ), radium-223 ( $^{223}\text{Ra}$ ), thorium-227 ( $^{227}\text{Th}$ ), and actinium-225 ( $^{225}\text{Ac}$ ) (Czerwinska et al. 2020). In 2013,  $^{223}\text{Ra}$  dichloride injections were approved by FDA for the treatment of patients with castration-resistant prostate cancer, with bone and lymph nodes metastasis, excluding visceral metastases (Das et al. 2015). Previously, the ALSYMPCA trial (phase III) showed an overall survival benefit with the addition of  $^{223}\text{Ra}$  to standard care, and after FDA approval, many other studies focusing on  $^{223}\text{Ra}$  have been performed to shift the paradigm of PCa treatment (Hoskin et al. 2014; Parker et al. 2013; Heidegger et al. 2018).

### **1.3.3. AE-emitting radionuclides**

AE are emitted by decaying radionuclides by electron capture and/ or internal conversion (Ramogida et al. 2013). These processes create a vacancy in the inner electron shell which is subsequently filled by electrons from higher energy shells triggering a cascade of radiative and non-radiative transitions (Czerwinska et al. 2020; Ramogida et al. 2013; Rosenkranz et al. 2020; Paillas et al. 2016). While radiative transitions may result in emission of X-ray,  $\gamma$ -rays, and  $\beta$ -particles, non-radiative transitions mainly correspond to the emission of AE, and Coster-Kronig and super Coster-Kronig electrons, collectively referred to as AEs (Knapp et al. 2016; Paillas et al. 2016). These are extremely low-energy electrons, with very limited tissue penetration (nanometers scale), generating high LET radiation (4–26 keV/ $\mu\text{m}$ ) (Czerwinska et al. 2020; Ramogida et al. 2013; Falzone et al. 2015; Kiess et al. 2015). The extremely localized deposition of energy allows targeting single cells or even subcellular organelles, ensuring high cytotoxicity, while lowering induced damage to surrounding tissue (Rosenkranz et al. 2020; Falzone et al. 2015; Sobolev et al. 2018; Costa et al. 2021). Importantly, the toxicity of AE is induced mainly through two mechanisms: 1) direct DNA damage by high LET radiation, generating SSB and DSB; or 2) indirect DNA damage by ROS generated during water radiolysis (Tafreshi et al. 2019; Ku et al. 2019; Rosenkranz

et al. 2020; Gudkov et al. 2016). Moreover, AE toxicity depends on the proximity of the decaying site to the target due to its low energy and high LET radiation. Several approaches have been followed, employing different delivery molecules, to ensure greater proximity between the radionuclide and the target and thus increase the biological effectiveness (Czerwinska et al. 2020; Kiess et al. 2015; Ku et al. 2019).

#### **1.4. Targeting strategies**

The relative biological effectiveness of radionuclide therapy depends on the specific targeting, which is achieved by intrinsic targeting properties of some radionuclides or by conjugating the radionuclide to a delivery molecule or vector (Ramogida et al. 2013; Dekempeneer et al. 2016). The delivery molecules currently used include antibodies, antibody fragments, peptides, small molecules, liposomes, dextrans, and microspheres (Dash et al. 2015; Ramogida et al. 2013). To choose the most suitable delivery system, it is necessary to consider the type of cancer and its features, namely its morphology and physiology (Dekempeneer et al. 2016). It is also necessary to bear in mind the properties of the delivery molecule that determine its pharmacokinetics (bioavailability, biospecificity, metabolism, excretion, and interaction on-target and off-target) to ensure maximum biological effectiveness of the modality. Emerging TRT approaches have been focused on a ligand-receptor mechanism., in which delivery molecules correspond to a ligand that targets and binds to a protein, the receptor. The success of this mechanism depends 1) on the affinity and specificity of the interaction between the ligand and the receptor, and 2) on the properties of the receptor, which is usually overexpressed in the malignant cells, allowing to selectively target the cancer cells, reducing the off-target damage (Ramogida et al. 2013; Dekempeneer et al. 2016). Specifically, for PCa, prostate-specific membrane antigen (PSMA) has shown enormous potential as target for imaging diagnosis and treatment purpose (Vaz et al. 2020).

#### **1.4.1. Prostate-specific membrane antigen**

PSMA, also known as glutamate carboxypeptidase II or folate hydrolase, is a 100–120 kDa protein with glutamate-carboxypeptidase and folate hydrolase I activity, playing a role in cell migration, cell survival, and proliferation (Emmett et al. 2017). This type II transmembrane glycoprotein, which is anchored at the prostate epithelial cell surface, is constituted by an intracellular domain with 18 amino acids, a transmembrane domain with 24 amino acids, and an extensive extracellular domain with 707 amino acids (O`driscoll et al. 2016). Upon binding to a ligand on the membrane surface, PSMA undergoes an internalization process via the endosome. This feature makes PSMA an attractive molecular target for cancer diagnostic imaging and treatment, as it has been shown to allow the internalization of PSMA-labelled radionuclides, ensuring a more efficient deposition of the pharmacophore within the cells (Emmett et al. 2017). PSMA is markedly overexpressed in prostatic cancer cells compared to other tissues, including normal prostatic tissue (Uijen et al. 2021). Moreover, high levels of PSMA expression are correlated with higher PCa malignancy and aggressiveness (Uijen et al. 2021; Chang 2004; Rahbar et al. 2018).

Despite its name, PSMA is also expressed in other normal tissues, such as brain, kidneys, small intestine, and salivary gland, playing different roles depending on the tissue. In the brain, its glutamate-carboxypeptidase regulates the release of key neurotransmitters by cleaving the neurotransmitter N-acetyl-L-aspartyl-L-glutamate (NAAG). Intestinal PSMA, on the other hand, displays folate hydrolase activity, which is characterized by the cleavage of polyglutamated peptides, playing a role in cellular uptake of dietary folate (Conway et al. 2006; Conway et al. 2016). Interestingly, PSMA seems to be universally upregulated in the neovasculature of solid tumors, such as those of the bladder, kidney, lung, and pancreas, while it is not expressed in the normal vasculature of tumors (Tumedei et al. 2021 Wang et al. 2015). This observation suggests that PSMA is a key player in tumor angiogenesis, which is an essential step in cancer invasion and in the development of metastasis (Conway et al. 2016; Wang et al. 2015; Russo et al. 2012). However, the underlying mechanism is not clear. Conway and colleagues suggested that PSMA acts downstream of metalloproteinase-2 (MMP-2),

generating a proteolytic cascade that promotes angiogenesis. Laminin, the predominant component of the extracellular matrix, is digested by MMP-2/PSMA into small laminin peptides that enhance endothelial cell adhesion and migration through the activation of integrins and adhesion kinases (Conway et al. 2006; Conway et al. 2016).

#### **1.4.2. Subcellular targeting of targeted radionuclide therapy**

The main target of different radiotherapy modalities, including TRT, is nuclear DNA. In fact, for many years, the central dogma of radiation biology sustains that the induction of genotoxicity was the responsible for biological effects of radiation. Currently, radiation-based therapies target other organelles, including mitochondria, lysosomes, and cell membranes (Chen et al. 2020), as it is believed that the distribution of IR in specific organelles could increase cytotoxicity and should also allow the use of lower radiation doses to reduce IR-associated adverse effects (Bavelaar et al. 2018). A study conducted by Maucksch et al., in 2016, an AE-emitting radionuclide,  $^{99m}\text{Tc}$ , was tested with three different ligands that ensured radiation deposition in the cytosol, plasma membrane and nucleus. The different subcellular distributions demonstrated alterations in the induced cytotoxicity which was not exclusively determined by DNA DSBs. The authors speculated that the observed differences in cytotoxicity were due to differential mitochondrial accumulation (Maucksch et al. 2016). This evidence highlights the importance of targeting extra-nuclear targets. In particular, mitochondrial DNA (mtDNA) has enormous potential as a target for novel radionuclide therapy modalities, as it is known to be extremely radiosensitive, but this potential has not yet been deeply explored. The interest in targeting mitochondria has increased recently due to their recognized role in tumorigenesis (Poole et al. 2021; Srinivasan et al 2017; Guo L 2021). Therefore, mitochondria are an excellent target for new therapies, especially targeted AE-emitting radionuclide therapy since it has high LET radiation with little tissue penetration, ensuring the deposition of IR in such small organelle (Badrinath et al. 2018; Czerwinska et al. 2020).

## 1.5. Mitochondria and cancer

In 2000, Hanahan and Weinberg proposed six hallmarks of cancer: sustaining proliferative signaling; evading growth suppressors; activating invasion and metastasis; enabling replicative immortality; inducing angiogenesis; resisting cell death. These are common features shared by most cancer cells that are acquired during the process of malignant transformation (Hanahan et al. 2000). Later, in 2011, the same authors suggested adding two emerging hallmarks: deregulating cellular energetics; avoiding immune destruction. The first one relies on reprogramming cellular metabolism to support malignant transformation and neoplastic proliferation. The second includes the capacity of cancer cells to avoid being destroyed by the immune system. Moreover, the authors suggested genome instability and mutation, and tumor-promoting inflammation as two enabling characteristics, i.e., characteristics that do not cause cancer themselves, but sustain the malignant transition (Hanahan et al. 2011). The first emerging hallmark, deregulating cellular energetics, includes alterations in cell bioenergetics through modifications in nutrient uptake and metabolic pathways leading to cell survival and proliferation (Hanahan et al. 2011).

Mammalian cells use two main processes to obtain energy, lactic acid glycolysis, and aerobic cellular respiration. Glycolysis occurs in the cytosol in which glucose is metabolized to pyruvate, generating two net molecules of ATP and two NADH molecules (Ashton et al. 2018). Subsequently, pyruvate may be reduced by lactate dehydrogenase, producing lactate (lactic acid fermentation), or may be converted to acetyl-CoA, which is fully oxidized in the tricarboxylic acid (TCA) cycle generating metabolic energy (ATP, indirectly through GTP) and reducing power (NADH, and complex II-bound FADH<sub>2</sub>). NADH and FADH<sub>2</sub> act as electron transporters, feeding the ETC with electrons, in a process called oxidative phosphorylation (OXPHOS), which occurs mainly in mitochondria in an oxygen-dependent manner. The electrons flow in the inner mitochondrial membrane (IMM) along four multiprotein ETC complexes (complex I (NADH: UQ oxidoreductase), II (succinate: UQ oxidoreductase), III (cytochrome *bc*<sub>1</sub> complex), and IV (cytochrome *c*)), creates an electron flux that allows the pumping of protons from the mitochondrial matrix to the intermembrane space, producing a high proton

gradient. These protons return to the mitochondrial matrix through the ATP synthase, leading to ATP formation by ADP phosphorylation. When arriving at complex IV, the electrons that flow along with the ETC are reduced to oxygen, the final electron acceptor, generating water (Payen et al. 2020). Despite the higher energy efficiency of respiration, compared to glycolysis, in 1923, Otto Warburg found evidence that cancer cells rely heavily on the latter to generate ATP. Initially, it was thought that the mitochondria of cancer cells were dysfunctional and therefore the cells had to rely on fermentation. Later, it was discovered that cancer cells produce ATP via glycolysis even though they have fully functional mitochondria and with oxygen available in which the acid lactic fermentation favors the cancer cells proliferation in the hypoxia microenvironment (Payen et al., 2020; San-Millán & Brooks, 2017; Xu et al., 2015)). This shift in cellular energetics is known as the Warburg effect or aerobic glycolysis and it is now known that it does not occur in all cancer cells, being dependent on cell type and type of cancer (Ashton et al. 2018; Xu et al. 2015; Wallace et al 2012).

Despite their role in the cellular energy metabolism, making this organelle known as the “powerhouse of the cell”, mitochondria are involved in many other cellular processes, including cell death, oxidative stress regulation and signaling (Hou et al. 2018). Moreover, cancer cells alter several signaling pathways to promote their malignant transformation and to induce cell proliferation and survival. The oncogenic signaling pathways have a direct influence on mitochondrial functioning, which is altered to favor cancer cells (Genovese et al. 2020; Vyas et al. 2016).

### **1.5.1. Mitochondrial dynamics**

Mitochondria is a very well-regulated organelle, which function can be modulated according to the cell host demand through biogenesis or turnover processes. This regulation depends on many factors, including cellular metabolic state, oxidative stress, temperature, and microenvironment (Jornayvaz et al. 2010). Mitochondrial biogenesis can be defined as the growth and division of mitochondria which could vary in number, size, and mass, when there is an increase in the need for their functions to maintain cell homeostasis (Bhatti et al. 2017). Mitophagy is a form of organelle-specific

autophagy selective for mitochondria turnover, ensuring a healthy mitochondrial population (Bernardini et al. 2017). Importantly, dysregulated mitochondrial function and dynamics are strictly associated with tumorigenesis and oncogenic signaling pathways (Popov et al. 2020; Maycotte et al. 2017).

Mitochondrial biogenesis is regulated by both nuclear and mitochondrial genomes, which encode mitochondrial proteins. The master regulator of the process is the peroxisome proliferator-activated receptor- $\gamma$  (PPAR- $\gamma$ ) coactivator  $\alpha$  (PGC-1 $\alpha$ ), a nuclear transcriptional coactivator that interacts with the nuclear receptor PPAR- $\gamma$ , regulating multiple transcription factors (Bhatti et al. 2017; Popov LD et al. 2020). LeBleu et al. performed a set of experiments where they found evidence of cancer cells dependent on PGC-1 $\alpha$ -mediated mitochondrial biogenesis (Lebleu et al. 2014). PGC-1 $\alpha$  has been shown to play a key role in metastatic potential, ensuring cancer cell growth in an anchorage-independent manner during their transit to target organs of metastasis (Popov et al. 2020; Lebleu et al. 2014). Moreover, LeBleu et al. observed that the suppression of PGC-1 resulted in impaired mitochondrial biogenesis and noticed a decrease in the frequency of metastases (Lebleu et al. 2014). In addition, according to Tan et al., PGC-1 $\alpha$ -mediated tumor suppression is due to the induction of intrinsic apoptotic pathway in colorectal and ovarian epithelial carcinoma cells and through induction of mitophagy in breast cancer (Tan et al. 2016).

The major mitophagy induction pathways are the PTEN-induced putative kinase 1 (PINK1)/Parkin pathway, and the adenovirus E1B 19 kDa-interacting protein 3 (BNIP3L)/NIP3-like protein X (NIX) pathway. These pathways are activated upon mitochondrial membrane depolarization resulting from the lack of reducing equivalents, hypoxia, and impaired electron transport (Bernardini et al. 2017; Vara-Perez et al. 2019). In normal conditions, PINK1 is translocated to the IMM in a voltage-dependent manner, where this kinase is cleaved by the mitochondrial protease PARL. Upon depolarization, PINK1 is translocated and accumulates in the outer mitochondrial membrane (OMM), where it phosphorylates Parkin. Consequently, several mitochondrial proteins are recruited and the mitophagy machinery is activated. Under hypoxia conditions, the hypoxia-inducible factor 1 (HIF-1) induces the expression of BNIP3L and NIX, which

contain an LC3-interacting domain that promotes activation of the mitophagy machinery (Ferro et al. 2020).

The relationship between mitophagy and cancer is not very clear. Mitophagy can be both pro- and anti-tumorigenic and its role and influence depend on cell type and cancer stage (Vara-Perez et al. 2019). In the early stages, mitophagy acts as a tumor suppressor, because the misregulation of mitophagy results in the release of mitochondrial signals and there is an increase in oxidative stress that induces a favorable microenvironment for tumor growth. In advanced-stage cancer, mitophagy is pro-tumorigenic, as it promotes tumor adaptation to the microenvironment, ensuring cancer survival (Vara-Perez et al. 2019; Ferro et al. 2020).

The metabolic state of a cell can be associated with the morphology and size of the mitochondrial network. Depending on the cell's physiological demands, mitochondria can alter their shape and size through fusion and fission processes (Maycotte et al., 2017). In mammalian cells, optic atrophy-1 (OPA1), mitofusin 1 (MFN1), and mitofusin 2 (MFN2) are three key proteins in fusion processes, and, on the other hand, the fission process is mediated by dynamin-related protein-1 (DRP1) and fission protein 1 (FIS1) (Maycotte P et al. 2017; Barbosa et al. 2012; Srinivasan et al. 2017; Dai et al. 2019). Mitochondria exist as either fused, tubular networks or as fragmented granules and the increase in mitochondria fusion gives a more elongated shape to mitochondria forming an extensive tubular network that is associated with an increase in OXPHOS capacity (Srinivasan et al. 2017). Multiple studies have revealed that dysregulation in mitochondrial fusion and fission processes is associated with several diseases including cancer (Srinivasan et al. 2017; Dai et al. 2019). The malignant imbalance is related to decreased mitochondrial fusion and increased fission resulting in a fragmented mitochondrial network. In many cancers, there is an enhanced DRP1 activity and downregulation of MFN2. Moreover, studies associate the high levels of DRP1 with the migratory phenotype, suggesting, once again, that mitochondria and their dynamics play a crucial role in metastasis (Dai et al. 2019).

### 1.5.2. Cell death

Apoptosis, a form of programmed cell death, is an essential mechanism to control cell proliferation and maintain tissue homeostasis, as it eliminates damaged and harmful cells, as well as superfluous cells (Goldar et al. 2015). This well-regulated mechanism has two major pathways: the extrinsic pathway (death receptor-mediated pathway) and the intrinsic pathway (mitochondrial-mediated pathway (Goldar et al. 2015; Ke et al. 2016). The first starts with the binding of an external signal such as tumor necrosis factor (TNF), Fas ligand (Fas-L), and TNF-related apoptosis-inducing ligand (TRAIL) to the extracellular domain of so-called death receptors. This ligand-receptor interaction activates a signaling cascade inside the cell, activating pro-caspase-8. During the process, the death-inducing signaling complex (DISC) is formed, which leads to auto-catalytic activation of pro-caspase-8. Subsequently, caspase-8 activates effector caspases that induce cell death by damaging the nucleus and other intracellular structures (Goldar et al. 2015; Ke et al. 2016). The second pathway is mediated by several internal stimuli such as DNA damage, oxidative stress, and increased cytosolic  $Ca^{2+}$  levels, which are recognized by intracellular proteins, leading to outer mitochondrial membrane permeabilization. Consequently, several apoptogenic factors are released, including cytochrome *c*, apoptosis-inducing factor (AIF), second mitochondria-derived activator of caspase (Smac)/ direct inhibitor of apoptosis protein (IAP) binding protein with low PI (DIABLO), and endonuclease G. Cytochrome *c* interacts with and activates the apoptosis protease activating factor (Apaf-1), forming a multi-protein complex known as apoptosome, which recruits and activates caspase-9, which is the effector caspase responsible for inducing cell death. The other apoptogenic factor also has a crucial role as Smac/DIABLO interacts with IAPs, facilitating caspase activation. AIF and endonuclease G is involved in other processes which result in cell death in a caspase-independent pathway. OMM permeabilization is mainly mediated by the B-cell lymphoma 2 protein (BCL-2) family, which can be divided into three different groups in mammalian cells. The BCL-2 family includes proteins with a pro-apoptotic role (e.g., Bax, Bak, and Bok), anti-apoptotic action (e.g., Bcl-2, Bcl-XL, Bcl-w, Mcl-L, and A1), and include proteins Bcl-2 homology (BH) domain-only such as Bim, Bad, Bid, Puma, and Noxa

which interact both with anti-apoptotic proteins inhibiting their action and with pro-apoptotic proteins stimulating their activity (Goldar et al. 2015; Ke et al. 2016; Maximchik et al. 2016).

Interestingly, cancer cells can alter the apoptotic pathways by transcriptional, translational, and post-translational mechanisms, leading to an advantage gain against apoptosis and thus ensuring their survival. This capacity to avoid death is one of the most important features contributing to cancer resistance against current therapies (Maximchik et al. 2016).

### **1.5.3. Mitochondrial DNA and ionizing radiation effects**

Mitochondria have their own genome, and the mtDNA of mammalian cells, in particular, is formed by a closed circle of double-stranded DNA, which contains 16,659 bases that encode 37 genes for rRNA, tRNA, and 13 proteins, in humans (Azzam et al. 2012; Yan et al. 2019). These 13 polypeptides are core elements of the OXPHOS complexes, being essential for OXOPHOS activity, as well as for all mitochondrial dynamics (Yan et al. 2019; Sharma et al. 2019). mtDNA is located in the mitochondrial matrix, being close to ETC, which is the main ROS-generator endogenous system (Fuhrmann et al. 2017). Importantly, since mtDNA lacks histones to regulate its structure, and effective repair systems, it is particularly susceptible to damage induced by IR and imbalances in the cellular redox status (Nissanka et al. 2018). Consequently, mtDNA is prone to numerous mutations, responsible for mitochondrial dysfunction, contributing to the aging process and is highly associated with several human diseases such as Alzheimer's disease, Parkinson's disease, and cancer (Yan et al. 2019; Nissanka et al. 2018; Sharma et al. 2019).

Altogether, mitochondria is a central cell organelle playing an essential role in energy metabolism, control of stress response, cell signaling, and is a hub for biosynthetic processes. Importantly, it is an extremely radiosensitive organelle, making mitochondria a potential target for novel radiotherapy-based therapies, reenforcing the shift in the paradigm of radiation biology to take in consideration the potential of other radiosensitive organelles, besides the nucleus.

## 1.6. Objectives

AugerTher project aim to synthesize dual-targeted (PCa and organelle) stable metal complexes containing DOTA chelators carrying a PSMA-binding motif (PSMA<sub>617</sub>) to ensure a specific internalization in PCa cells. These complexes also contain a DNA intercalator or a mitochondriotropic group (tri-phenyl-phosphonium (TPP)), to further direct the pharmacophore to the nucleus or mitochondria, respectively, enhancing their anticancer effects. This innovative strategy can lead to a shift in the radiation biology paradigm, as TRT based on AE-emitting radionuclides targeting mitochondria is almost unexplored, despite their well-recognized radiosensitivity and association to tumorigenesis (McCann et al. 2021).

Particularly, in the present study we performed preliminary work for AugerTher project. Specifically, we aim to assess the biological effect of PSMA<sub>617</sub> and the cold surrogate <sup>nat</sup>In-DOTAGA-AO, the first synthesized compounds in the AugerTher project, in four *in vitro* cell models. Specifically, we evaluated the impact of both compounds on cellular metabolism by assessing 1) mitochondrial respiration, 2) mitochondrial membrane potential, and 3) mitochondrial superoxide levels, and 4) glycolytic function. Mitochondria-related factors were evaluated in normal prostate cells (PNT2) compared with malignant PCa cells (LNCaP). PC3-PIP cells, which express the human PSMA protein, were also used to assess the role/influence of PSMA in PCa cancer cells metabolism and compared to PC3-FLU cells (respective control).



## 2. Material and Methods

### 2.1. Novel compounds

PSMA<sub>617</sub> (Figure 2A) and the cold surrogate <sup>nat</sup>In-DOTAGA-AO (Figure 2B) were synthesized by a multidisciplinary team led by Doctor António Paulo, from the Center for Nuclear Sciences and Technologies (C<sup>2</sup>TN), from Instituto Superior Técnico of the University of Lisboa.

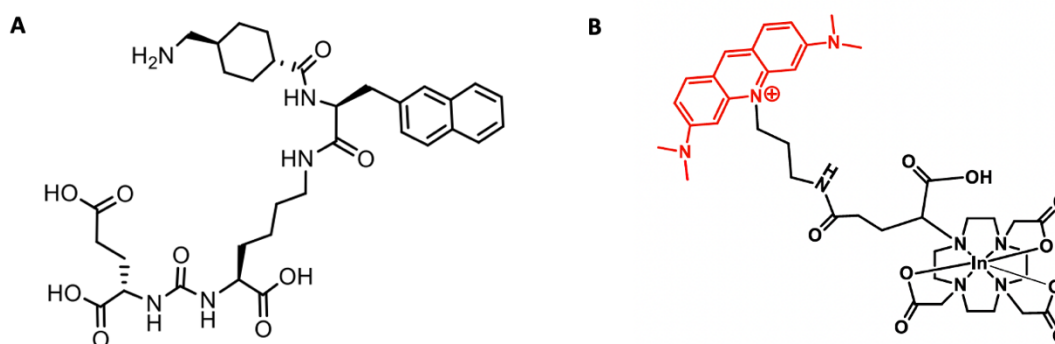


**Figure 2.** Chemical structure of the compounds under investigation in the present study. (A) PSMA<sub>617</sub> with 655.74 g/mol molecular weight and (B) natIn-DOTAGA-AO with 893.71 g/mol molecular weight.

### 2.2. Cell culture

In the present study, four different cell lines were used as *in vitro* models, PNT2, LNCaP, PC3-FLU, and PC3-PIP. The cell line PNT2, derived from normal prostate epithelium immortalized with SV40, was the control of the malignant LNCaP cells derived from a lymph node metastatic prostate carcinoma. PC3 cells are a prostate cancer cell line derived from bone metastasis that do not express PSMA. In particular, PC3-PIP cells were generated by transduction using VSV-G pseudotyped lentiviral vector expressing human PSMA; and isogenic PSMA negative PC3-FLU cells. All cell lines were cultured in RPMI-1640 medium containing 2 g/L sodium bicarbonate and 10% fetal bovine serum (FBS). For the culture of PC3-PIP and PC3-FLU cells, and the medium was further supplemented with 20 µg/mL puromycin dihydrochloride (A11138-03, Gibco™), for selection and maintenance of cells with VSV-G pseudotyped lentiviral vector incorporated. Cells were maintained at 37 °C in a humidified atmosphere of 5% CO<sub>2</sub>

/95% air and were passage every 3–4 days, at 80–90% confluence. For subculturing, the medium was removed, and the monolayers were rinsed with phosphate-buffered saline 1x (PBS). Cells were individualized and detached from the substrate using a solution of 0.05% trypsin/EDTA(1x) (25300-062, Gibco™) at 37 °C for ca. 5 minutes. Fresh medium was added to inactivate trypsin and the cell suspension was centrifuged at 150 x g for 5 minutes. Next, cells were split into a new 25 cm<sup>2</sup> flask (10062-872, VWR®) in a 1:10 to 1:20 ratio. LNCaP cells were cultured in flasks coated with Poly- L -Lysine (PLL) to improve attachment to the flasks. In addition, the seeding density for this cell line was twice the seeding density used with the other cell lines. Cells were tested for mycoplasma by the MYCOPLASMA CHECK protocol (GATC-Biotech).

### **2.3. Preparation of total cell extracts**

To assess the impact of <sup>nat</sup>In-DOTAGA-AO on mitochondrial protein expression, cells were seeded on a pre-coated 6 multi-well plate (10062-892, VWR®) with PLL. PNT2, PC3-PIP and PC3-FLU were seeded with a cellular density of 1.0 x 10<sup>4</sup> cells/cm<sup>2</sup>, and LNCaP were seeded with a cellular density of 2.0x10<sup>4</sup> cells/cm<sup>2</sup>. After 24 hours in culture, cells were treated or not with 50 μM <sup>nat</sup>In-DOTAGA-AO and incubated at 37 °C, in a 5% CO<sub>2</sub> atmosphere for 72 hours. Then, cells were harvested with trypsinization and isolated by centrifugation at 150 rpm for 5 minutes. Pellets were stored at -80 °C until assayed.

For protein extraction, cell pellets were resuspended in RIPA buffer supplemented with 0.5 mM PMSF, 20 mM NaF, 10 mM NAM, 5 mM sodium butyrate, 0.5% DOC, and PIC (diluted 1:400 (v/v)). Next, cellular suspensions were sonicated, and their protein content was assessed using the Bradford method, using the Bio-Rad Protein Assay kit (5000001, Bio-Rad) and Bovine Serum Albumin (BSA) as standard. First, the working reagent was diluted in ultrapure water (1:3) as suggested by the kit's protocol. The reaction was initiated by adding 120 μL of working reagent to 1 μL of sample and 79 μL of water in a micro test flat-base 96-well plate (82.1581, SARSTEDT AG). After 15 minutes of incubation at room temperature and in the dark, absorbance was read at 595 nm, using a BioTEK® Cytation3™ (BioTek).

## 2.4. Western blotting

After total protein quantification, samples were denatured with sample buffer 6x at 95 °C for 5 minutes. Then, 18 to 25 µg of protein was loaded into the wells of an 8% dodecyl sulfate (SDS-polyacrylamide gel (SDS-PAGE) and separated by electrophoresis at a constant voltage of 80 V, for 90 minutes, at room temperature using a PowerPac™ Basic Power Supply (Bio-Rad). In each gel, a molecular weight standard (Precision Plus Protein Dual Color Standards, Bio-Rad) was loaded to allow for molecular weight estimation. Next, proteins were transferred to a pre-activated (5 seconds in 100% methanol followed by 15 minutes in water and 15 minutes in TBS-T) polyvinylidene difluoride membrane (PVDF, 0.45 µm, Millipore) using the Trans-Blot® Turbo™ Transfer System (Bio-Rad) at a constant voltage of 0,75V, for 2 hours. Once protein transfer was complete, the membrane was incubated with a blocking solution (5% non-fat dry milk), at room temperature, for 1 hour. Afterwards, membranes were incubated overnight and at 4 °C with a primary antibody (Table 1), under continuous stirring. On the following day, membranes were washed three times with TBS-T, 5 minutes each time, and were incubated with the respective Horseradish Peroxidase (HRP)-conjugated secondary antibody (Table 1) at room temperature, for 1 hour. Both primary and secondary antibodies were prepared in 1% non-fat dry milk in TBS-T. Finally, membranes were washed again three times with TBS-T and incubated with Clarity™ Western ECL Substrate detection kit (Bio-Rad). Chemi-fluorescence was detected using the VWR® Gel Documentation System Imager Chemi 5QE. Densitometry analysis was performed using the ImageLab software (Bio-Rad).

**Table 1.** Antibodies used in western blotting analysis.

Protein	MW (kDa)	Host Species	Dilution	Gel (%)	Catalog Number	Manufacturer
$\beta$ -Actin	43	Mouse (monoclonal)	1:10,000	8	MAB1501	Cell Signaling
PSMA	100	Mouse (monoclonal)	1:1000	8	sc-514444	Santa Cruz
Anti-Mouse	–	Horse	1:10000	8	7076	Cell Signaling

## 2.5. Resazurin assay

The resazurin assay is commonly used as an indirect measure of cytotoxicity/cell proliferation by measuring the dehydrogenase activity of cell cultures. In this technique, the blue non-fluorescent resazurin is reduced to resofurin through the dehydrogenases activity of viable cells. The resulting resofurin is a pink-fluorescent metabolite detected by spectrofluorometers (Prabst et al. 2017; Silva et al. 2016).

Cells were seeded on a pre-coated 96 multi-well plate (10062-900, VWR®) at a density of  $1.0 \times 10^4$  cells/cm<sup>2</sup> for PNT2, PC3-PIP and PC3-FLU and  $2.0 \times 10^4$  cells/cm<sup>2</sup> for LNCaP. After 24 hours of incubation, PSMA<sub>617</sub> or <sup>nat</sup>In-DOTAGA-AO were directly added to the culture medium, to final concentrations of 0.1; 1; 10; and 50  $\mu$ M. Resazurin reduction was evaluated at 0 h (time zero), 48, and 72 hours after PSMA<sub>617</sub> addition. For <sup>nat</sup>In-DOTAGA-AO, the resazurin assay was performed after 0 hours, 24 hours, 48 hours, and 72 hours after the addition of the compound. For each timepoint, the medium of the respective wells was removed and substituted by 10  $\mu$ g/mL solution of resazurin prepared in microscopy medium (0.1 M NaCl; 20 mM NaHCO<sub>3</sub>; 6 mM KH<sub>2</sub>PO<sub>4</sub>; 5 mM KCl; 0.9 mM CaCl<sub>2</sub>; 5 mM Na<sub>2</sub>HPO<sub>4</sub>; 0.4 mM MgSO<sub>4</sub>; 10 mM glucose; 10% FBS; pH= 7.2)). Cells were then incubated at 37 °C and in a 5% CO<sub>2</sub> atmosphere for 120 minutes. The amount of produced resofurin was measured by fluorescence at an excitation wavelength of 540 nm and emission wavelength of 590 nm, using the BioTEK ®

Cytation3™ system (BioTek). Afterwards, wells were washed with PBS 1x and allowed to dry until the end of the whole experiment, at which time cells were fixated overnight with 1% (v/v) acetic acid, at -20 °C. Subsequently, the Sulforhodamine B (SRB) assay (Silva et al. 2016) was performed as described below (section 2.6).

## **2.6. Sulforhodamine B assay**

SRB is a colorimetric assay that provides an estimate of cell mass based on the measurement of cellular protein content. This assay employs the sodium salt of SRB, which is a red fluorescent dye that binds basic amino acid residues under mild acidic conditions (Silva et al. 2016; van Tonder et al. 2015). In this work, SRB assay was used both to complement the cytotoxicity/cell proliferation evaluation, but also for normalization purposes.

Firstly, the fixation solution (1% (v/v) acetic acid or methanol or 60% (w/v) trichloroacetic acid (TCA) was discarded and the plate was left to dry at 37 °C. Further, 100 µL of 0.05 % SRB in acetic acid were added to each well and the plate was incubated at 37 °C for 1 hour. Then, the SRB solution was removed, and the plate was washed with 1% (v/v) acetic acid. When dried, 250 µL of 10 mM Tris pH 10.5 were added to the plates that subsequently were shaken for 15 minutes. Finally, absorbance was read at 540 nm, using the BioTEK ® Cytation3™ (BioTek) system.

## **2.7. Real-time cell metabolic analysis**

To assess the impact of PSMA<sub>617</sub> and <sup>nat</sup>In-DOTAGA-AO on metabolism, the Agilent Seahorse XF Cell Mito Stress Test Kit and the Agilent Seahorse XF Glycolysis Stress Test Kit were performed. The Seahorse XFe96 Analyzer (Seahorse Bioscience, Billerica, MA, USA) measures in real-time the oxygen consumption rate (OCR) and extracellular acidification rate (ECAR), which can be taken as a measure of the bioenergetic status of the cultures under analysis. ORC and ECAR are key indicators of the energy metabolism of cells providing information about mitochondrial respiration, lactic acid fermentation, and ATP production (Divakaruni et al. 2014).

In the Agilent Seahorse XF Cell Mito Stress Test, different modulators of respiration are sequentially injected during the assay to monitor mitochondrial function. The injected compounds include oligomycin, carbonyl cyanide-4 (trifluoromethoxy) phenylhydrazone (FCCP), rotenone, and antimycin A. The first compound injected is oligomycin, an ATP synthase inhibitor ( $F_0$  subunit of complex V), which leads to a decrease in the electron flow through the ETC, ultimately decreasing the mitochondrial respiration. The second compound injected is FCCP, which is an uncoupler that promotes the dissipation of the electrochemical proton gradient, thus disrupting the mitochondrial membrane potential. As a result of both injections, the electron flow through ETC is inhibited and the oxygen consumption by complex IV is maximal. Finally, a mix of rotenone and antimycin is injected, which are complex I and complex III inhibitors, respectively. At this point, OXPHOS is completely inactivated, and the measured OCR results from non-mitochondrial processes (Figure 3). This assay allows for the calculation of different mitochondrial function parameters, including basal, maximal, ATP production-linked, and proton leak-linked respiration, as well as spare respiration capacity, coupling efficiency, and non-mitochondrial respiration (Table 2).

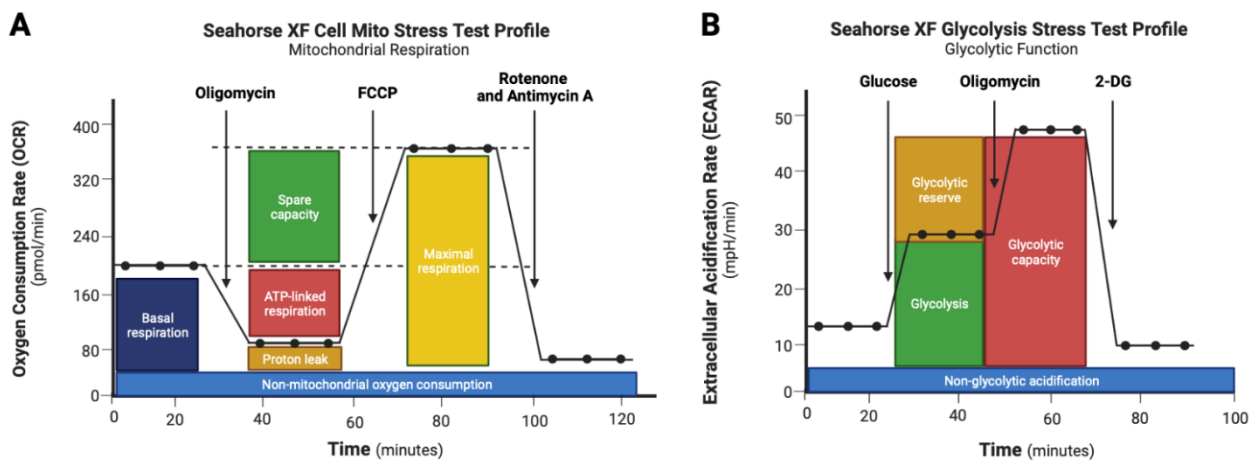


**Figure 3.** Seahorse XF profile and respective parameters of the performed. (A) Seahorse XF Cell Mito Stress Test Profile. (B) Seahorse XF Glycolysis Stress Test Profile. Figure 3 was created with BioRender. FCCP, carbonyl cyanide-4 (trifluoromethoxy) phenylhydrazone; 2-DG, 2-deoxy-glucose.

**Table 2.** Key parameters of mitochondrial respiration and formulas used in their evaluation when performing the Agilent Seahorse XF Cell Mito Stress Test

<b>Parameter</b>	<b>Indicator</b>	<b>Formula</b>
Basal Respiration	Cellular energy demand under baseline conditions	(Late rate measurement before 1 <sup>st</sup> injection) – (Non-mitochondrial respiration rate)
ATP Production	Mitochondrial ATP produced mitochondria to meet the energy needs of the cell	(Late rate measurement before oligomycin injection) – (Minimum rate measurement after oligomycin injection)
H <sup>+</sup> (Proton) Leak	Mitochondrial damage, or mechanism to regulate the mitochondrial ATP production	(Minimum rate measurement after oligomycin injection) – (Non-mitochondrial respiration)
Maximal Respiration	The maximum rate of respiration that the cell can achieve	(Maximum rate measurement after FCCP injection) – (Non-mitochondrial respiration)
Spare respiration capacity	Cell fitness or flexibility	(Maximal respiration) – (Basal respiration)
Non-mitochondrial respiration	Oxygen consumption by other cellular enzymes	Minimum rate measurement after rotenone and antimycin A injection

The Agilent Seahorse XF Glycolysis Stress Test Kit monitors the glycolytic function of cells by measuring the extracellular medium acidification, reported as ECAR. During lactic acid, pyruvate generated from glucose by glycolysis is converted to lactate, with all steps occurring in the cytosol. This results in an extrusion of protons to the extracellular medium and its consequent acidification (Adeva-Andany et al. 2014). In this assay, cells are incubated in a glycolysis stress test medium without glucose or pyruvate. Further, glucose, oligomycin, and 2-deoxy-glucose (2-DG) are injected. The injected glucose is metabolized in glycolysis, with some of the pyruvate formed converted to

lactate production, acidifying the extracellular medium. Next, oligomycin is added, shifting the production of energy to the glycolytic pathway, resulting in ECAR augment, revealing the maximal cellular glycolytic capacity. Finally, 2-DG, which is a glucose analogue, inhibits the glycolytic pathway by competitive binding to glucose hexokinase. As result, ECAR decreases confirming, that the acidification of the medium was due to glycolysis function. This assay allows the assessment of glycolysis, glycolytic capacity, glycolytic reserve, and non-glycolytic acidification (Table 3).

**Table 3.** Key parameters of glycolytic function and respective formulas used in their evaluation when performing the Agilent Seahorse XF Cell Glycolytic Stress Test

Parameter	Indicator	Formula
Glycolysis	Glycolytic function after addition of saturating amounts of glucose	(Maximum rate measurement before oligomycin injection) – (Last rate measurement before glucose injection)
Glycolytic capacity	Maximal glycolytic capacity after shutting down OXPHOS	(Maximum rate measurement after oligomycin injection) – (Last rate measurement before glucose injection)
Glycolytic reserve	Glycolytic response to an energetic demand	(Glycolytic capacity) – (Glycolysis)
Non-glycolytic acidification	Other sources of extracellular acidification	Last rate measurement prior to glucose injection

In these assays, two different concentrations were tested (10  $\mu$ M and 50  $\mu$ M, for both PSMA<sub>617</sub> and <sup>nat</sup>In-DOTAGA-AO), as well as two different times of exposure (6 and 72 hours). Firstly, cells were seeded on an Agilent Seahorse XF96 Cell Culture Microplate (101085-004, Agilent) pre-coated with PLL at a density of 1.5 x 10<sup>4</sup> cells/cm<sup>2</sup> for PNT2, PC3-PIP and PC3-FLU cells and 3.0 x 10<sup>4</sup> cells/cm<sup>2</sup> for LNCaP cells, in 80  $\mu$ L of culture medium. On the following day, 70  $\mu$ L solutions of PSMA<sub>617</sub> and <sup>nat</sup>In-DOTAGA-AO prepared in culture medium were added directly to the cells in culture, to final concentrations of 10  $\mu$ M and 50  $\mu$ M. Non-treated cultures received 70  $\mu$ L of culture medium. Further, cells were incubated at 37 °C and in a 5% CO<sub>2</sub> atmosphere for 72 hours

exposed to the compounds. Six hours previously to the assay, the culture medium was discarded, and 150  $\mu\text{L}$  of 10  $\mu\text{M}$  and 50  $\mu\text{M}$  of both PSMA<sub>617</sub> and <sup>nat</sup>In-DOTAGA-AO were added. On the day before the assay, the XFe96 sensor cartridge was hydrated overnight and at 37 °C in with Seahorse XF Calibrant in a non-CO<sub>2</sub> incubator.

On the day of the experiment, the assay medium was prepared by supplementing the Seahorse RPMI medium with 10 mM glucose and 2 mM glutamine, for the Mito stress test assay, or with 2 mM glutamine, for the glycolysis stress test. Next, the medium pH was adjusted to 7.4 and warmed to 37 °C in a water bath, before usage. Microplates containing cells were washed 3 times with the warmed assay medium and then 175  $\mu\text{L}$  of assay medium were added to each well of the cell culture microplate, which was then incubated at 37 °C in a non-CO<sub>2</sub> incubator for 45 minutes. Further, the sensor cartridge ports were loaded with 25  $\mu\text{L}$  of the different modulators, previously prepared in the assay medium. The concentrations of these solutions were such as to obtain the following final concentrations: for Mito stress test port A – oligomycin (2  $\mu\text{M}$ ); port B – FCCP (0.2  $\mu\text{M}$  for PNT2, and 0.5  $\mu\text{M}$  for PC3-PIP, PC3-FLU, and LNCaP); port C – rotenone + antimycin A (2  $\mu\text{M}$ ). For glycolysis stress test port A – glucose (10 mM); port B – oligomycin (2 $\mu\text{M}$ ); port C – 2-DG (10 mM). During the assay, the modulators were injected automatically, port by port.

At the end of the experiment, 50  $\mu\text{L}$  of TCA 60% were added to each well, to a final concentration of 10% TCA to fixate cells, at 4 °C overnight. Further, an SRB assay was performed, as previously described, to normalize the data. SRB absorbance values were inserted on the Agilent Seahorse Wave Desktop Software (Agilent) to obtain OCR and ECAR values normalized to cell mass.

## **2.8. Evaluation of <sup>nat</sup>In-DOTAGA-AO internalization and localization**

To assess <sup>nat</sup>In-DOTAGA-AO internalization and co-localization, confocal images were obtained using a Plan-Apochromat/1.4NA 63 $\times$  lens on an Axio Observer.Z1 confocal microscope (Zeiss Microscopy, Germany) with Zeiss LSM 710 software. FIJI (ImageJ, National Institute of Health, USA) was used for image analysis. <sup>nat</sup>In-DOTAGA-AO internalization was assessed by analyzing compound fluorescence and co-

localization within nucleus and mitochondria analysis were achieved using Macros in Fiji designed by Dr. Jorge Valero. Briefly, image background was normalized using the function Subtract Background, included in Fiji. Mitochondria-targeting tetramethylrhodamine methyl ester (TMRM) images were extracted to grayscale. FindFoci function was then used to allow the identification of peak intensity regions (Herbert et al. 2014) to show mitochondria-specific fluorescence. A threshold was applied to optimally resolve individual mitochondria. Mitochondrial outlines were traced through the Analyze Particles function. To obtain information about protein co-localization with mitochondria, a selection of mitochondrial ROIs was done, and the respective protein Integrated Density inside the ROIs was considered.

## **2.9. Assessment of mitochondrial membrane potential**

The red fluorescent TMRM dye was used to measure the mitochondrial membrane potential (MMP). TMRM is a lipophilic cationic dye that accumulates within active mitochondria with intact MMP (Creed et al. 2019; Chazotte 2011).

Cells seeded at a density of  $1.0 \times 10^4$  cells/cm<sup>2</sup> (for PNT2, PC3-PIP and PC3-FLU cells) and  $2.0 \times 10^4$  cells/cm<sup>2</sup> (for LNCaP cells) on a  $\mu$ -Slide 8 Well ibiTreat (80826, ibidi®) pre-coated with PLL were treated for 72 h 24 hours post-seeding with 10 or 50  $\mu$ M <sup>nat</sup>In-DOTAGA-AO. Control cultures received the same volume of the addition vehicle. On the day of the experiment, cells were washed with microscopy medium and incubated for 30 minutes with a solution of 100 nM TMRM and 1  $\mu$ g/mL Hoechst 33342, prepared in microscopy medium. Confocal images were acquired as described in section 2.8.

## **2.10. Measurement of mitochondrial superoxide levels**

MitoSOX<sup>TM</sup> (M36002, Invitrogen<sup>TM</sup>) was used to assess mitochondrial O<sub>2</sub><sup>-</sup> production. MitoSOX<sup>TM</sup> is a fluorogenic dye that specifically targets mitochondria in live cells. It is quickly oxidized by O<sub>2</sub><sup>-</sup>, but not by other ROS or RNS. The resulting product emits highly red fluorescence that can be detected by spectrofluorometers or for live-cell imaging (Kalyanaraman B 2020; Kauffman M et al. 2016).

Cells were seeded on a 96-well black/clear bottom polystyrene microplate (3603, Corning®) pre-coated with PLL. PNT2, PC3-PIP and PC3-FLU were seeded with a cellular density of  $1.0 \times 10^4$  cells/cm<sup>2</sup>, and LNCaP were seeded with a cellular density of  $2.0 \times 10^4$  cells/cm<sup>2</sup>. 24 hours after seeding, cells were treated with 10  $\mu$ M and 50  $\mu$ M <sup>nat</sup>In-DOTAGA-AO and incubated at 37 °C and in a 5% CO<sub>2</sub> atmosphere for 72 hours. Then, the culture medium was discarded and MitoSOX™ 5  $\mu$ M prepared in pre-heated microscopy medium were added to each well. The microplate containing cells was incubated at 37 °C in a non-CO<sub>2</sub> incubator for 45 minutes. Next, the microplate was washed once with microscopy medium and 100  $\mu$ L of the same medium was added to each well. The fluorescence of the produced metabolite was measured using a BioTEK® Cytation3™ system (BioTek), at an excitation wavelength of 510 nm and emission wavelength of 580 nm, for 20 minutes. Finally, cells were fixed with 1% (v/v) acetic acid in methanol, at -20 °C overnight. Subsequently, an SRB assay was performed to normalize the data to cell mass.

### **2.11. Statistical analysis**

Data were expressed as the mean  $\pm$  SEM of the number of experiments or elements (neuritis or mitochondria) indicated in the figure legends. The normal distribution of each population was analyzed, and all experimental groups were considered non-parametric. Thus, comparisons among multiple groups (relative to control or to treatment) were performed by non-parametric one-way analysis of variance (ANOVA) followed by the Kruskal–Wallis Multiple Comparison post-hoc test. Mann–Whitney U test was also performed for comparison between two populations, as described in figure legends. Significance was defined as  $p < 0.05$ .



### 3. Results

#### 3.1. Cell lines characterization: PSMA expression levels

PSMA is markedly overexpressed in prostatic cancer cells compared to other tissues, including normal prostatic tissue (Uijen et al 2021). Moreover, high levels of PSMA expression are correlated with higher PCa malignancy and aggressiveness (Uijen et al 2021; Chang 2004; Rahbar et al 2018). Since AugerTher project aims to synthesize novel dual-targeted TRT compounds with specific targeting to PSMA, we initially characterized the in vitro models used in this study by assessing PSMA levels (Figure 4).

Results evidenced that PNT2, a normal prostate epithelial cell line, does not express PSMA, as expected. In contrast, LNCaP cells, which derived from a lymph node metastatic prostate carcinoma, expressed PSMA as shown in Figure XB. Importantly, beside the 100 kDa band corresponding to PSMA, we were also able to detect a band at approximately 200 kDa corresponding to PSMA dimers as shown by Liu et al 2014 (Liu et al 2014). PC3 cells are a prostate cancer cell line derived from bone metastasis that do not express PSMA. In contrast, PC3-PIP, transduced with human PSMA overexpress the protein. In addition to the expression of 100 kDa PSMA, PC3-PIP cells also express 200 kDa PSMA and lower levels of PSMA glycoforms (Liu et al 2014, Yuan et al 2022). Comparing the cell lines that express the protein of interest, PC3-PIP have a higher expression of PSMA than LNCaP.

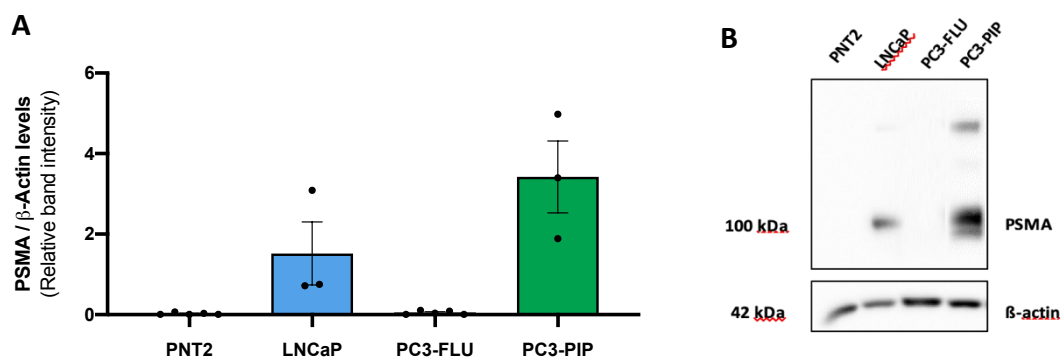


**Figure 4.** Characterization of the cell lines: expression of PSMA in PNT2, LNCaP, PC3-FLU and PC3-PIP. **(A)** Levels of PSMA protein normalized for  $\beta$ -actin protein levels used as loading control. **(B)** Representative Western Blotting analysis of PSMA and  $\beta$ -actin labelling. Data are the mean  $\pm$  SEM of 3-5 independent experiments.

## **3.2. Effect of PSMA<sub>617</sub> compound in cell viability and metabolism**

### **3.2.1. PSMA<sub>617</sub> did not induce cell mass or metabolic activity alterations**

PSMA<sub>617</sub> was the initial compound to be synthesized in the context of this project. This ligand is intended to be present in the structure of synthesized compounds in the future to be used as a tag to PCa cells which overexpress PSMA protein. Therefore, we assessed the cytotoxicity of PSMA<sub>617</sub>, itself, in the four cell lines used in this study, using the SRB and the resazurin assays to evaluate cell mass and metabolic activity, respectively (Figure X). Cells were treated with 0.1, 1, 10, or 50  $\mu\text{M}$  PSMA<sub>617</sub> or vehicle for 48 and 72 hours. Treatment with 250  $\mu\text{M}$  H<sub>2</sub>O<sub>2</sub> showing high cytotoxicity as described (Xiang et al 2016), was used as positive control to induce cell death. Data evidenced that none of the four concentrations of PSMA<sub>617</sub> tested affect significantly neither the cell mass, neither the metabolic activity. Importantly, treatment with H<sub>2</sub>O<sub>2</sub> decreases significantly both parameters as expected.

To evaluate if the changes in metabolic activity were related with changes in cell mass, we replotted results from graphics i) and ii) into a correlation graphic iii) for each cell line. Results show a positive correlation between both parameters in PNT2 ( $\rho = 0.97$ ;  $r^2 = 0.94$ ), LNCaP ( $\rho = 0.91$ ;  $r^2 = 0.83$ ), PC3-FLU ( $\rho = 0.97$ ;  $r^2 = 0.94$ ), and PC3-PIP ( $\rho = 0.96$ ;  $r^2 = 0.92$ ), indicating that the change observed in the metabolic activity are the result of an increase in cell mass and very likely due to cell proliferation.

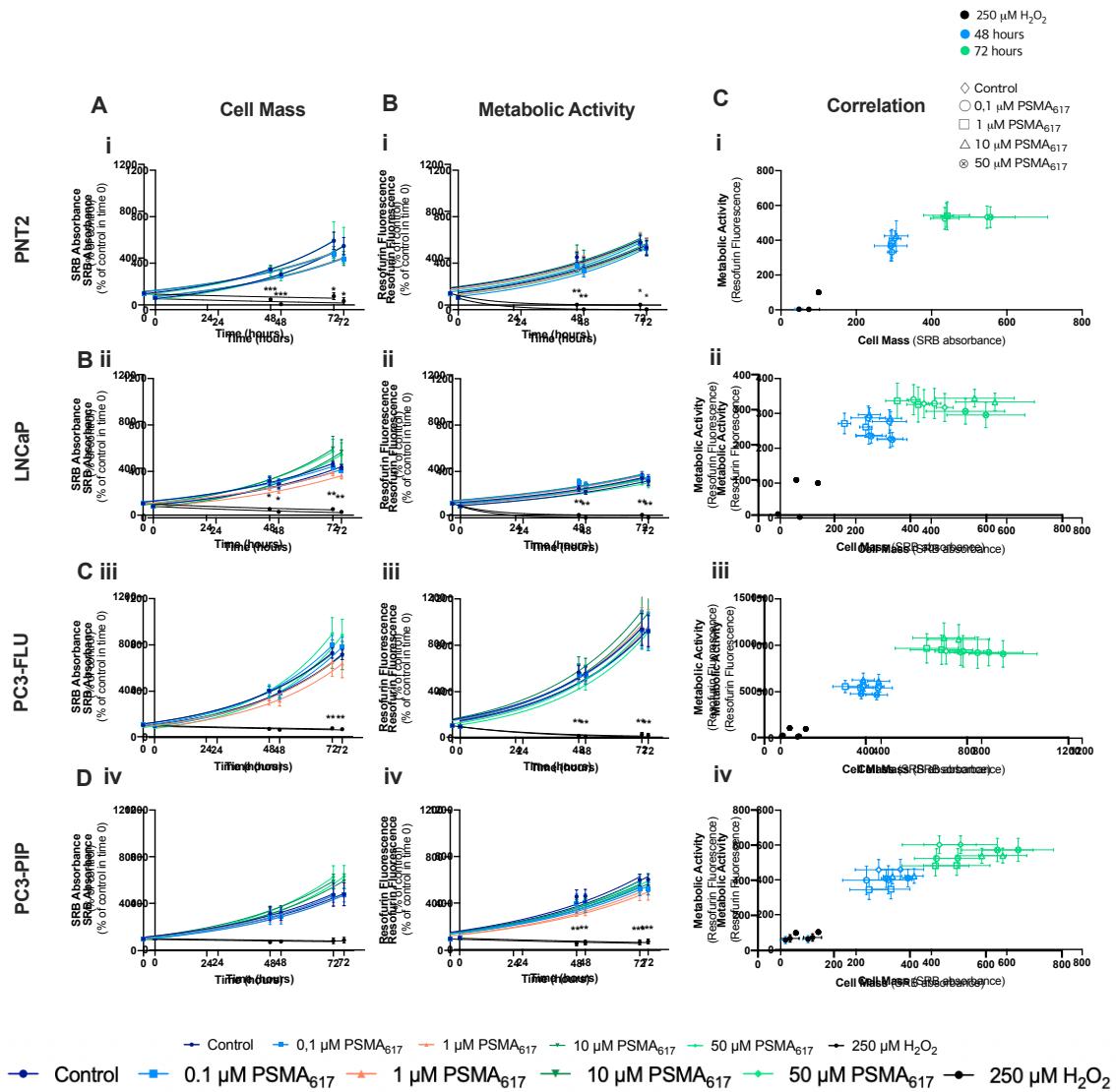


**Figure 5.** Cytotoxic effect of PSMA<sub>617</sub> on PNT2, LNCaP, PC3-FLU and PC3-PIP cells. **(A)** The sulforhodamine B (SRB) assay was used to measure cell mass of untreated cells (control) and cells treated with 0,1  $\mu\text{M}$ ; 1  $\mu\text{M}$ ; 10  $\mu\text{M}$  and 50  $\mu\text{M}$  PSMA<sub>617</sub> for 0 (time 0), 48, and 72 hours. Data are the mean  $\pm$  SEM of 4 independent experiments in triplicate and expressed as percentage of the time 0 value. The different conditions were compared to the control by a two-way ANOVA (\*  $p < 0.05$ ; \*\*  $p < 0.01$ ; \*\*\*  $p < 0.001$ ). **(B)** The metabolic activity of untreated cells (control) and cells treated with 0,1  $\mu\text{M}$ ; 1  $\mu\text{M}$ ; 10  $\mu\text{M}$  and 50  $\mu\text{M}$  PSMA<sub>617</sub> for 0, 48, and 72 hours was measured by resazurin assay. Data are the mean  $\pm$  SEM of 4–6 independent experiments in triplicate and expressed as percentage of the respective control. The different conditions were compared to the control by a two-way ANOVA (\*  $p < 0.05$ ; \*\*  $p < 0.01$ ; \*\*\*  $p < 0.001$ ). **(C)** The values of SRB and resazurin assay were re-plotted to assess the correlation between cell mass and metabolic activity. The Pearson correlation coefficients ( $\rho$ ) are: 0.97 for PNT2; for 0.91 LNCaP; 0.97 for PC3-FLU; 0.96 for PC3-PIP.

### 3.2.2. Long-term PSMA<sub>617</sub> exposure affect mitochondrial respiration of PCa cells

PSMA is a transmembrane protein that internalize upon interaction with a ligand (Emmett et al 2017). Thus, we hypothesize that the interaction of PSMA<sub>617</sub> with PSMA protein might lead to the internalization of both and that once in the cell, PSMA<sub>617</sub> could induce changes in mitochondrial function. Although no differences were noticed in the metabolic activity of the cells (Figure 5), we sought to understand the impact of PSMA<sub>617</sub> on mitochondrial respiration using the Agilent Seahorse XF Cell Mito Stress Test Kit. Moreover, considering the Warburg effect and the capacity of cancer cells to remodel their metabolism (Ashton et al 2018; Xu et al 2015), we evaluated the impact of short-term (6 hours, Figure 6) and long-term (72 hours; Figure 7) incubation with PSMA<sub>617</sub> in PNT2, normal prostate cells, and LNCaP, PCa cells. As PSMA<sub>617</sub> did not induce cytotoxicity (Figure 5), we used 10 and 50  $\mu$ M, the two highest concentrations of compound, for this experiment.

Data suggested that exposure to PSMA<sub>617</sub> for 6 hours did not induce significant alterations in the mitochondrial function of PNT2 and LNCaP cells. Thus, we do not see significant differences between control and treated cells regarding basal (Figure 6D), maximal (Figure 6E), ATP production-linked (Figure 6F), proton leak-linked (Figure 6G), spare respiratory capacity (Figure 6H), coupling efficiency (Figure 6I) and non-mitochondrial respiration (Figure 6J). However, LNCaP cells present higher OCR values over time (Figure 6A), when compared to PNT2 cells, which on the opposite, present higher ECAR values (Figure 6B). This observation is supported by the energy phenotype profile (Figure 6C) which evidence that LNCaP cells as more aerobic, using mitochondrial respiration predominantly, while PNT2 cells appear to be more glycolytic. Importantly, PNT2 cells exposed to both 10 and 50  $\mu$ M PSMA<sub>617</sub> showed a more energetic profile, both metabolic pathways, glycolysis and OXPHOS, are used to produce energy (Figure 6, A-C) evidencing that although PSMA<sub>617</sub> does not induce significant changes in mitochondrial respiration-related parameters, in PNT2 cells it induces a small shift in the energetic profile.

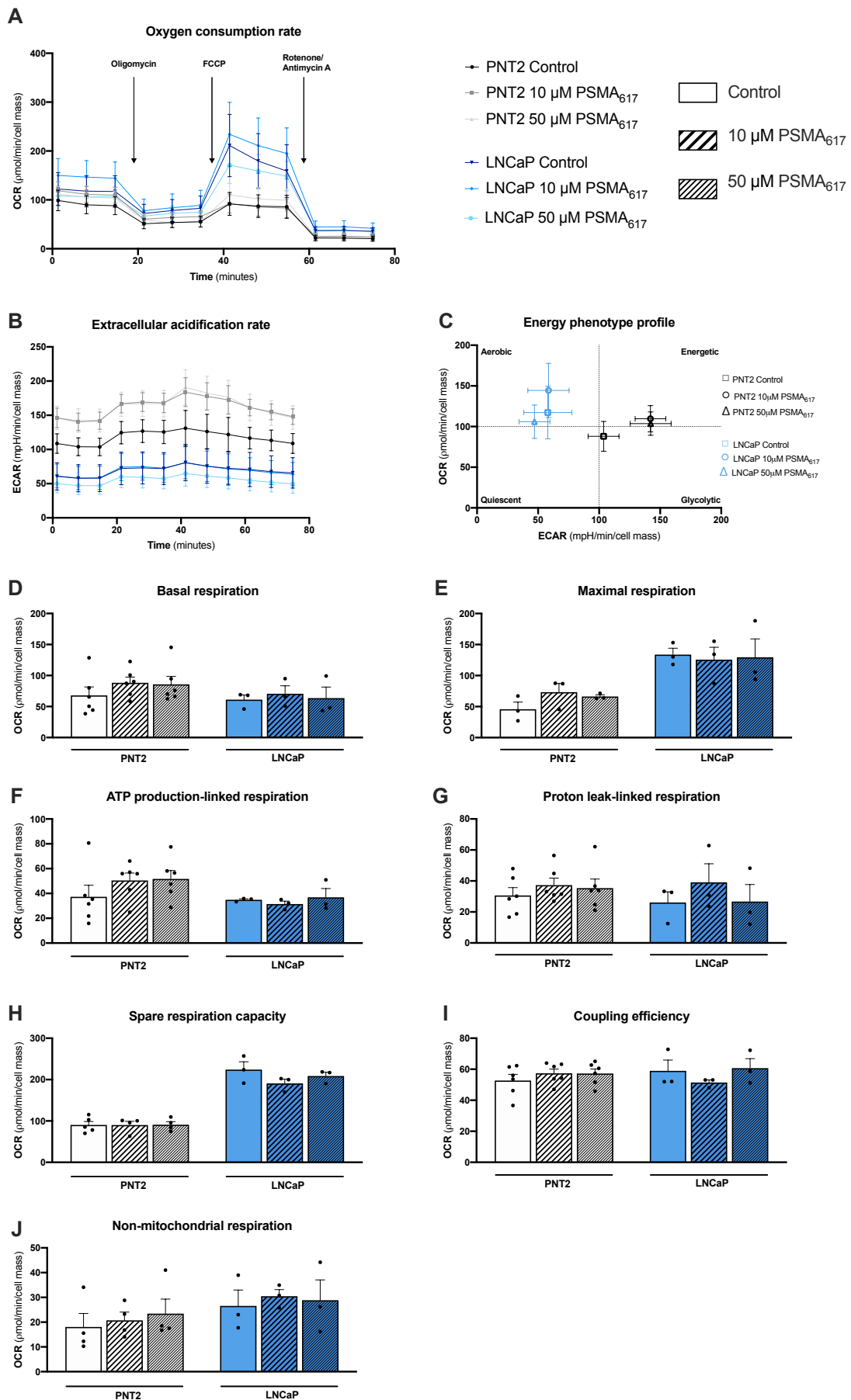


**Figure 6. Impact of short-term exposure to PSMA<sub>617</sub> on mitochondrial oxygen consumption of PNT2 and LNCaP cells.** The Seahorse XF<sup>96</sup> Extracellular Flux Analyzer was used to measure Oxygen Consumption Rate (OCR) expressed as pmol/min (**A**), and Extracellular Acidification Rate (ECAR) expressed in mpH//min (**B**), both normalized per cell mass of cells untreated (control) and treated with 10  $\mu$ M and 50  $\mu$ M PSMA<sub>617</sub> for 6 hours. (**C**) The values of the last OCR and ECAR rate measured before first injection were displayed as a scatter plot to assess the energetic profile. Several respiratory parameters were evaluated: (**D**) basal OCR; (**E**) maximal OCR; (**F**) ATP production-linked OCR (**G**) proton leak-linked OCR; (**H**) spare respiration capacity OCR; (**I**) coupling efficiency OCR; and (**J**) non-mitochondrial OCR. Data are the mean  $\pm$  SEM of 4-6 independent experiments in triplicate. The different conditions were compared to the control by Kruskal-Wallis's followed by Dunn's post-hoc test.

Results depicted in Figure 7 evidence that although no significant changes were observed in most of the mitochondrial respiration parameters assessed with the Mito Stress test, the spare capacity of 10  $\mu$ M PSMA<sub>617</sub>-treated LNCaP cells was significantly decreased when compared to control cells (Figure 7H). Moreover, long-term exposure to PSMA<sub>617</sub> appear to induce a shift in the energetic profile of LNCaP cells. Thus, tumoral cells LNCaP slightly shift their metabolism to a quiescent profile when treated with PSMA<sub>617</sub> for 72 hours. Importantly, the switch from glycolytic to energetic profile observed in non-tumoral PNT2 cells after a short-term exposure to the compound (Figure 6C) is maintained at 72 hours (Figure 7C).

Altogether, our results suggest that although PSMA<sub>617</sub> did not induce changes in cell proliferation (Figure 5), it affected the metabolic profile of tumoral cells by inducing a shift to a more quiescent profile, which could be of interest in the context of cancer therapeutic.

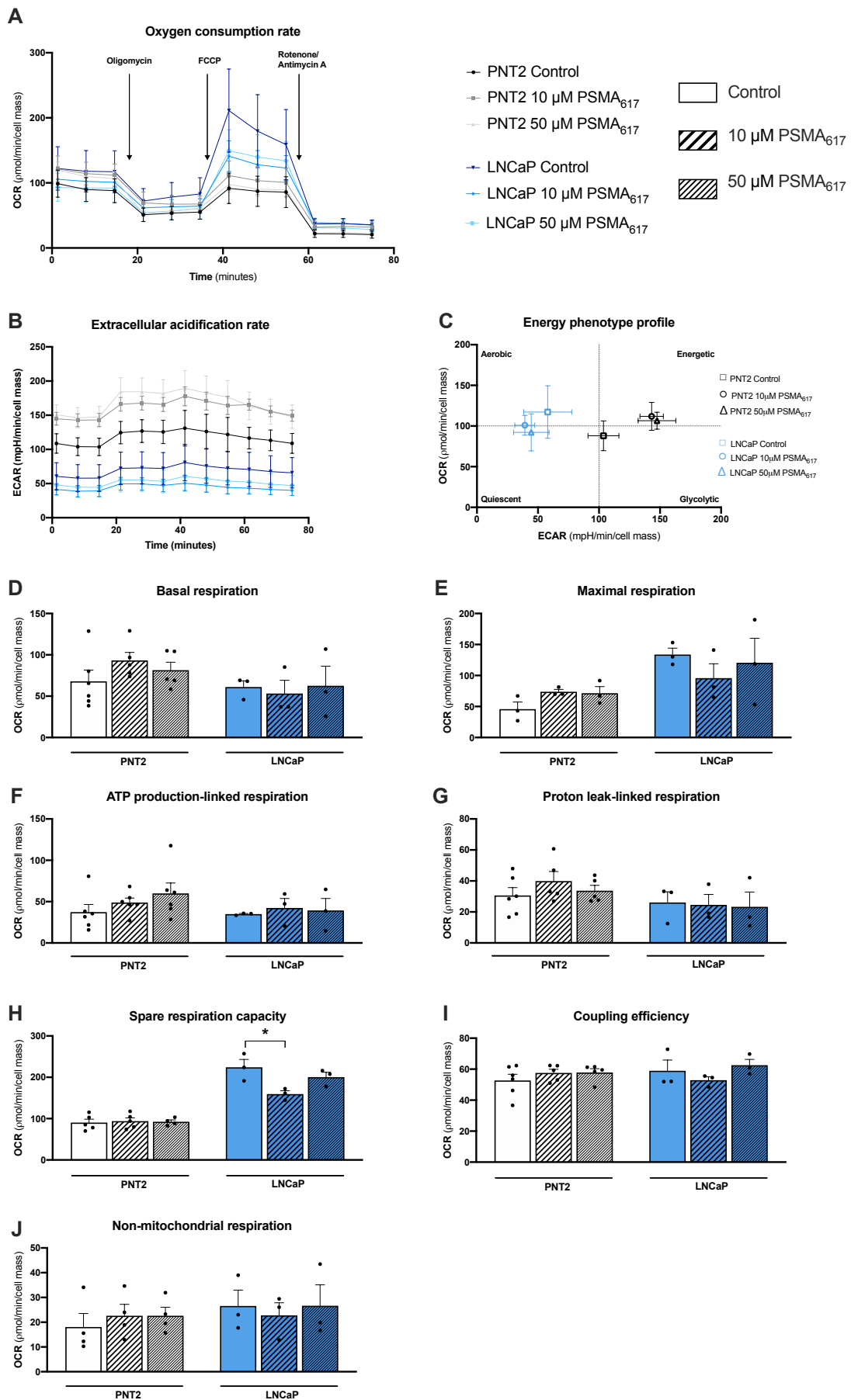


**Figure 7. Impact of long-term exposure to PSMA<sub>617</sub> on mitochondrial oxygen consumption of PNT2 and LNCaP cells.** The Seahorse XF<sup>96</sup> Extracellular Flux Analyzer was used to measure Oxygen Consumption Rate (OCR) expressed as pmol/min (**A**), and Extracellular Acidification Rate (ECAR) expressed in mpH//min (**B**), both normalized per cell mass of cells untreated (control) and treated with 10  $\mu$ M and 50  $\mu$ M PSMA<sub>617</sub> for 72 hours. (**C**) The values of the last OCR and ECAR rate measured before first injection were displayed as a scatter plot to assess the energetic profile. Several respiratory parameters were evaluated: (**D**) basal OCR; (**E**) maximal OCR; (**F**) ATP production-linked OCR (**G**) proton leak-linked OCR; (**H**) spare respiration capacity OCR; (**I**) coupling efficiency OCR; and (**J**) non-mitochondrial OCR. Data are the mean  $\pm$  SEM of 3-6 independent experiments in triplicate. The different conditions were compared to the control by Kruskal-Wallis's followed by Dunn's post-hoc test. Significant differences in LNCaP cells are marked by \* ( $p < 0.05$ ).

### **3.2.3. Short- and long-term exposure to PSMA<sub>617</sub> increases the glycolytic function of normal prostate PNT2 cells**

Since we observed some slight changes in the energetic profile of cells treated with PSMA<sub>617</sub>, we also assessed the glycolytic function of the cells through the Agilent Seahorse XF Glycolysis Stress Test Kit, after both short- (Figure 8) and long-term exposure (Figure 9). This assay allows the determination of ECAR, but also glycolytic parameters based on extracellular acidification.

Results depicted in Figure 8A evidence an increase in ECAR values over time in PNT2 cells treated with PSMA<sub>617</sub> for 6 hours. Of note, this effect was dependent of the concentration of compound. The glycolytic parameters calculated from the Figure 8A are plotted in B-E and show that PNT2 cells treated with 50  $\mu$ M PSMA<sub>617</sub> present a significant increase in glycolysis (Figure 8B), glycolytic capacity (Figure 8C) and glycolytic reserve (Figure 8D). Treatment with 10  $\mu$ M PSMA<sub>617</sub> also induce an increase in those parameters, although only changes in glycolytic reserve appears to be statistically significant. No changes were observed regarding the non-glycolytic acidification. On the other hand, tumoral cell line LNCaP glycolytic pathway is not affected by short-term exposure to both 10 and 50  $\mu$ M PSMA<sub>617</sub>.

Results obtained after 72 hours treatment evidence a similar increase in the ECAR value of both 10 and 50  $\mu$ M treated cells when compared to respective control (Figure 9A). Moreover, although changes in glycolytic pathway-associated parameters were not statistically significant, results showed an increase in glycolysis (Figure 9B), glycolytic capacity (Figure 9C) and glycolytic reserve (Figure 9D) in PNT2 cells treated

with PSMA<sub>617</sub>. LNCaP cells did not suffer significant alterations in any of the glycolytic parameters under long-term treatment with 10 or 50  $\mu$ M PSMA<sub>617</sub> (Figure 9, B-E).

Altogether, our results indicate that PSMA<sub>617</sub> alone already induce changes in normal prostate cells (PNT2) increasing the contribution of the glycolytic pathway to energy production. However, it has no effect on PCa cells (LNCaP).

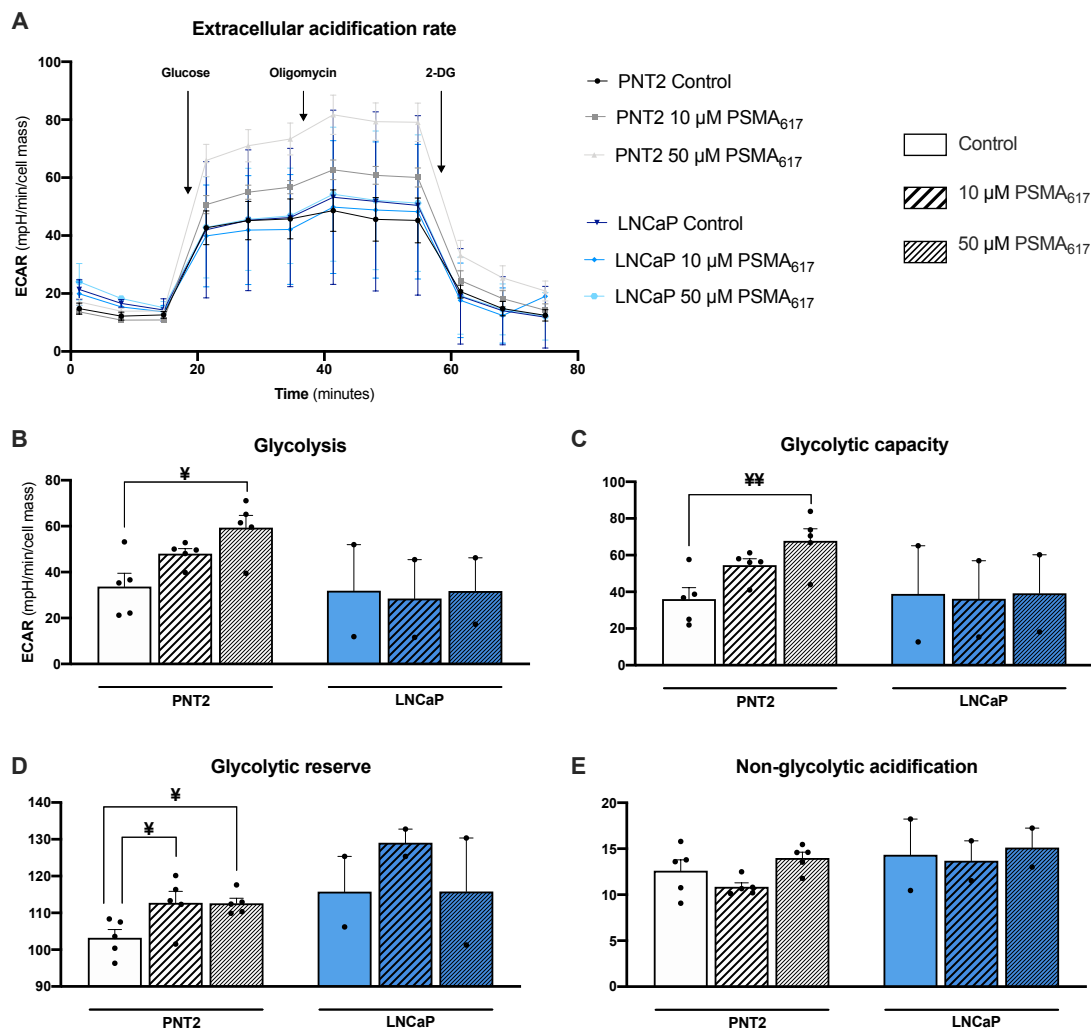


**Figure 8. Impact of short-term exposure to PSMA<sub>617</sub> on glycolytic function of PNT2 and LNCaP cells.** The Seahorse XF<sup>®</sup>96 Extracellular Flux Analyzer was used to measure Extracellular Acidification Rate (ECAR) expressed in mpH//min (A), normalized per cell mass of cells untreated (control) and treated with 10  $\mu$ M and 50  $\mu$ M PSMA<sub>617</sub> for 6 hours. Several glycolytic parameters were evaluated: (B) glycolysis ECAR; (C) glycolysis capacity ECAR; (D) glycolytic reserve ECAR (E) and non-glycolytic acidification ECAR. Data are the mean  $\pm$  SEM of 2 or 3 independent experiments in triplicate. The different conditions were compared to the control by Kruskal-Wallis' followed by Dunn's post-hoc test. Significant differences in PNT2 cells are marked by ¥ (p < 0.05) and ¥¥ (p < 0.01).

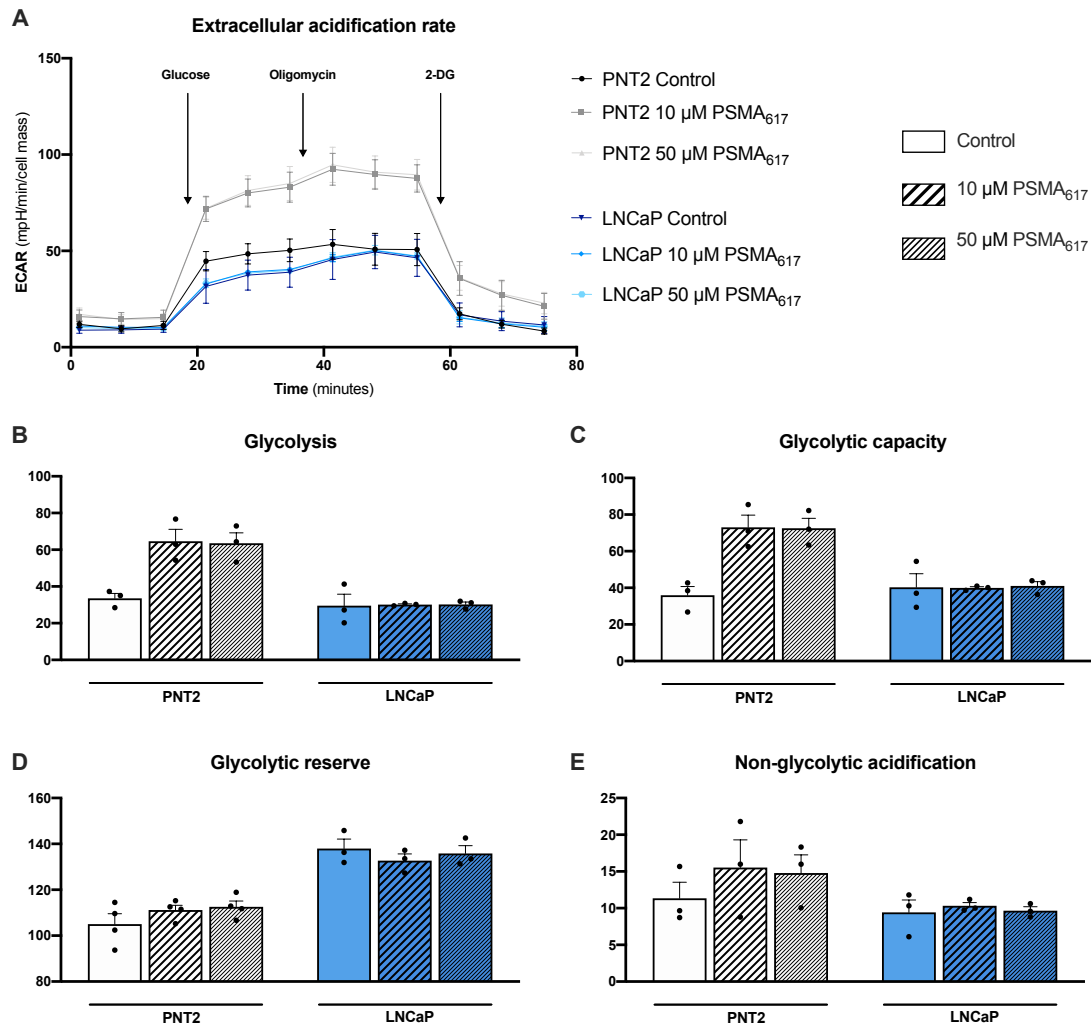


**Figure 9. Impact of long-term exposure to PSMA<sub>617</sub> on glycolytic function of PNT2 and LNCaP cells.** The Seahorse XF<sup>96</sup> Extracellular Flux Analyzer was used to measure Extracellular Acidification Rate (ECAR) expressed in mpH//min (A), normalized per cell mass of cells untreated (control) and treated with 10  $\mu$ M and 50  $\mu$ M PSMA<sub>617</sub> for 72 hours. Several glycolytic parameters were evaluated: (B) glycolysis ECAR; (C) glycolysis capacity ECAR; (D) glycolytic reserve ECAR (E) and non-glycolytic acidification ECAR. Data are the mean  $\pm$  SEM of 3 independent experiments in triplicate. The different conditions were compared to the control by Kruskal-Wallis's followed by Dunn's post-hoc test.

### 3.2.4 Exposure to PSMA<sub>617</sub> has no effect on PC3-PIP cells but induce an energetic switch in PC3-FLU cells

PSMA<sub>617</sub> has already been shown to have high PSMA cellular specificity and fast pharmacokinetics (Czerwinska et al 2020). Results obtained above (Figure 6 – 9) shows almost no significant effects of PSMA<sub>617</sub> on tumoral cells LNCaP. Thus, we assessed the same parameters on a tumoral cell line overexpressing PSMA protein, PC3-PIP, and

compared to its isogenic control, PC3-FLU. As previously, we evaluated the impact of short-term (6 hours; Figure 10) and long-term (72 hours; Figure 11) incubation with PSMA<sub>617</sub> (10 or 50  $\mu$ M) in PC3-FLU tumoral cells (non-expressing PSMA) and in PC3-PIP tumoral cells overexpressing PSMA.

Results in Figure 10A and B show that there are no significant differences in OCR and ECAR values between PC3-FLU and PC3-PIP cells treated for 6 hours and their respective control. This result is supported by Figure 10C which show that both cell lines, regardless of the treatment, have an aerobic energetic profile, producing energy mainly through OXPHOS. Looking at mitochondrial respiration-related parameters, PC3-FLU cells presented a significant concentration-dependent increase in basal respiration when treated with PSMA<sub>617</sub> for 6 hours (Figure 10D), while other parameters remain unchanged. No effects were detected in the PC3-PIP cell line.

Figure 11 depicted the same parameters but after a long-term incubation with the compound (72 hours). Data evidenced that the long-term treatment with PSMA<sub>617</sub> induced a shift in the energetic profile of PC3-FLU cells to a more energetic profile, producing energy through both OXPHOS and glycolysis (Figure 11C), in a concentration-dependent manner. This shift is also represented in the ECAR values over time which are increased in PC3-FLU treated cells, comparing to control cells (Figure 11B). Concomitantly, PC3-FLU presented a dose-dependent increase in basal respiration (Figure 11D) and ATP production (Figure 11F) as well as in maximal respiration (Figure 11E) although this last is not statistically significant. PC3-PIP cells treated with the lower concentration of PSMA<sub>617</sub> (10  $\mu$ M) only present a decrease in spare respiratory capacity (Figure 11H) which is probably related with the non-significant increase in the same condition of basal respiration (Figure 11B).

Altogether, our results suggest that the tumoral cell line PC3-PIP, overexpressing the PSMA protein, is not sensitive to PSMA<sub>617</sub>; while, interestingly, the cell line non-expressing the PSMA protein shows a concentration-dependent response to the compound.

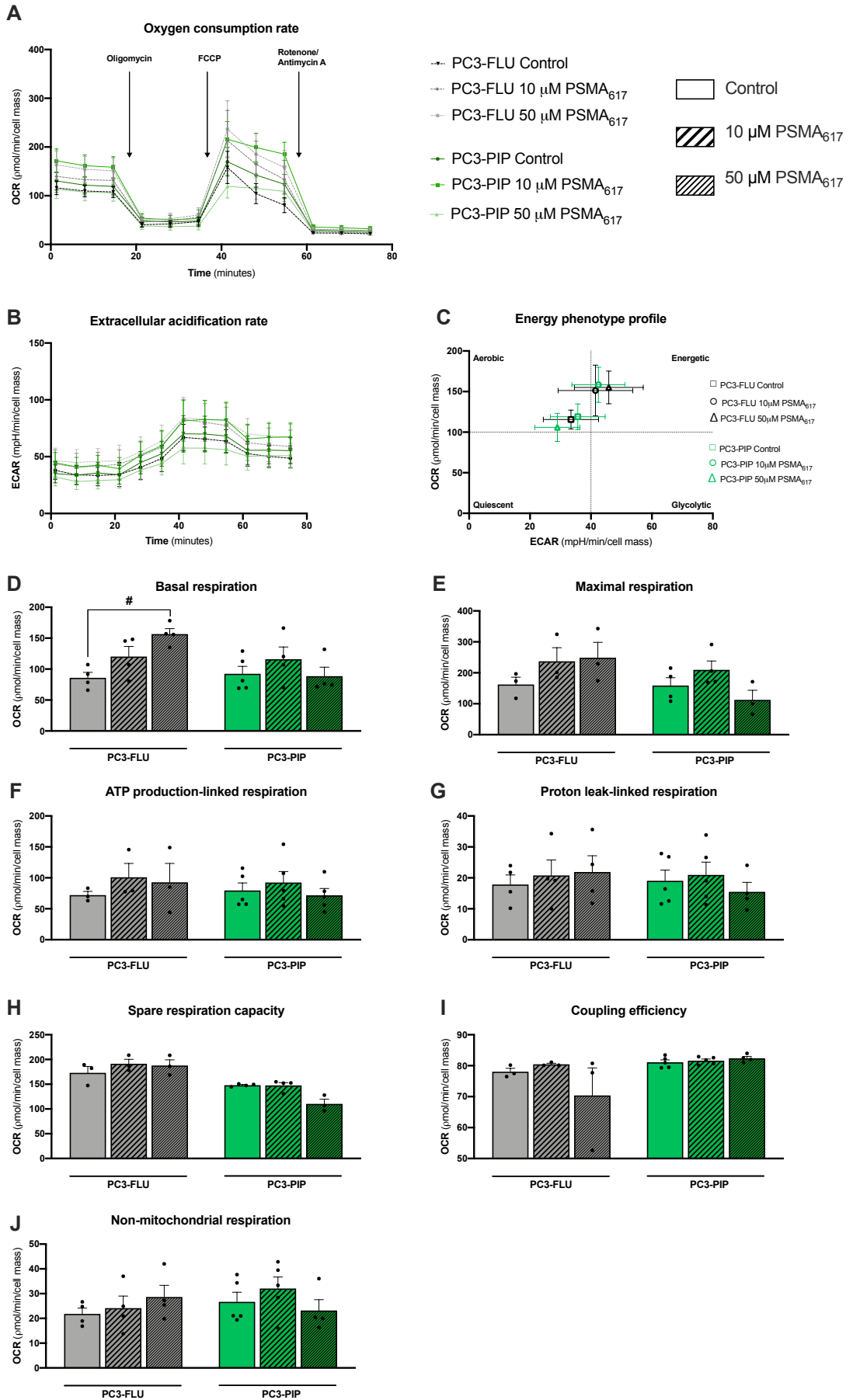


**Figure 10. Impact of short-term exposure to PSMA<sub>617</sub> on mitochondrial oxygen consumption of PC3-FLU and PC3-PIP cells.** The Seahorse XF<sup>®</sup>96 Extracellular Flux Analyzer was used to measure Oxygen Consumption Rate (OCR) expressed as pmol/min (**A**), and Extracellular Acidification Rate (ECAR) expressed in mpH//min (**B**), both normalized per cell mass of cells untreated (control) and treated with 10 μM and 50 μM PSMA<sub>617</sub> for 6 hours. (**C**) The values of the last OCR and ECAR rate measured before first injection were displayed as a scatter plot to assess the energetic profile. Several respiratory parameters were evaluated: (**D**) basal OCR; (**E**) maximal OCR; (**F**) ATP production-linked OCR (**G**) proton leak-linked OCR; (**H**) spare respiration capacity OCR; (**I**) coupling efficiency OCR; and (**J**) non-mitochondrial OCR. Data are the mean ± SEM of 3-6 independent experiments in triplicate. The different conditions were compared to the control by Kruskal-Wallis' followed by Dunn's post-hoc test. Significant differences in PC3-FLU cells are marked by # (p < 0.05).

### **3.2.5 PSMA<sub>617</sub> treatment did not induce alterations on the glycolytic function of PC3-FLU and PC3-PIP cells**

The previous results suggest that PC3-FLU cells become more energetic after treatment with PSMA<sub>617</sub>, starting to produce energy also through the glycolytic pathway and not predominantly through OXPHOS. Thus, we assessed the glycolytic function of PC3-FLU and PC3-PIP under PSMA<sub>617</sub> treatment and sought to understand the influence of PSMA expression in the cellular response to treatment. Thus, we performed the Glycolytic Stress assay on both PC3-FLU and PC3-PIP treated with PSMA<sub>617</sub> (10 and 50 μM) for 6 hours to evaluate the short-term exposure (Figure 12) and for 72 hours to evaluate the long-term exposure to the compound (Figure 13). Results evidence that the glycolytic rate of the cells is not significantly affected by PSMA<sub>617</sub> treatment.

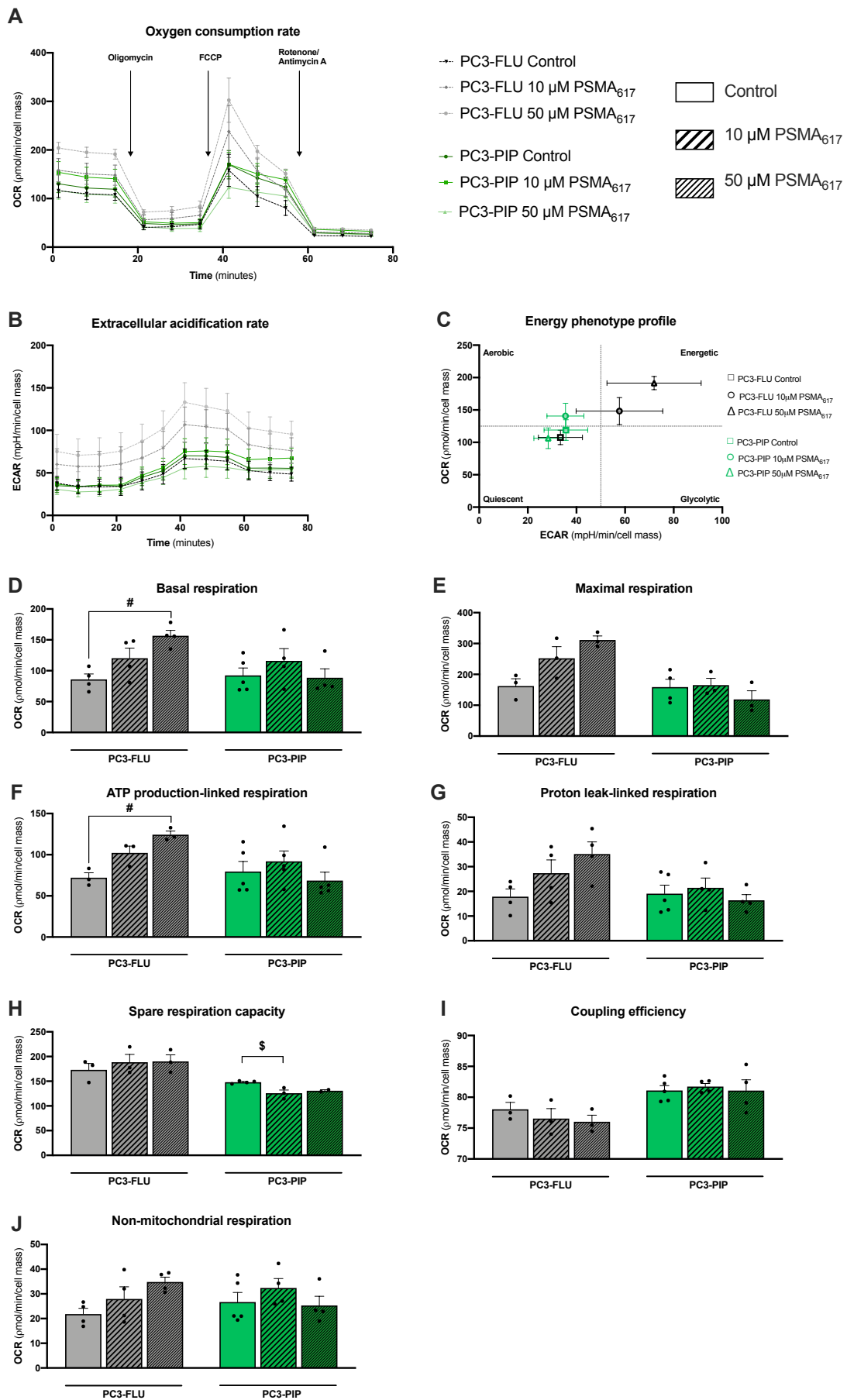


**Figure 11. Impact of long-term exposure to PSMA<sub>617</sub> on mitochondrial oxygen consumption of PC3-FLU and PC3-PIP cells.** The Seahorse XF<sup>96</sup> Extracellular Flux Analyzer was used to measure Oxygen Consumption Rate (OCR) expressed as pmol/min (A), and Extracellular Acidification Rate (ECAR) expressed in mpH//min (B), both normalized per cell mass of cells untreated (control) and treated with 10  $\mu$ M and 50  $\mu$ M PSMA<sub>617</sub> for 72 hours. (C) The values of the last OCR and ECAR rate measured before first injection were displayed as a scatter plot to assess the energetic profile. Several respiratory parameters were evaluated: (D) basal OCR; (E) maximal OCR; (F) ATP production-linked OCR (G) proton leak-linked OCR; (H) spare respiration capacity OCR; (I) coupling efficiency OCR; and (J) non-mitochondrial OCR. Data are the mean  $\pm$  SEM of 3-5 independent experiments in triplicate. The different conditions were compared to the control by Kruskal-Wallis followed by Dunn's post-hoc test. Significant differences in PC3-FLU cells are marked by # ( $p < 0.05$ ). Significant differences in PC3-PIP cells are marked by \$ ( $p < 0.05$ ).

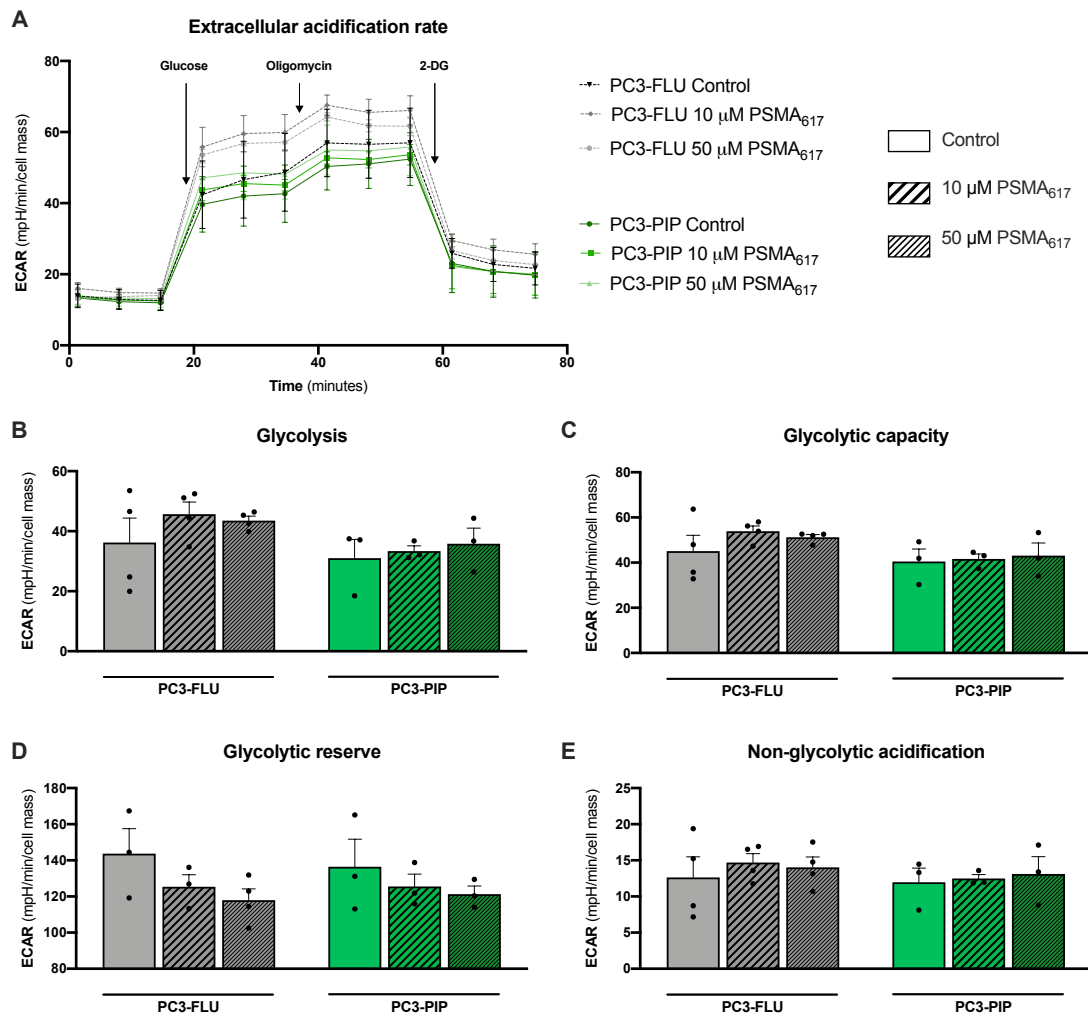


**Figure 12. Impact of short-term exposure to PSMA<sub>617</sub> on glycolytic function of PC3-FLU and PC3-PIP cells.** The Seahorse XF<sup>96</sup> Extracellular Flux Analyzer was used to measure Extracellular Acidification Rate (ECAR) expressed in mpH//min (A), normalized per cell mass of cells untreated (control) and treated with 10  $\mu$ M and 50  $\mu$ M PSMA<sub>617</sub> for 6 hours. Several glycolytic parameters were evaluated: (B) glycolysis ECAR; (C) glycolysis capacity ECAR; (D) glycolytic reserve ECAR (E) and non-glycolytic acidification ECAR. Data are the mean  $\pm$  SEM of 3 independent experiments in triplicate. The different conditions were compared to the control by Kruskal-Wallis followed by Dunn's post-hoc test.

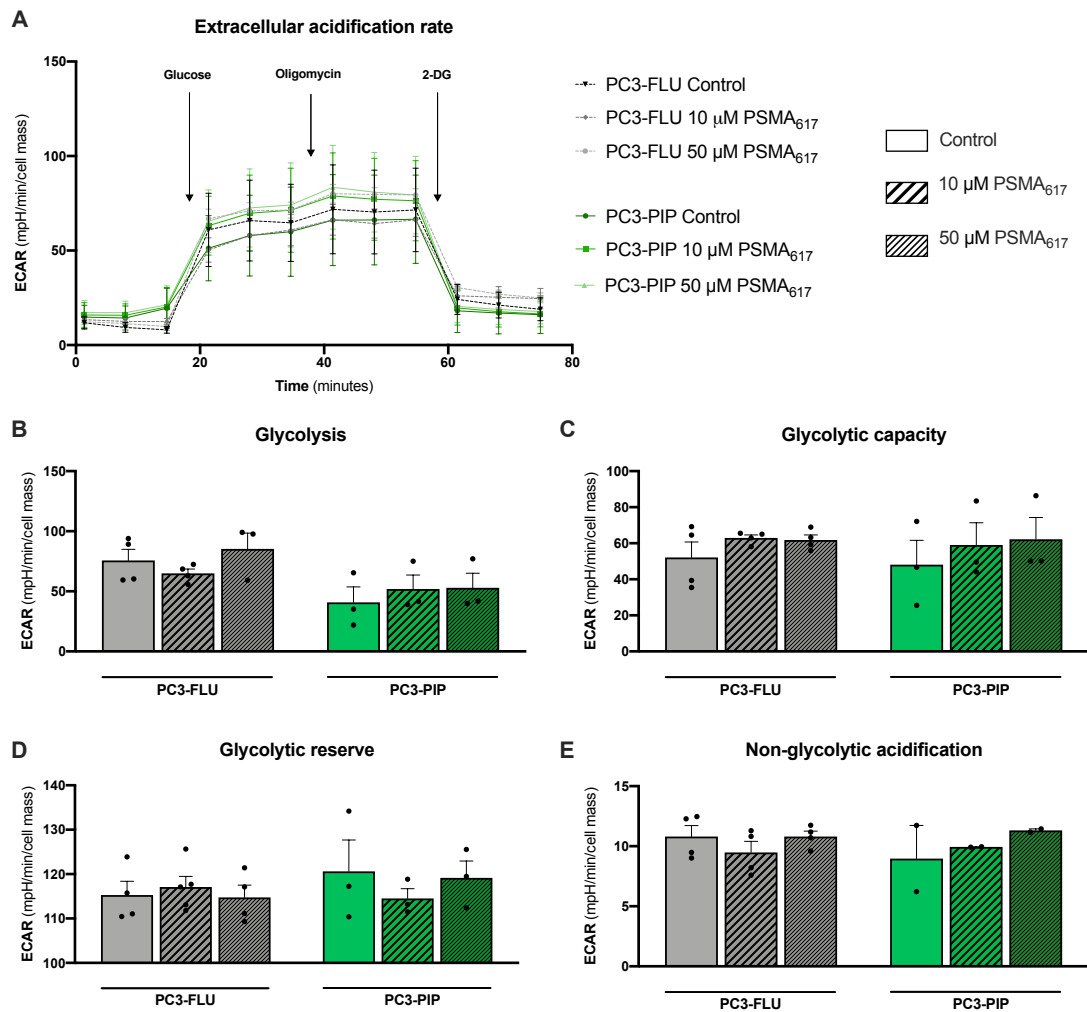


**Figure 13. Impact of long-term exposure to PSMA<sub>617</sub> on glycolytic function of PC3-FLU and PC3-PIP cells.** The Seahorse XF<sup>e</sup>96 Extracellular Flux Analyzer was used to measure Extracellular Acidification Rate (ECAR) expressed in mpH//min (**A**), normalized per cell mass of cells untreated (control) and treated with 10  $\mu$ M and 50  $\mu$ M PSMA<sub>617</sub> for 72 hours. Several glycolytic parameters were evaluated: (**B**) glycolysis ECAR; (**C**) glycolysis capacity ECAR; (**D**) glycolytic reserve ECAR (**E**) and non-glycolytic acidification ECAR. Data are represented as the mean  $\pm$  SEM of 2 or 3 independent experiments in triplicate. The different conditions were compared to the control by Kruskal-Wallis's followed by Dunn's post-hoc test.

### 3.3 Effects of $^{nat}\text{In}$ -DOTAGA-AO compound in cell viability and metabolism

#### 3.3.1 $^{nat}\text{In}$ -DOTAGA-AO internalizes and co-localizes with the nucleus and mitochondria

In the present study we performed preliminary work for AugerTher project that aim to develop a novel dual-targeting TRT modality based on AE-emitting radionuclide. Thus, we evaluate the cellular effects of  $^{nat}\text{In}$ -DOTAGA-AO on four *in vitro* models This cold surrogate is constituted by a native form of  $^{111}\text{In}$  isotope chelated with DOTAGA and functionalized with an AO attached ligand. The AO intercalate with nucleic acids, ensuring the targeting of nuclear DNA or mtDNA (Baskic et al 2006; Agorastos et al 2007), with any specific cell type target. Firstly, we assessed the internalization and co-localization of  $^{nat}\text{In}$ -DOTAGA-AO within nucleus and mitochondria by analyzing the compound fluorescence using confocal microscopy and Fiji software (Figure 14).  $^{nat}\text{In}$ -DOTAGA-AO successfully internalizes into PNT2, LNCaP and PC3-PIP cells, and is distributed within the nucleus (Figure 14B) and mitochondria (Figure 14C). Data evidence no significant difference between the compound co-localization in the nucleus of normal prostate PNT2 cells and LNCaP or PC3-PIP tumor cells (Figure 14B). We also observed accumulation of  $^{nat}\text{In}$ -DOTAGA-AO within PC3-FLU nucleus (data not shown) but have not evaluated its accumulatio in mitochondria. Moreover,  $^{nat}\text{In}$ -DOTAGA-AO internalization is significantly higher in PCa LNCaP cells compared to normal prostate PNT2 cells, while no changes are observed in PC3-PIP cells compared to PNT2 (Figure 14C). In addition, data suggest that LNCaP are the cells with more compound internalization within both nucleus and mitochondria. Interestingly, PC3-PIP appears to accumulate more  $^{nat}\text{In}$ -DOTAGA-AO within the mitochondria than in the nucleus.

Overall, data evidence that  $^{nat}\text{In}$ -DOTAGA-AO internalize in both tumoral and non-tumoral prostate cells, in both mitochondria and nucleus. In addition, LNCaP cells show higher internalization of  $^{nat}\text{In}$ -DOTAGA-AO.

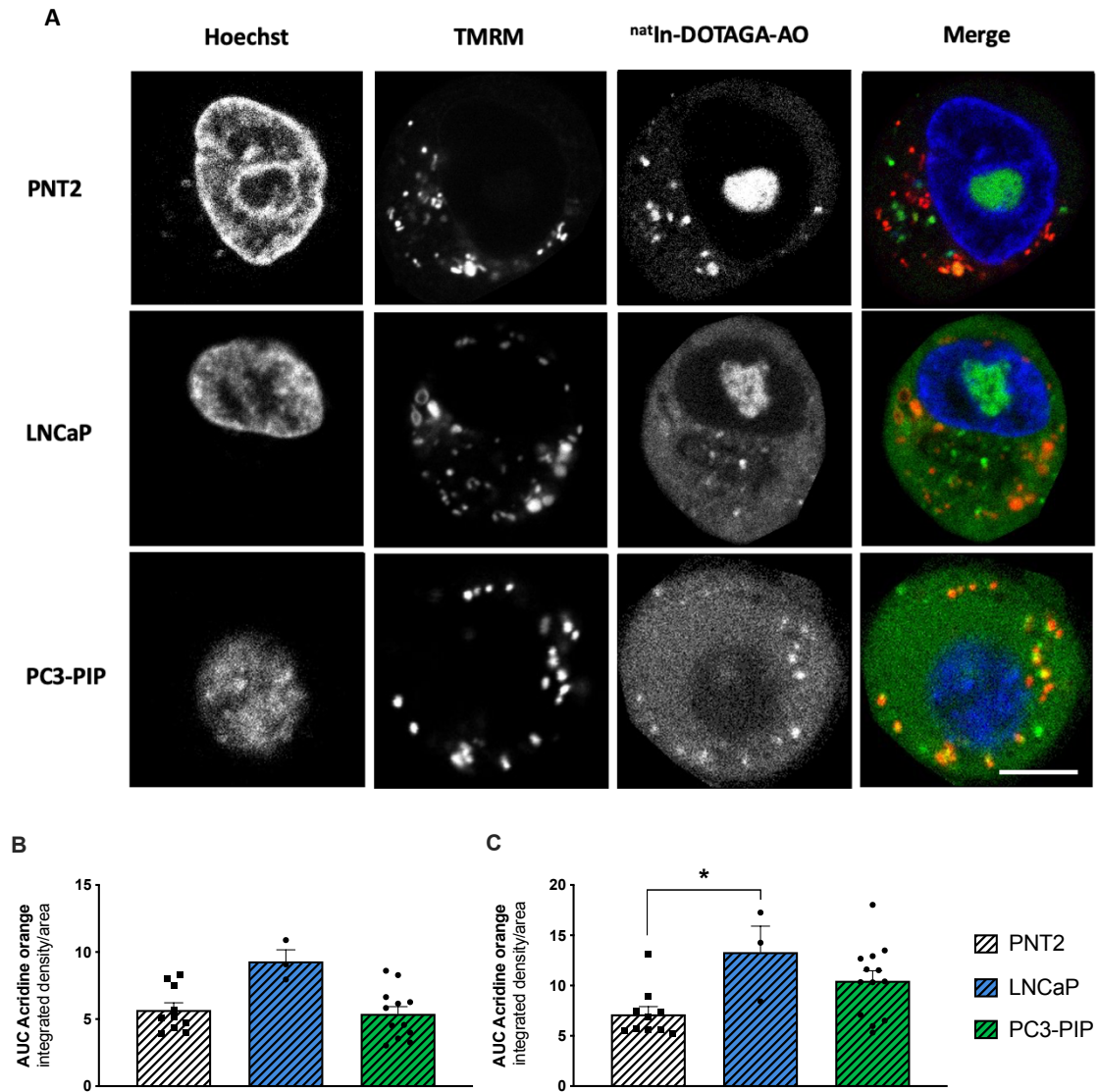


**Figure 14. <sup>nat</sup>In-DOTAGA-AO internalization and co-localization within the nucleus and mitochondria.** (A) Representative confocal images of PNT2, LNCaP, and PC3-PIP cells treated with <sup>nat</sup>In-DOTAGA-AO for 72 hours obtained using TMRM and Hoechst for mitochondrial and nuclei labeling, respectively. Scale bar = 10  $\mu$ m. (B-C) Area under the curve (AUC) of single cell integrated density per area (from threshold 1-21) in the nucleus (B) and in the mitochondria (C). Data are the mean  $\pm$  SEM for 10 PNT2 cells, 3 LNCaP cells, and 13 PC3-PIP cells, obtained from one single experiment. LNCaP and PC3-PIP treated cells were compared to the PNT2 treated cells by a one-way ANOVA followed by Kruskal-Wallis's post-test. Significant differences in LNCaP cells are marked by \* ( $p < 0.05$ ).

### 3.3.2 <sup>nat</sup>In-DOTAGA-AO did not induce cell mass or metabolic activity alterations

We further evaluate the cytotoxicity of <sup>nat</sup>In-DOTAGA-AO in the four cell lines used in this study. Cells were treated or not (control) with 0.1, 1, 10, or 50  $\mu\text{M}$  <sup>nat</sup>In-DOTAGA-AO for 24, 48 and 72 hours and the cell mass (Figure 15i) and metabolic activity (Figure 15ii) were evaluated through SRB and rezasurin assays, respectively. Data evidence that none of the four concentrations of <sup>nat</sup>In-DOTAGA-AO affect neither the cell mass, neither the metabolic activity. To assess if the changes in metabolic activity were related with changes in cell mass, we replotted results from graphics i) and ii) into a correlation graphic iii) for each cell line. Results show a positive correlation between both parameters in PNT2 ( $\rho = 0.94$ ;  $r^2 = 0.88$ ), LNCaP ( $\rho = 0.87$ ;  $r^2 = 0.76$ ), PC3-FLU ( $\rho = 0.98$ ;  $r^2 = 0.96$ ) and PC3-PIP ( $\rho = 0.97$ ;  $r^2 = 0.94$ ), indicating that the change observed in the metabolic activity are the result of an increase in cell mass and very likely due to cell proliferation.

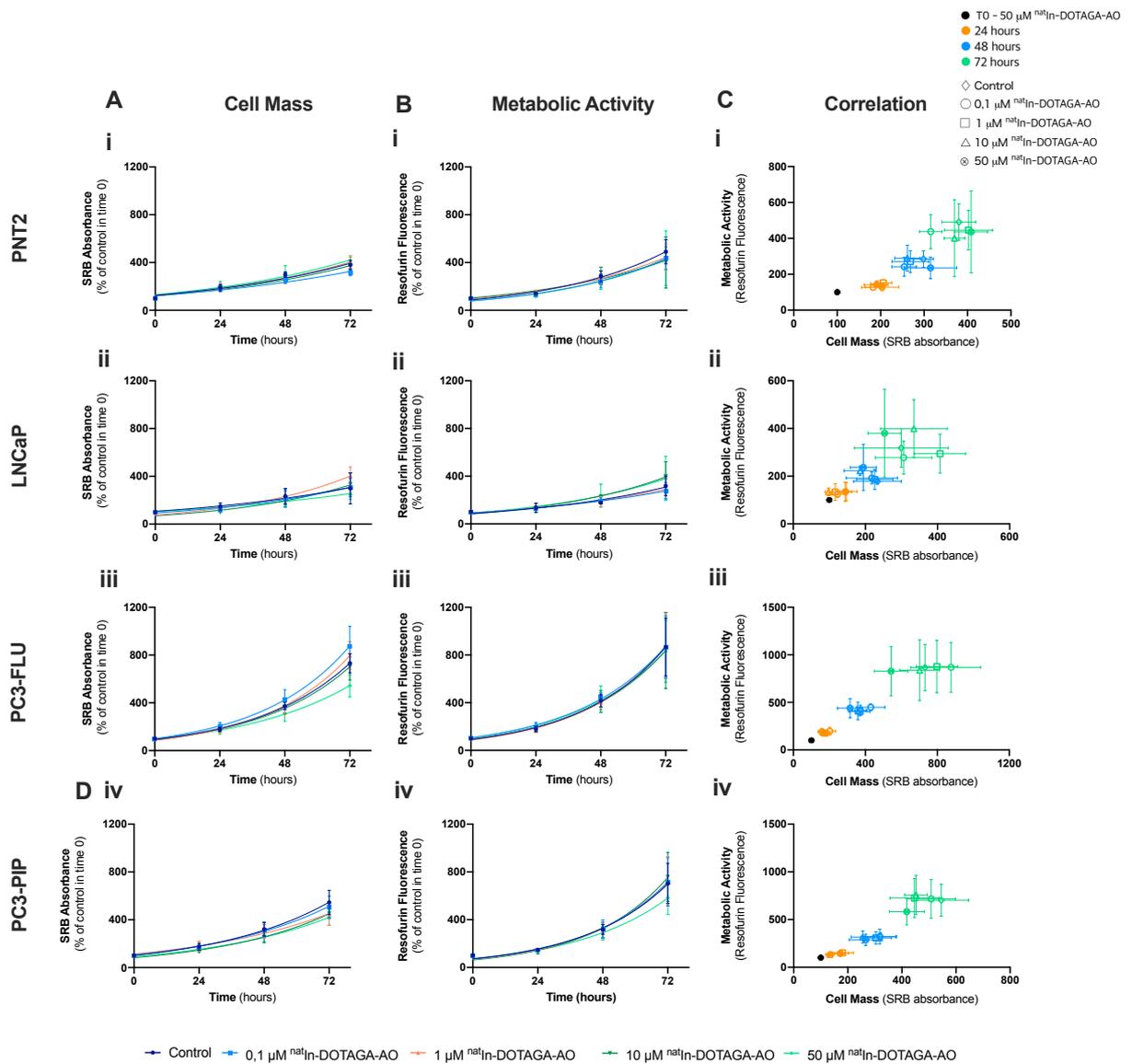


**Figure 15.** Cytotoxic effect of  $^{111}\text{In}$ -DOTAGA-AO on PNT2, LNCaP, PC3-FLU and PC3-PIP cells. **(A)** The sulforhodamine B (SRB) assay was used to measure cell mass of untreated cells (control) and cells treated with 0,1  $\mu\text{M}$ ; 1  $\mu\text{M}$ ; 10  $\mu\text{M}$  and 50  $\mu\text{M}$   $^{111}\text{In}$ -DOTAGA-AO for 0 (time 0), 24, 48, and 72 hours. Data are the mean  $\pm$  SEM of 4 independent experiments in triplicate and expressed as percentage of the time 0 value. The different conditions were compared to the control by a two-way ANOVA. **(B)** The metabolic activity of untreated cells (control) and cells treated with 0,1  $\mu\text{M}$ ; 1  $\mu\text{M}$ ; 10  $\mu\text{M}$  and 50  $\mu\text{M}$  PSMA<sub>617</sub> for 0, 24, 48, and 72 hours was measured by resazurin assay. Data are represented as the mean  $\pm$  SEM of 4–6 independent experiments in triplicate and expressed as percentage of the respective control. The different conditions were compared to the control by a two-way ANOVA. **(C)** The values of SRB and resazurin assay were re-plotted to assess the correlation between cell mass and metabolic activity. The Pearson correlation coefficients are: 0.94 for PNT2; 0.87 for LNCaP; 0.98 for PC3-FLU; 0.97 for PC3-PIP.

### 3.3.2 Long-term exposure to <sup>nat</sup>In-DOTAGA-AO impaired mitochondrial function of non-tumoral and tumoral cells

As for PSMA<sub>617</sub>, we also sought to understand the impact of short- (6 hours) and long-term (72 hours) exposure to <sup>nat</sup>In-DOTAGA-AO on mitochondrial function of normal prostate cells and PCa cells. Thus, mitochondrial respiration was assessed in PNT2 and LNCaP cells in the absence or the presence of 10 or 50  $\mu\text{M}$  <sup>nat</sup>In-DOTAGA-AO using the the Agilent Seahorse XF Cell Mito Stress Test Kit.

Data presented in Figure 16 show that PNT2 cells treated for 6 hours with 10  $\mu\text{M}$  <sup>nat</sup>In-DOTAGA-AO present significantly higher levels of basal (Figure 16D) and maximal respiration (Figure 16E), concomitantly with increased ATP production-linked respiration although not significant. Curiously, the treatment with 50  $\mu\text{M}$  <sup>nat</sup>In-DOTAGA-AO did not induce significant changes in mitochondrial respiration except in coupling efficiency (Figure 16I). Results suggest that the mitochondrial function of LNCaP was not affected by the treatment with <sup>nat</sup>In-DOTAGA-AO in our conditions. Importantly and similar to what happened with PSMA<sub>617</sub>, PNT2 cells treated with <sup>nat</sup>In-DOTAGA-AO show a slight shift in the energetic profile increasing ECAR values overtime (Figure 16C).

Regarding long-term exposure, results depicted in Figure 17 evidence that PNT2 cells responded to long-term exposure <sup>nat</sup>In-DOTAGA-AO in the opposite way to short-term exposure. Thus, PNT2 cells treated with 50  $\mu\text{M}$  <sup>nat</sup>In-DOTAGA-AO showed a significantly lower basal (Figure 17D), maximal (Figure 17E), ATP production-linked (Figure 17F), and proton leak-linked respiration (Figure 17G). Moreover, although the effects of 10  $\mu\text{M}$  <sup>nat</sup>In-DOTAGA-AO are not significant, the compound seems to have a concentration-dependent effect. Treatment of PNT2 cells with 10  $\mu\text{M}$  <sup>nat</sup>In-DOTAGA-AO also increases the coupling efficiency. These changes translate into a shift to quiescent PNT2 cells (Figure 17C). Interestingly, long-term exposure to <sup>nat</sup>In-DOTAGA-AO significantly affected the mitochondrial respiration of PCa cells, LNCaP. Thus, LNCaP presented a significant decrease in basal (Figure 17D), maximal (Figure 17E), ATP production-linked (Figure 17F), and proton leak-linked respiration (Figure 17G), as well as decreased spare respiration capacity (Figure 17H). Moreover, tumoral cells LNCaP treated with 50  $\mu\text{M}$  <sup>nat</sup>In-DOTAGA-AO for 72 hours also presented a shift in their

energetic profile from aerobic to quiescent (Figure 17C), suggesting that the compound could have a beneficial effect to decrease cell metabolic activity although we did not observe any effect on cell proliferation at the same time point.

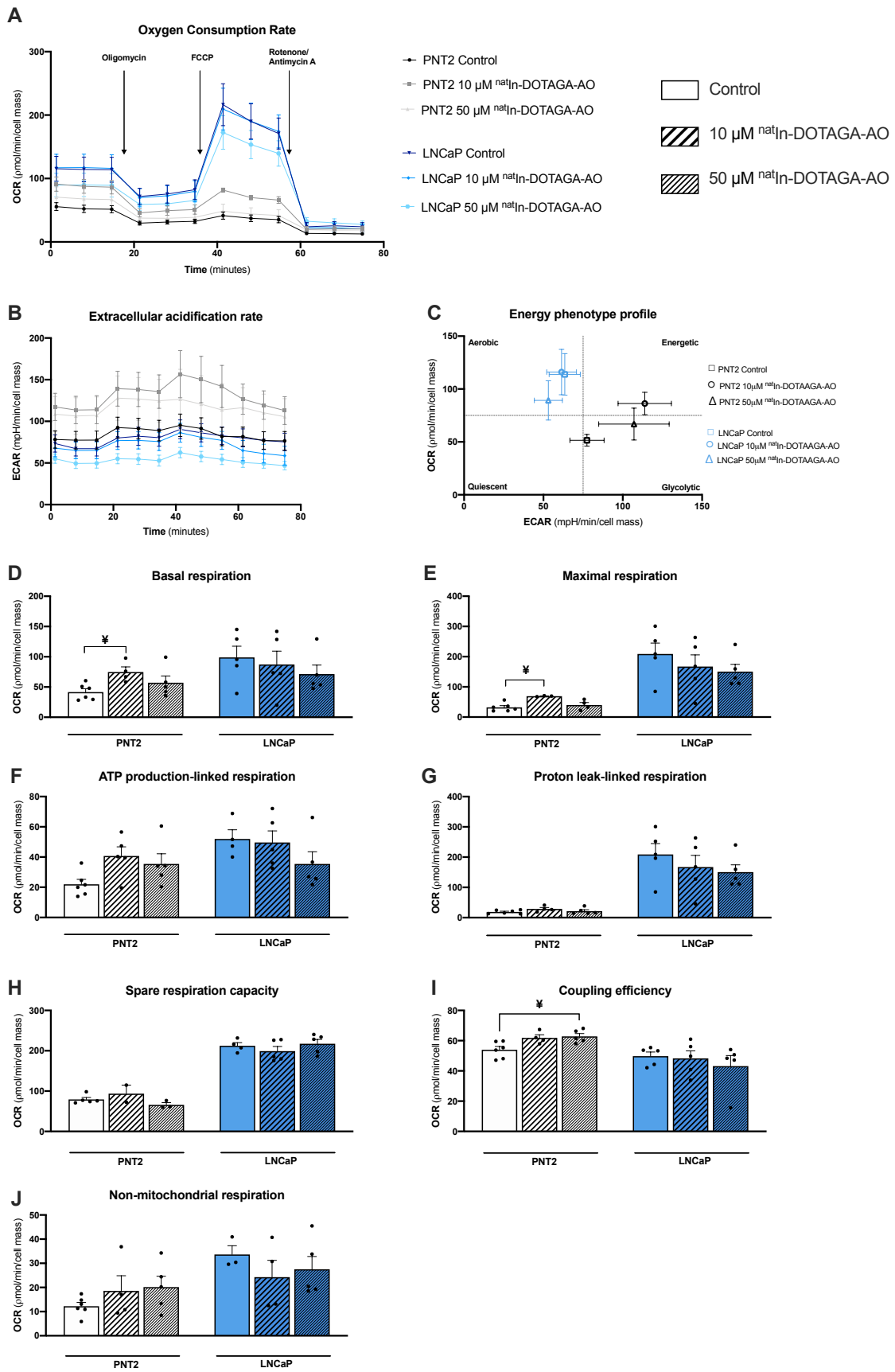


**Figure 16. Impact of short-term exposure to <sup>nat</sup>In-DOTAGA-AO on mitochondrial oxygen consumption of PNT2 and LNCaP cells.** The Seahorse XF<sup>e</sup>96 Extracellular Flux Analyzer was used to measure Oxygen Consumption Rate (OCR) expressed as pmol/min (**A**), and Extracellular Acidification Rate (ECAR) expressed in mpH//min (**B**), both normalized per cell mass of cells untreated (control) and treated with 10 μM and 50 μM <sup>nat</sup>In-DOTAGA-AO for 6 hours. (**C**) The values of the last OCR and ECAR rate measured before first injection were displayed as a scatter plot to assess the energetic profile. Several respiratory parameters were evaluated: (**D**) basal OCR; (**E**) maximal OCR; (**F**) ATP production-linked OCR (**G**) proton leak-linked OCR; (**H**) spare respiration capacity OCR; (**I**) coupling efficiency OCR; and (**J**) non-mitochondrial OCR. Data are represented as the mean ± SEM of 3-6 independent experiments in triplicate. The different conditions were compared to the control by Kruskal-Wallis' followed by Dunn's post-hoc test. Significant differences in PNT2 cells are marked by ¥ (p < 0.05).

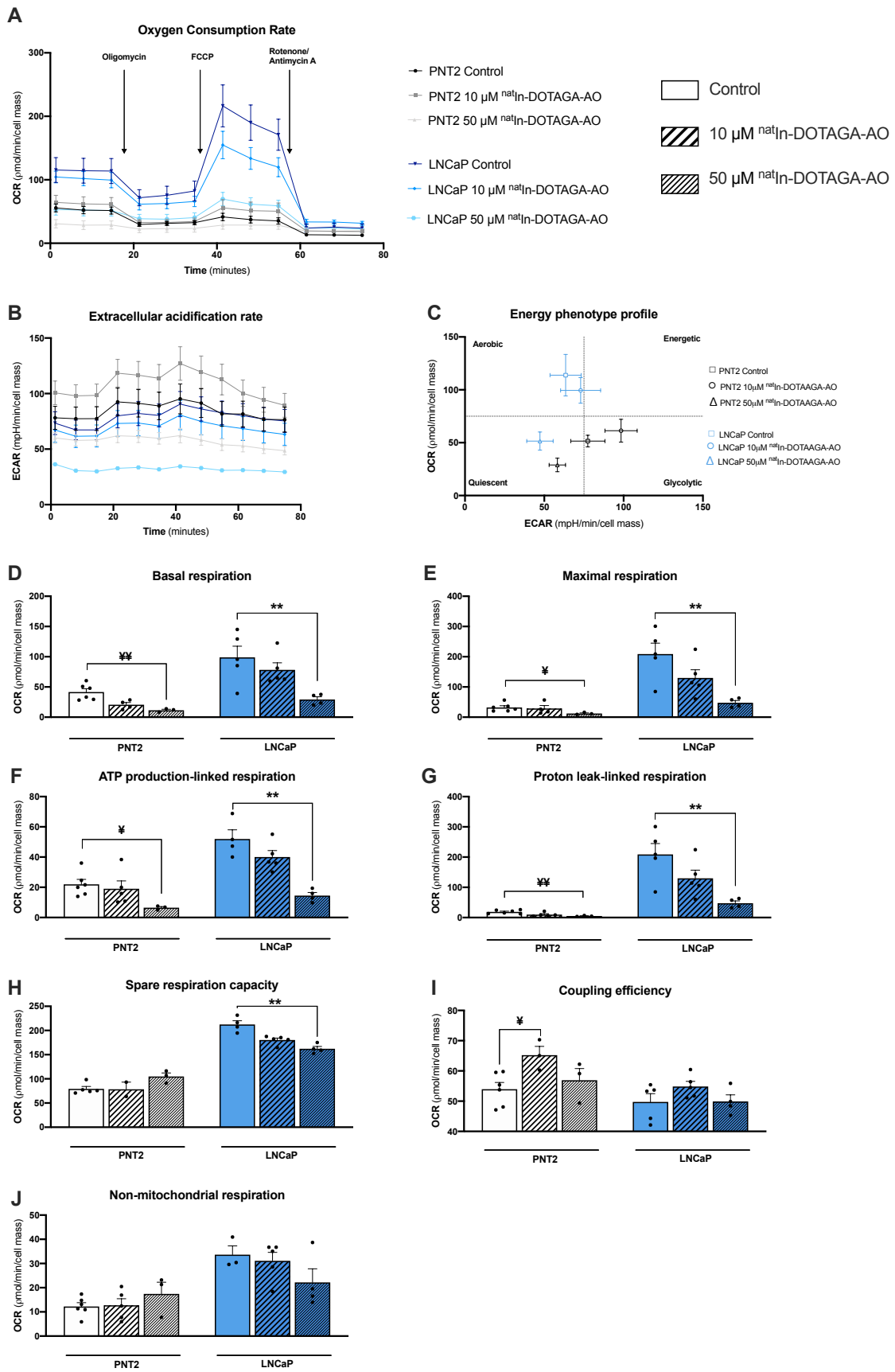


**Figure 17. Impact of long-term exposure to <sup>nat</sup>In-DOTAGA-AO on mitochondrial oxygen consumption of PNT2 and LNCaP cells.** The Seahorse XF<sup>e</sup>96 Extracellular Flux Analyzer was used to measure Oxygen Consumption Rate (OCR) expressed as pmol/min (**A**), and Extracellular Acidification Rate (ECAR) expressed in mpH//min (**B**), both normalized per cell mass of cells untreated (control) and treated with 10  $\mu$ M and 50  $\mu$ M <sup>nat</sup>In-DOTAGA-AO for 72 hours. (**C**) The values of the last OCR and ECAR rate measured before first injection were displayed as a scatter plot to assess the energetic profile. Several respiratory parameters were evaluated: (**D**) basal OCR; (**E**) maximal OCR; (**F**) ATP production-linked OCR (**G**) proton leak-linked OCR; (**H**) spare respiration capacity OCR; (**I**) coupling efficiency OCR; and (**J**) non-mitochondrial OCR. Data are represented as the mean  $\pm$  SEM of 3-6 independent experiments in triplicate. The different conditions were compared to the control by Kruskal-Wallis's followed by Dunn's post-hoc test. Significant differences in PNT2 cells are marked by ¥ ( $p < 0.05$ ), ¥¥ ( $p < 0.01$ ). Significant differences in LNCaP cells are marked by \* ( $p < 0.05$ ), \*\* ( $p < 0.01$ ).

### 3.3.3 <sup>nat</sup>In-DOTAGA-AO increases the glycolytic function of PNT2 cells

To better understand how exposure to <sup>nat</sup>In-DOTAGA-AO may affect the metabolism of normal prostate cells and PCa cells, we proceeded with the Glycolytic stress test to assess the glycolytic rate of cells. Thus, PNT2 and LNCaP cells were treated with <sup>nat</sup>In-DOTAGA-AO (10 and 50  $\mu$ M) for 6 hours (Figure 18) or 72 hours (Figure 19).

Results depicted in Figure 14 show that PNT2 cells treated with <sup>nat</sup>In-DOTAGA-AO have higher ECAR values over time compared to respective control. This alteration reflects in the glycolytic parameters in graphics B-D. Thus, we observed a significant increase in glycolysis (Figure 18B), glycolysis capacity (Figure 18C), and glycolytic reserve (Figure 18D) of PNT2 cells treated with 10  $\mu$ M <sup>nat</sup>In-DOTAGA-AO. These same parameters are also increased in PNT2 cells treated with 50  $\mu$ M <sup>nat</sup>In-DOTAGA-AO, although not significant. In contrast, the treatment with <sup>nat</sup>In-DOTAGA-AO did not induce significant alterations in the glycolytic function of LNCaP cancer cells, although we observed a slight tendency to decrease glycolytic parameters under 50  $\mu$ M <sup>nat</sup>In-DOTAGA-AO treatment. Of note, experiments performed with LNCaP are preliminary and have a lower sample size (2 independent experiments), for which the variability is elevated. Thus, more assays are needed with this experimental condition.

Data represented in Figure 15 show the glycolytic activity of PNT2 and LNCaP cells after a long-term incubation with <sup>nat</sup>In-DOTAGA-AO. Results evidenced that the effect observed after 6 hours incubation with the compound is maintained after 72 hours. Thus, normal prostate PNT2 cells, 10  $\mu$ M <sup>nat</sup>In-DOTAGA-AO for 72 hours induced a significant increase in glycolysis (Figure 15B), and glycolytic capacity (Figure 19C). Of

note, PCa LNCaP cells treated with 50  $\mu\text{M}$   $^{nat}\text{In}$ -DOTAGA-AO evidence a slight decrease in some glycolysis parameters, namely glycolysis capacity (Figure 19C) and glycolytic reserve (Figure 19D).

Altogether, data suggest that  $^{nat}\text{In}$ -DOTAGA-AO has an impact on the glycolytic rate of normal prostate PNT2 cells. In addition, although preliminary, our results reveal a promising effect of 50  $\mu\text{M}$   $^{nat}\text{In}$ -DOTAGA-AO in tumoral-cells by decreasing some glycolysis parameters.

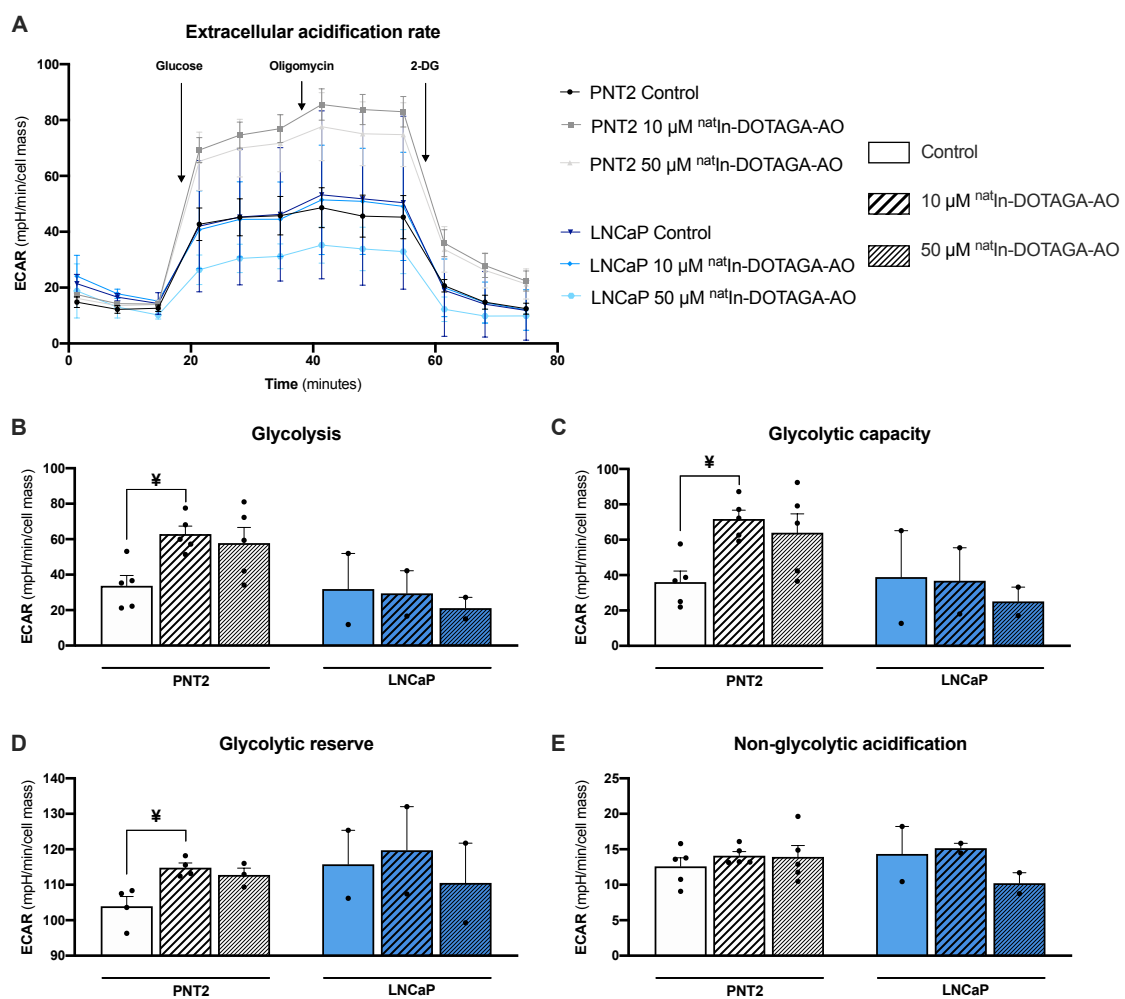


**Figure 18. Impact of short-term exposure to  $^{nat}\text{In}$ -DOTAGA-AO on glycolytic function of PNT2 and LNCaP cells.** The Seahorse XFe96 Extracellular Flux Analyzer was used to measure Extracellular Acidification Rate (ECAR) expressed in mpH//min (A), normalized per cell mass of cells untreated (control) and treated with 10  $\mu\text{M}$  and 50  $\mu\text{M}$   $^{nat}\text{In}$ -DOTAGA-AO for 6 hours. Several glycolytic parameters were evaluated: (B) glycolysis ECAR; (C) glycolysis capacity ECAR; (D) glycolytic reserve ECAR (E) and non-glycolytic acidification ECAR. Data are represented as the mean  $\pm$  SEM of 2 or 3 independent experiments in triplicate. The different conditions were compared to the control by Kruskal-Wallis' followed by Dunn's post-hoc test. Significant differences in PNT2 cells are marked by  $\text{¥}$  ( $p < 0.05$ ).

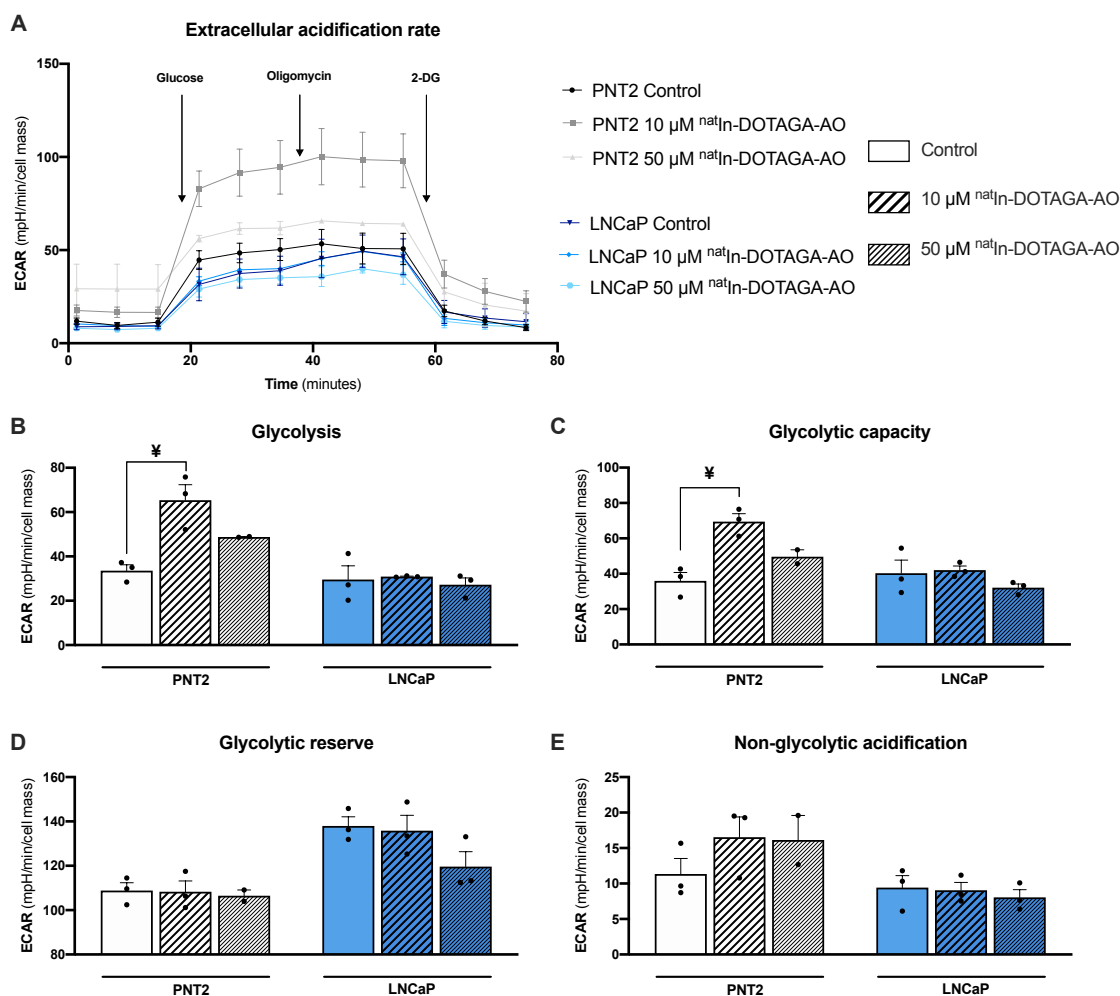


**Figure 19. Impact of long-term exposure to  $^{nat}\text{In-DOTAGA-AO}$  on glycolytic function of PNT2 and LNCaP cells.** The Seahorse XF<sup>e</sup>96 Extracellular Flux Analyzer was used to measure Extracellular Acidification Rate (ECAR) expressed in mpH//min (A), normalized per cell mass of cells untreated (control) and treated with 10  $\mu\text{M}$  and 50  $\mu\text{M}$   $^{nat}\text{In-DOTAGA-AO}$  for 72 hours. Several glycolytic parameters were evaluated: (B) glycolysis ECAR; (C) glycolysis capacity ECAR; (D) glycolytic reserve ECAR (E) and non-glycolytic acidification ECAR. Data are represented as the mean  $\pm$  SEM of 2 or 3 independent experiments in triplicate. The different conditions were compared to the control by Kruskal-Wallis' followed by Dunn's post-hoc test. Significant differences in PNT2 cells are marked by ¥ ( $p < 0.05$ ).

### 3.3.4. Short-term $^{nat}\text{In-DOTAGA-AO}$ treatment increased basal and ATP production-linked respiration of PC3-FLU cells while long-term exposure to 50 $\mu\text{M}$ $^{nat}\text{In-DOTAGA-AO}$ decreases mitochondrial function of cells overexpressing PSMA

Although the compound  $^{nat}\text{In-DOTAGA-AO}$  does not have a tag to target the PSMA protein, we evaluated its potential off-target effects on the mitochondrial respiration of tumoral cells PC3-FLU (no PSMA expression) and PC3-PIP (PSMA

overexpression) cells. Once again, the impact of short- (Figure 16) and long-term (Figure 17)  $^{nat}In$ -DOTAGA-AO (10 or 50  $\mu$ M) treatment were assessed through the Mito stress assay.

Data depicted in Figure 20 indicate that PC3-FLU cells treated with both 10  $\mu$ M and 50  $\mu$ M evidenced a slight increase in basal (Figure 20D), maximal (Figure 20E), ATP production-linked (Figure 20F,  $p < 0.05$  for 50  $\mu$ M vs control), and proton leak-linked respiration (Figure 20G) as well as non-mitochondrial respiration (Figure 20J). On the other hand, treatment of PC3-PIP has no effect on mitochondrial respiration.

Then, we evaluated the long-term exposure to  $^{nat}In$ -DOTAGA-AO, treating PC3-FLU and PC3-PIP cells with  $^{nat}In$ -DOTAGA-AO (10 and 50  $\mu$ M) for 72 hours. The results obtained are shown in Figure 21. Overall,  $^{nat}In$ -DOTAGA-AO treatment appears to decrease mitochondrial respiration of treated cells. Contrary to what was observed in PC3-FLU cells treated with  $^{nat}In$ -DOTAGA-AO for 6 hours the OCR values appear to decrease, with increasing the exposure time. In addition, although there are no statistically significant results, all the parameters of mitochondrial respiration of PC3-FLU cells seem to be affected by  $^{nat}In$ -DOTAGA-AO, with a strong decrease in basal (Figure 21D), maximal (Figure 21E), and ATP production-linked respiration (Figure 21F). Additionally, proton leak-linked respiration (Figure 21G), spare respiratory capacity (Figure 21H), coupling efficiency (Figure 21I) and non-mitochondrial respiration (Figure 21J) were slightly decrease. Interestingly, the long-term treatment of PC3-PIP cells significantly affect it mitochondrial respiration in a concentration-dependent manner and induce a switch from an energetic profile to a glycolytic one (Figure 21C). Thus, 50  $\mu$ M  $^{nat}In$ -DOTAGA-AO significantly decreased basal (Figure 21D), maximal (Figure 21E), ATP production-linked (Figure 21F), and proton leak-linked respiration (Figure 21G), as well as coupling efficiency (Figure 21I) in tumoral PC3-PIP cells.

Therefore, overall data suggest that  $^{nat}In$ -DOTAGA-AO negatively affects the mitochondrial activity of PC3-PIP cells in a concentration- and time-dependent manner. Furthermore, data shows a shift in the metabolism of both PC3-FLU and PC3-PIP cells treated with 50  $\mu$ M  $^{nat}In$ -DOTAGA-AO, becoming more glycolytic mainly by reducing OXPHOS-dependent respiration.

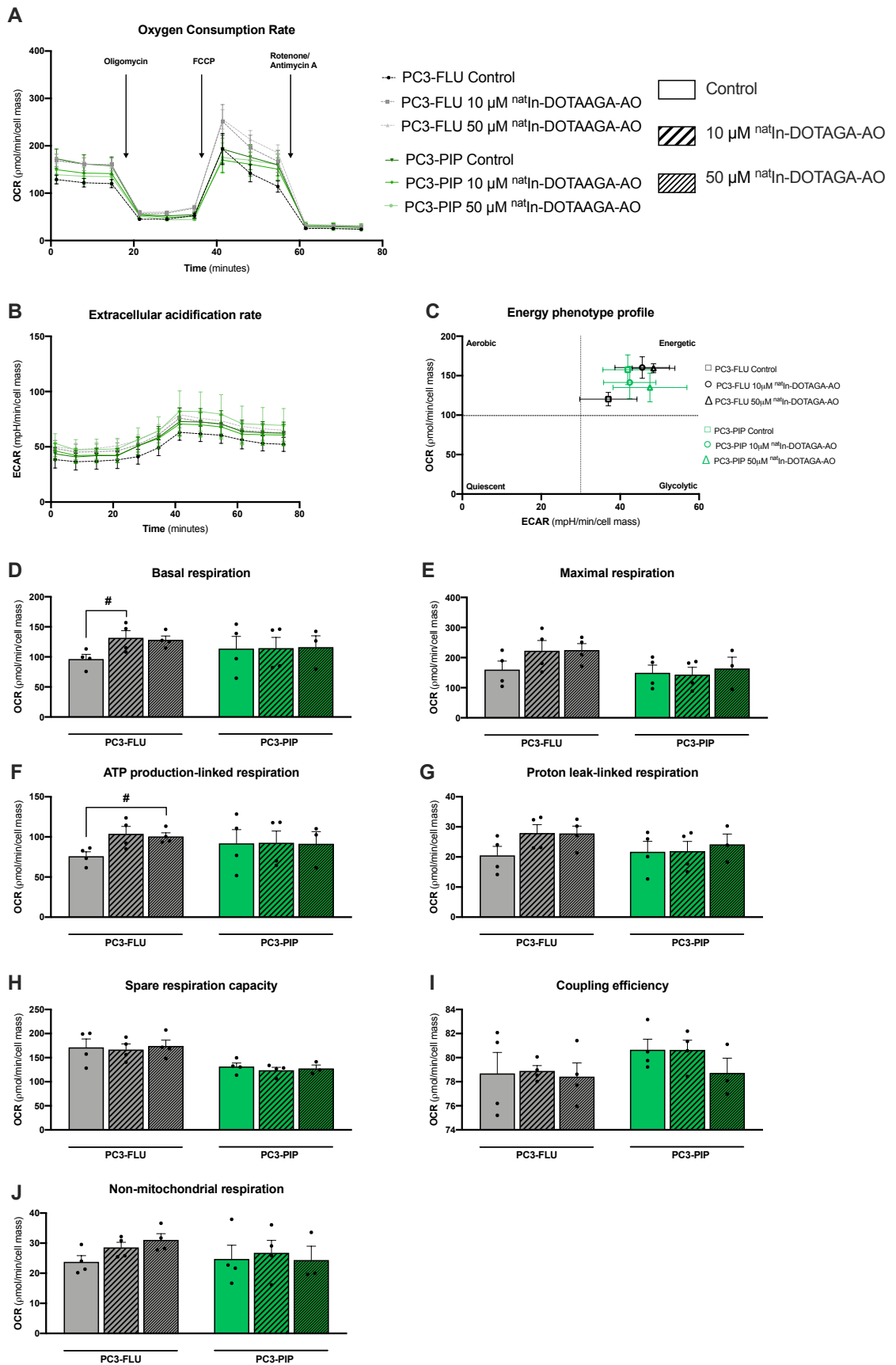


**Figure 20. Impact of short-term exposure to <sup>nat</sup>In-DOTAGA-AO on mitochondrial oxygen consumption of PC3-FLU and PC3-PIP cells.** The Seahorse XF<sup>e</sup>96 Extracellular Flux Analyzer was used to measure Oxygen Consumption Rate (OCR) expressed as pmol/min (**A**), and Extracellular Acidification Rate (ECAR) expressed in mpH//min (**B**), both normalized per cell mass of cells untreated (control) and treated with 10 μM and 50 μM <sup>nat</sup>In-DOTAGA-AO for 6 hours. (**C**) The values of the last OCR and ECAR rate measured before first injection were displayed as a scatter plot to assess the energetic profile. Several respiratory parameters were evaluated: (**D**) basal OCR; (**E**) maximal OCR; (**F**) ATP production-linked OCR (**G**) proton leak-linked OCR; (**H**) spare respiration capacity OCR; (**I**) coupling efficiency OCR; and (**J**) non-mitochondrial OCR. Data are represented as the mean ± SEM of 3-6 independent experiments in triplicate. The different conditions were compared to the control by Kruskal-Wallis' followed by Dunn's post-hoc test. Significant differences in PC3-FLU cells are marked by # (p < 0.05).

### **3.3.5 Long-term <sup>nat</sup>In-DOTAGA-AO treatment increases PC3-FLU cells glycolytic reserve**

Considering the switch in energetic profile in tumoral PC3-FLU and PC3-PIP cells observed in Figure 21, we performed the Glycolytic stress test on both cells under exposure to <sup>nat</sup>In-DOTAGA-AO. Figure 22 evidence no effect of 6 hours incubation with <sup>nat</sup>In-DOTAGA-AO in both PC3-FLU and PC3-PIP cells while Figure 23 show a significant increase of the glycolytic reserve of PC3-FLU cells after 72 hours treatment with 50 μM <sup>nat</sup>In-DOTAGA (Figure 23D). Thus, results suggest that changes in glycolytic profile obtained from the Mito Stress assay are not directly related with major changes in the glycolytic pathway but rather to changes in the OXPHOS respiration.

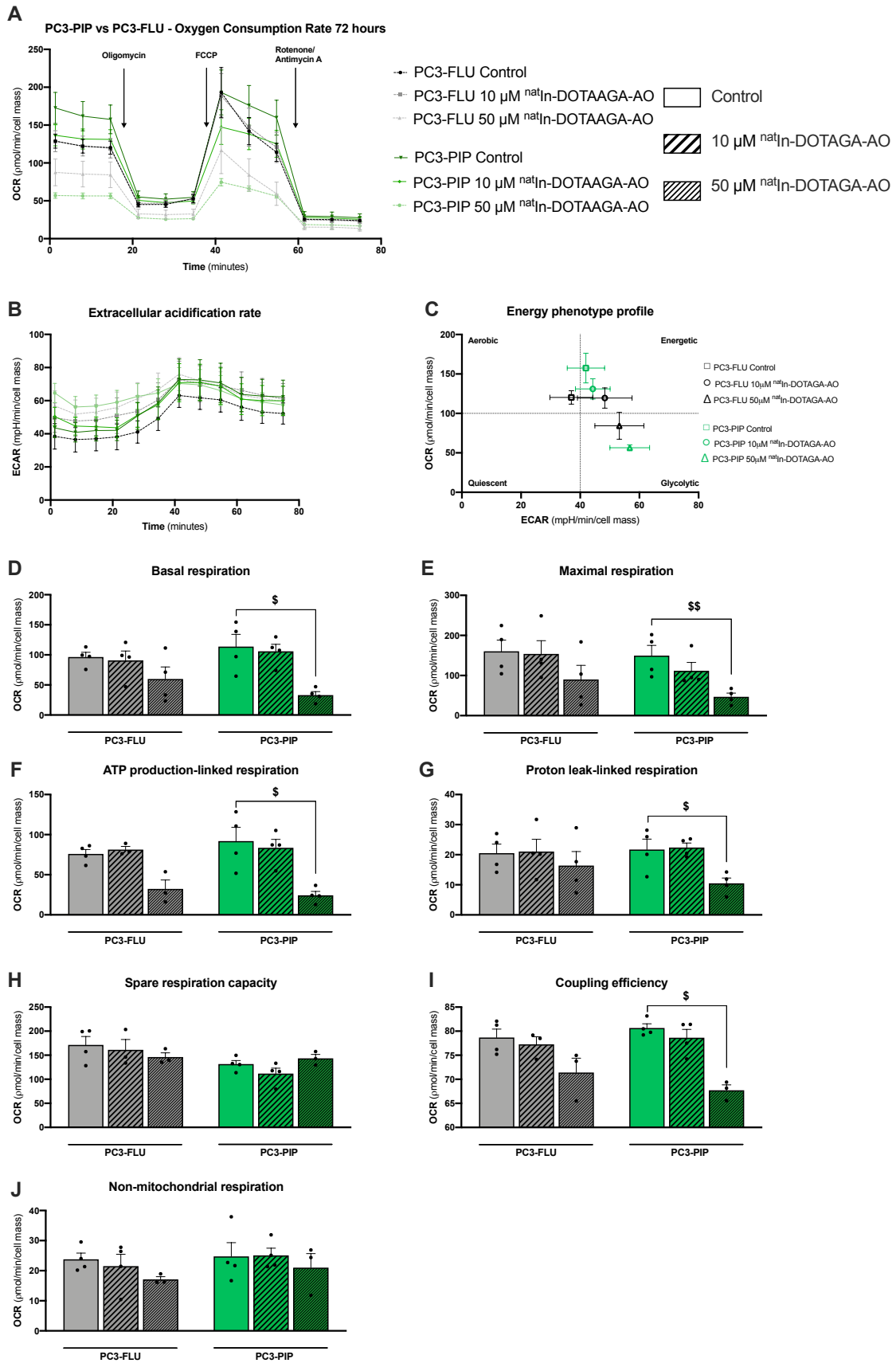


**Figure 21. Impact of long-term exposure to <sup>nat</sup>In-DOTAGA-AO on mitochondrial oxygen consumption of PC3-FLU and PC3-PIP cells.** The Seahorse XF<sup>e</sup>96 Extracellular Flux Analyzer was used to measure Oxygen Consumption Rate (OCR) expressed as pmol/min (A), and Extracellular Acidification Rate (ECAR) expressed in mpH//min (B), both normalized per cell mass of cells untreated (control) and treated with 10 μM and 50 μM <sup>nat</sup>In-DOTAGA-AO for 72 hours. (C) The values of the last OCR and ECAR rate measured before first injection were displayed as a scatter plot to assess the energetic profile. Several respiratory parameters were evaluated: (D) basal OCR; (E) maximal OCR; (F) ATP production-linked OCR (G) proton leak-linked OCR; (H) spare respiration capacity OCR; (I) coupling efficiency OCR; and (J) non-mitochondrial OCR. Data are represented as the mean ± SEM of 3-6 independent experiments in triplicate. The different conditions were compared to the control by Kruskal-Wallis's followed by Dunn's post-hoc test. Significant differences in PC3-PIP cells are marked by \$ (p < 0.05), \$\$ (p < 0.01).

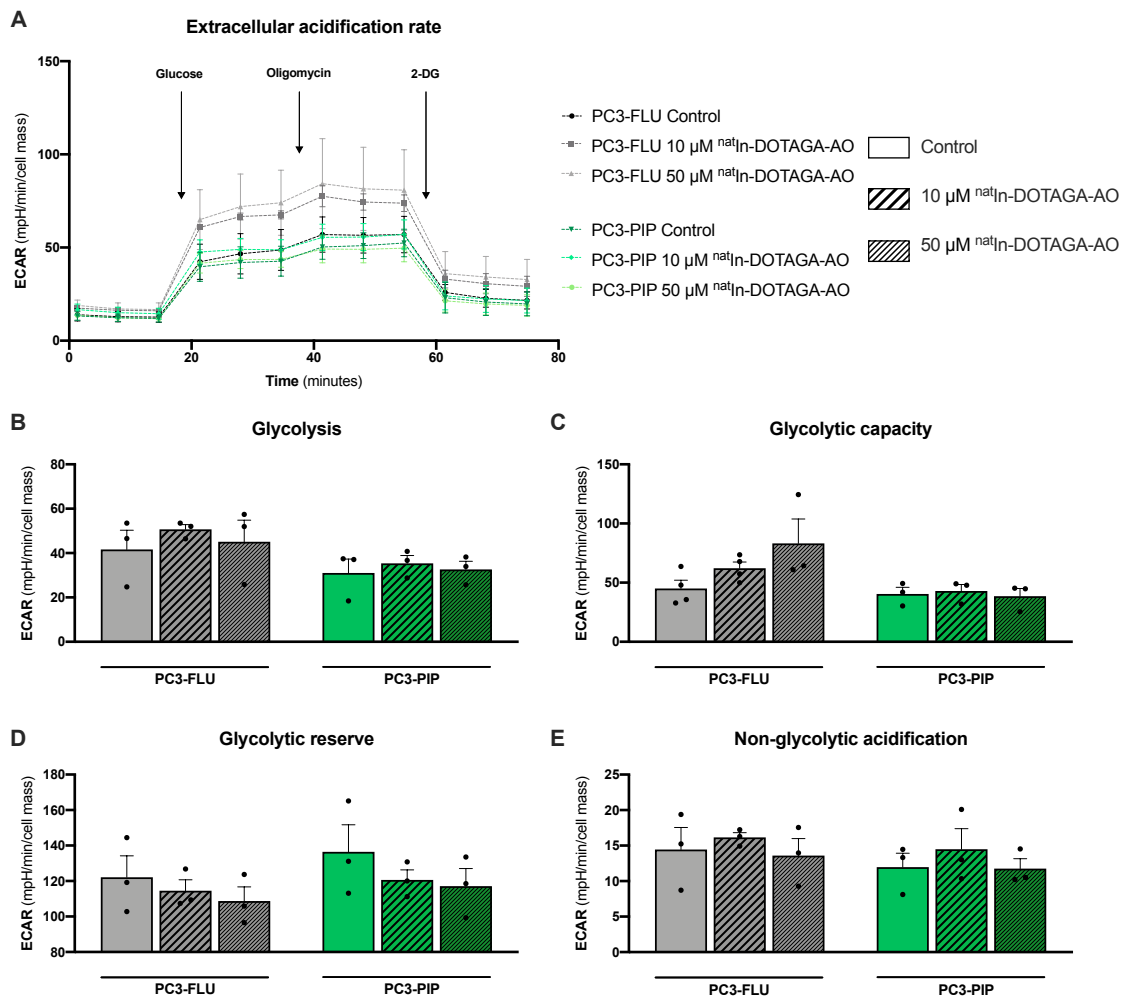


**Figure 22. Impact of short-term exposure to <sup>nat</sup>In-DOTAGA-AO on glycolytic function of PC3-FLU and PC3-PIP cells.** The Seahorse XF<sup>e</sup>96 Extracellular Flux Analyzer was used to measure Extracellular Acidification Rate (ECAR) expressed in mpH//min (A), normalized per cell mass of cells untreated (control) and treated with 10 μM and 50 μM <sup>nat</sup>In-DOTAGA-AO for 6 hours. Several glycolytic parameters were evaluated: (B) glycolysis ECAR; (C) glycolysis capacity ECAR; (D) glycolytic reserve ECAR (E) and non-glycolytic acidification ECAR. Data are represented as the mean ± SEM of 2 or 3 independent experiments in triplicate. The different conditions were compared to the control by Kruskal-Wallis's followed by Dunn's post-hoc test.

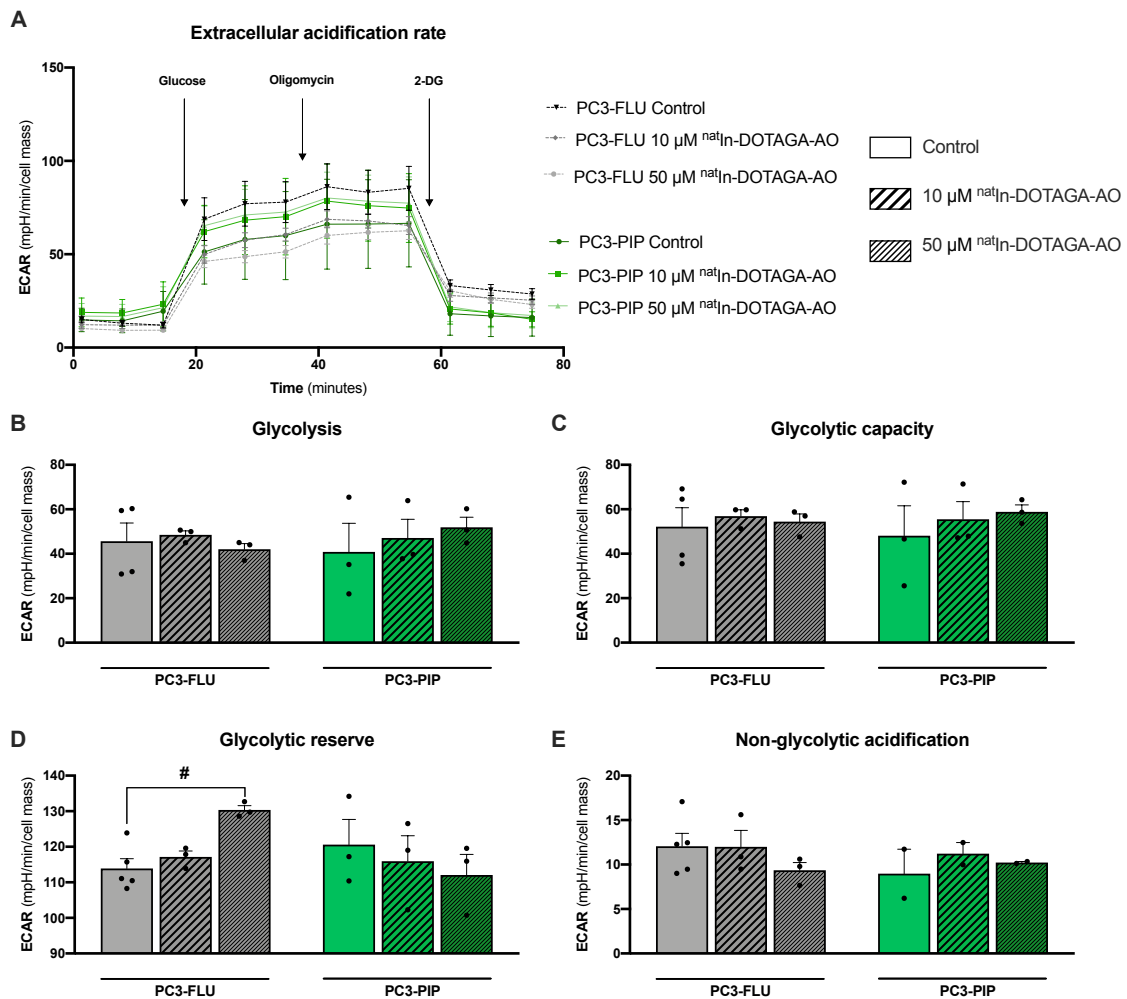


**Figure 23. Impact of short-term exposure to  $^{nat}\text{In-DOTAGA-AO}$  on glycolytic function of PC3-FLU and PC3-PIP cells.** The Seahorse XF<sup>e</sup>96 Extracellular Flux Analyzer was used to measure Extracellular Acidification Rate (ECAR) expressed in mpH//min (A), normalized per cell mass of cells untreated (control) and treated with 10  $\mu\text{M}$  and 50  $\mu\text{M}$   $^{nat}\text{In-DOTAGA-AO}$  for 72 hours. Several glycolytic parameters were evaluated: (B) glycolysis ECAR; (C) glycolysis capacity ECAR; (D) glycolytic reserve ECAR (E) and non-glycolytic acidification ECAR. Data are represented as the mean  $\pm$  SEM of 2 or 3 independent experiments in triplicate. The different conditions were compared to the control by Kruskal-Wallis's followed by Dunn's post-hoc test. Significant differences in PC3-FLU cells are marked by # ( $p < 0.05$ ).

### 3.3.6. $^{nat}\text{In-DOTAGA-AO}$ decreases the mitochondrial membrane potential of PNT2 cells while it increases the mitochondrial membrane potential of PC3-PIP cells

To uncover the differences in the mitochondrial function observed above, mitochondrial membrane potential was indirectly assessed using TMRM dye by confocal imaging after treatment with 50  $\mu\text{M}$   $^{nat}\text{In-DOTAGA-AO}$  for 72 hours (Figure 24) Interestingly, data evidence that the compound induces a significant decrease in the

mitochondrial membrane potential of normal prostate PNT2 cells, and, in contrast, a significant increase in tumoral PC3-PIP cells. No differences were found in PCa LNCaP cells treated with  $\mu\text{M}^{\text{nat}}\text{In-DOTAGA-AO}$  for 72 hours.

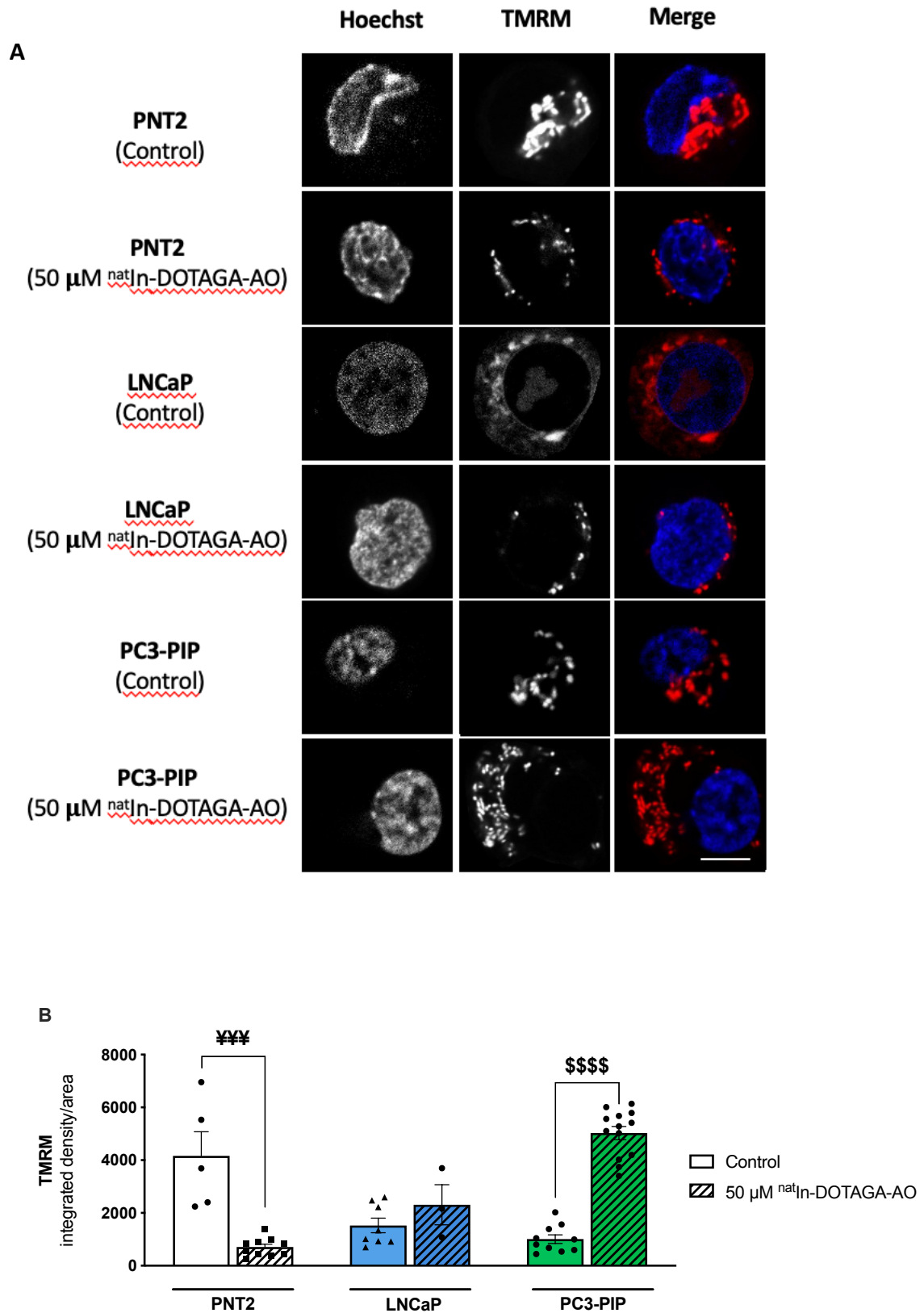


**Figure 24. Impact of  $^{nat}In$ -DOTAGA-AO treatment on mitochondrial network area and mitochondrial membrane potential.** (A) Representative confocal images of PNT2, LNCaP, and PC3-PIP cells treated or not (control) with  $^{nat}In$ -DOTAGA-AO for 72 hours obtained using TMRM and Hoechst for mitochondrial and nuclei labeling, respectively. Scale bar = 10  $\mu$ m. (B) Area under the curve of single cell integrated density per area (from threshold 1-254). Data are expressed as mean  $\pm$  SEM for 5 untreated PNT2 cells and 10 treated PNT2 cells; 8 untreated LNCaP cells and 3 treated LNCaP cells; 10 untreated PC3-PIP cells and 13 treated PC3-PIP cells, obtained from one single experiment. Each treated cells condition of each cell line was compared to the respective untreated cells condition. Statistical analysis was performed using the non-parametric test Mann-Whitney. Significant differences in PNT2 cells are marked by ¥¥¥ (p < 0.001). Significant differences in PC3-PIP cells are marked by \$\$\$\$ (p < 0.0001).

### 3.3.7 $^{nat}In$ -DOTAGA-AO treatment increased mitochondrial reactive oxygen species levels in LNCaP cells

Since our results evidence that long-term treatment with  $^{nat}In$ -DOTAGA-AO induces a significant decrease in the mitochondrial respiration in both tumoral cell lines LNCaP and PC3-PIP cells, we evaluate if changes in mitochondrial respiration could be related with changes in mitochondrial superoxide levels. For that purpose, cells were treated with  $^{nat}In$ -DOTAGA-AO (10 and 50  $\mu$ M) for 72 hours and the mitochondrial superoxide anion levels were quantified using MitoSOX (Figure 25 and 26).

Graphics of the fluorescence variation along time (Figure 25 and 26, i) evidenced no major detectable changes during the 20 minutes of acquisition. Thus, we replotted the basal value of fluorescence for each condition on graphics ii of Figure 25 and 26. Normal prostate cells PNT2 show no significant difference in superoxide levels (Figure 25Ai), although there is a tendency to an increase. In tumoral cells,  $^{nat}In$ -DOTAGA-AO induced a concentration-dependent significant increase in the levels of superoxide as depicted in Figure 25Bii (LNCaP), Figure 26 A and B ii (PC3-FLU and PC3-PIP, respectively). Therefore, results suggest that long-term exposure to 50  $\mu$ M  $^{nat}In$ -DOTAGA induce an increase in non-tumoral and tumoral cell lines.

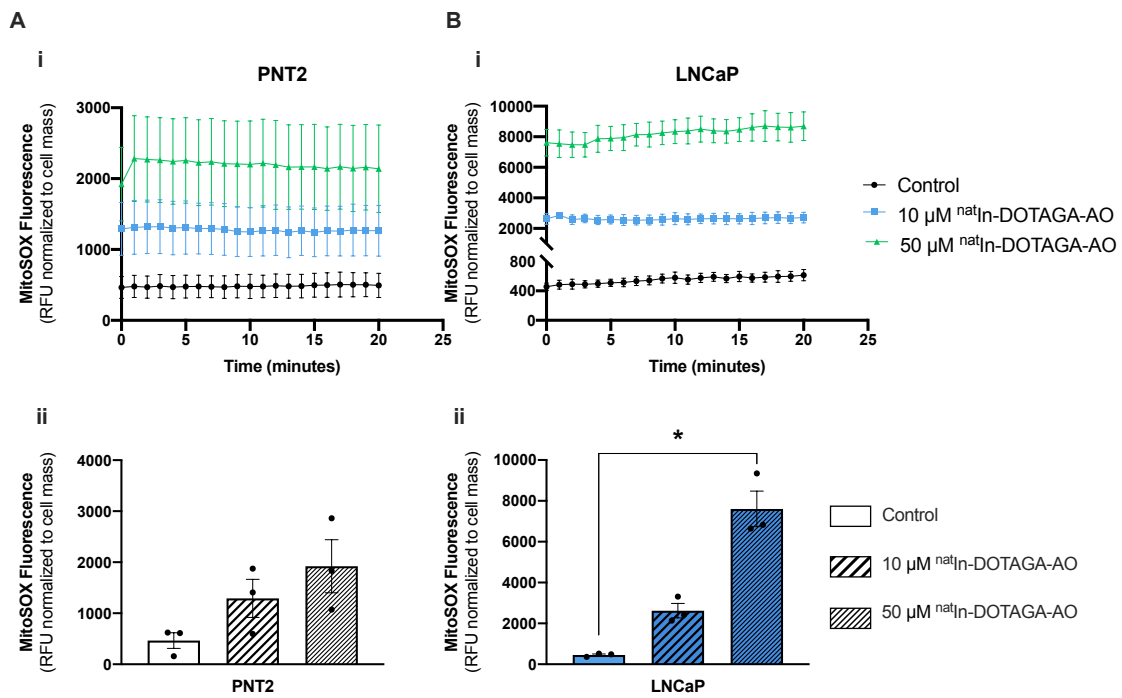


**Figure 25. Impact of  $^{nat}\text{In}$ -DOTAGA-AO treatment on mitochondrial superoxide anion production on PNT2 and LNCaP cells.** (A) The fluorescent report molecule (MitoSOX) was used to measure the mitochondrial superoxide anion levels (over time) of PNT2 and LNCaP cells untreated (control) and treated with 10  $\mu\text{M}$  and 50  $\mu\text{M}$   $^{nat}\text{In}$ -DOTAGA-AO for 72 hours. (B) Basal mitochondrial superoxide anion levels. Data are represented as the mean  $\pm$  SEM of 3 independent experiments in triplicate. The different conditions were compared to the control by Kruskal-Wallis' followed by Dunn's post-hoc test. Significant differences in LNCaP cells are marked by \* ( $p < 0.05$ ).

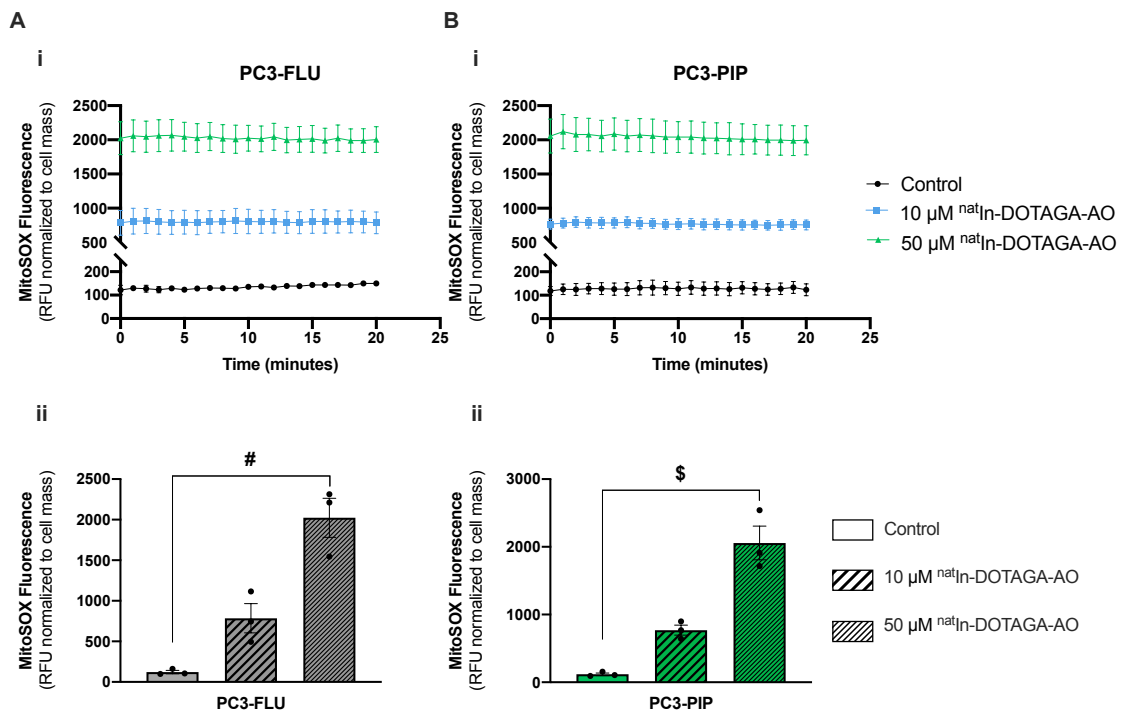


**Figure 26. Impact of  $^{nat}\text{In-DOTAGA-AO}$  treatment on mitochondrial superoxide anion production on PC3-FLU and PC3-PIP cells. (A)** The fluorescent report molecule (MitoSOX) was used to measure the mitochondrial superoxide anion levels (over time) of PC3-FLU and PC3-PIP cells untreated (control) and treated with 10  $\mu\text{M}$  and 50  $\mu\text{M}$   $^{nat}\text{In-DOTAGA-AO}$  for 72 hours. **(B)** Basal mitochondrial superoxide anion levels. Data are represented as the mean  $\pm$  SEM of 3 independent experiments in triplicate. The different conditions were compared to the control by a one-way ANOVA followed by Kruskal-Wallis's post-test. Significant differences in PC3-FLU cells are marked by # ( $p < 0.05$ ). Significant differences in PC3-PIP cells are marked by \$ ( $p < 0.05$ ).

## 4. Discussion

During the last decades, TRT has emerged as an efficient intervention for cancer treatment (Pouget et al. 2015; Chang T et al. 2020). TRT strategies involves the use of radiocomplexes comprising a high-affinity PCa cell-targeting ligand attached to therapeutic and diagnostic radionuclides which emit charged particles during decaying process. The specific targeting is achieved by intrinsic targeting properties of some radionuclides or by conjugating the radionuclide to a delivery molecule or vector, which specifically targets to biomarkers present in malignant tissue (Ramogida et al. 2013; Dekempeneer et al. 2016). For PCa, targeting PSMA has shown enormous potential since it is a transmembrane protein markedly overexpress on the cell surface of prostate malignant tissue (Uijen et al. 2021; Chang S 2004; Rahbar et al. 2018). Indeed, PSMA is an excellent target for both diagnosis and treatment of PCa, and it has been focused on several studies (Haberkorn et al. 2016; Muller et al. 2019). The most common strategies to target PSMA are an antibody-based modality that uses antibodies as targeting vectors, and approaches that use small-molecule enzyme inhibitors or binding agents (Haberkorn et al. 2016). Considering the antibody based TRT targeting to PSMA, several preclinical studies have been performed using different murine monoclonal antibodies (mAb), including mu7E11, muJ591, muJ533 and muE99, and humanized antibody huJ591 (Czerwinska et al. 2020). Of note, 7E11 mAb conjugated with capromab peptide (CYT-365) radiolabeled with the  $\gamma$ -emitter  $^{111}\text{In}$  ( $^{111}\text{In}$ -7E11/CYT-365), was the first radioimmunoconjugate designed and approved by the FDA for PCa patients (Kahn et al. 1994), followed by others (Czerwinska et al. 2020; Dev et al. 1996; do Pazo et al. 2021)

In 2000, the first  $\alpha$ -emitting radionuclides-based therapy targeting PSMA, the radioconjugate  $^{213}\text{Bi}$ -J591, was tested by McDevitt and colleagues *in vitro* (LNCaP cells) and in an *in vivo* model. The promising results of this first agent triggered new studies with antibodies conjugated with  $\alpha$ -emitting radionuclides (Czerwinska et al. 2020; McDevitt et al. 2000). Thus, in May 2021, Telix Pharmaceuticals started the phase III trial of a radiopharmaceutical targeting PSMA, TLX591 ( $^{177}\text{Lu}$ -DOTArosopatomab) (do Pazo et al. 2021). As previously mentioned, another strategy to target PSMA is using small-

molecule enzyme inhibitors or binding agents. So far, only three structures have been synthesized to target PSMA successfully: PSMA-11, PSMA<sub>617</sub> and PSMAI&T. These compounds are based on the same binding moiety that binds the enzymatic pocket of PSMA, inhibiting the glutamate carboxypeptidase activity of this protein (Miyahira et al 2018). In recent years, these compounds labeled with different radionuclides, namely  $\alpha$ -,  $\beta$ -, and AE-emitting radionuclides, have been used in numerous clinical studies (Czerwinska et al. 2020). In general, PSMA-11, PSMA<sub>617</sub> and PSMAI&T demonstrated high PSMA cellular specificity and fast pharmacokinetics, however, adverse effects have also been reported due to accumulated radioactivity in various off-target organs (Czerwinska et al. 2020). Additionally, in the last years, Novartis carries out three different phases III trial, one of them using <sup>177</sup>Lu-PSMA<sub>617</sub> [NCT 03511664] (do Pazo et al. 2021), which was recently approved by FDA for the treatment of PSMA-positive metastatic castration-resistant PCa (Novartis, March 2022)

In the AugerTher project, we aimed to develop novel TRT strategies based on AE-radionuclide emitters attached to PSMA<sub>617</sub> to ensure a specific internalization by PCa cells. The characterization of our cells evidenced that PNT2, a normal prostate epithelial cell line, did not express PSMA. Same results were observed with PC3-FLU cells which do not express PSMA. In contrast, LNCaP, derived from a lymph node metastatic prostate carcinoma, and PC3-PIP, transduced to overexpress PSMA showed PSMA positive labelling by Western blotting. Moreover, besides the 100 kDa band, which corresponds to PSMA, our Western blotting also detected a slight band at 200 kDa, as well as positive bands between 100 and 200 kDa. Liu et al. 2014 hypothesized that the labelling detected by Western blotting after incubation with an anti-PSMA antibody could be either from the cell surface PSMA or the vesicle PSMA, which is internalized into endosomes. Their data suggest that PSMA can be enriched in endosomes, exhibiting a higher content of glycosylation and partial proteolysis in comparison to cellular PSMA. (Liu T et al. 2014) In this sense, Yuan et al. 2022 evidenced that PSMA structure has numerous sites susceptible to glycosylation and identified several PSMA glycoforms in prostate human cell lines and prostate tissue, which, they believe, could be associated with different prostate cancer staging (Yuan W et al. 2022), an information that could be used to improve PCa diagnosis. Thus, the different bands that we observed only on

PSMA-expressing cells are probably labelling PSMA and reflect different cell phenotypes.

In our study, we initially assessed the cellular effects of the synthesized PSMA<sub>617</sub> compound and verified no toxicity in the used models. Indeed, we did not register any changes neither in cell mass nor in metabolic activity of cells treated with PSMA<sub>617</sub> for 72 hours. Additionally, we assessed the impact of short- and long-term exposure to PSMA<sub>617</sub> on the metabolism of normal prostate cells (PNT2) and PCa cells (LNCaP) through the Seahorse XFe96 Analyzer using the Mito stress test and Glycolytic stress test to assess mitochondrial- or glycolytic-associated parameters, respectively. Although we found no differences in the evaluated mitochondrial parameters in PNT2 cells, PSMA<sub>617</sub> treatment increased glycolysis, glycolytic capacity, and glycolytic reserve of cells treated with 50  $\mu$ M PSMA<sub>617</sub> for 6 hours. Moreover, curiously, long-term treatment with PSMA<sub>617</sub> (10 and 50  $\mu$ M) did not the glycolytic parameters of PNT2 cells, suggesting that these cells are sensitive to the treatment in a time-independent manner. Furthermore, our data showed that treatment with PSMA<sub>617</sub> in LNCaP cells only induced a decreased spare respiration capacity in cells treated with 10  $\mu$ M PSMA<sub>617</sub> for 72 hours. In the parameters associated with glycolysis, neither the short- nor the long-term treatment induced significant changes in LNCaP cells. Additionally, data showed that normal prostate PNT2 cells produce energy predominantly through the glycolytic pathway and the PCa LNCaP are more aerobic cells, using mitochondrial respiration as main source of energy. In 1923, Otto Warburg found evidence that cancer cells rely heavily on glycolysis to generate ATP. Initially, it was thought that the mitochondria of cancer cells were dysfunctional and therefore the cells opted for the glycolytic pathway. However, it was later discovered that cancer cells produce ATP via glycolysis even though they have fully functional mitochondria and oxygen available, in which acid lactic fermentation favors the cancer cells proliferation in the hypoxia microenvironment (Payen et al., 2020; San-Millán & Brooks, 2017; Xu et al., 2015)). This shift in cellular energetics is known as the Warburg effect and it is not common to all cancer cells, being dependent on cell type and type of cancer (Ashton et al. 2018; Xu et al. 2015; Wallace et al 2012). Importantly, in the 1940s, Huggins and colleagues (Barron and Hugging et al. 1944) characterized prostate metabolism using isolated dog and rabbit prostate tissue and found that

normal prostate tissue relies on the glycolytic pathway instead of OXPHOS even under aerobic conditions. Following studies evidenced that peripheral prostatic epithelium has an androgen receptor-mediated metabolic program that favors the production, accumulation, and secretion of citrate into the prostatic fluid (Putluri et al. 2011; Bader and McGuire 2020). Outstanding, the citrate synthesis relies on the condensation of aspartate-derived oxaloacetate and glucose-derived acetyl-CoA in the mitochondrial matrix. In addition, zinc-mediated aconitase 2 inhibition prevents citrate oxidation, resulting in citrate production, which is coupled with a mandatory physiological truncation of the TCA cycle. Consequently, normal prostate tissue uses the glycolytic pathway to produce energy because it cannot produce reducing equivalents in the TCA cycle to power the ETC chain (Mycielska et al. 2009; Costello and Franklin 2016; Bader and McGuire 2020). In contrast, prostate adenocarcinoma relies on OXPHOS to produce energy. During the malignant transformation of normal prostate tissue, the physiological truncation of the TCA is abolished. Once again, the metabolic reprogramming is predominantly under androgen receptor control, which when activated drives to clinical progression of PCa by lipogenesis and OXPHOS enhancement (Costello and Franklin 2016; Bader and McGuire 2020). Moreover, in prostate adenocarcinoma, mitochondrial aconitase 2 is activated because of zinc depletion. Consequently, citrate is oxidized in the TCA cycle or exported to the cytoplasm for use as de novo lipogenic substrate (Costello and Franklin 2016; Bader and McGuire 2020; Mycielska et al. 2009). Thus, our results are in accordance with the literature. In fact, in basal or control conditions, normal prostate PNT2 cells produce energy mainly through the glycolytic pathway while the PCa LNCaP are more aerobic cells, using mitochondrial respiration as predominant source of energy.

PNT2 cells do not express PSMA, however, they are sensitive to PSMA<sub>617</sub>. We sought to find whether the presence or absence of PSMA could play a role in the metabolic response of tumoral cells to PSMA<sub>617</sub> treatment. Thus, we used two tumoral cell lines derived from the PC3 cell line which do not express PSMA: the PC3-PIP cells, generated by transduction using VSV-G pseudotyped lentiviral vector expressing human PSMA to overexpress PSMA; and isogenic PSMA negative cells PC3-FLU. Data evidence that the tumoral cell line PC3-PIP is not sensitive to PSMA<sub>617</sub>, while the cell line PC3-FLU

shows a concentration-dependent response to the compound, similarly to what happened with the LNCaP and PNT2 cells, respectively. These results suggest that cell lines without PSMA are more sensitive to PSMA<sub>617</sub> than cells expressing the PSMA protein which is surprising. Moreover, we found that untreated (control) PC3-FLU and PC3-PIP cells have both a predominantly aerobic metabolism, using OXPHOS as the main energy source. Curiously, PSMA<sub>617</sub> treatment induce a metabolic shift only in PC3-FLU cells which became more energetic (producing energy by both OXPHOS and glycolysis) in a concentration-dependent manner. The analysis of the glycolytic function of PC3-FLU and PC3-PIP cells treated with PSMA<sub>617</sub> evidenced no alterations, which is not surprising since PCa cells rely on OXPHOS to produce energy. Thus, our data suggest that the response of cells to PSMA<sub>617</sub> treatment is independent of whether cell has a normal or cancerous phenotype. Moreover, cells without PSMA protein seems to be more sensitive to PSMA<sub>617</sub> than cells expressing the protein.

The function of PSMA within the cell remains unclear (Emmett et al. 2017; Uijen et al. 2021). Moreover, so far, we do not know if there is any interaction between PSMA<sub>617</sub> compound and PSMA protein as well as if the compound is internalized. Xi Hong and colleagues performed metabolomic and transcriptomic analysis in PSMA-knockdown LNCaP and 22rv1 cell lines to assess the effect of PSMA on PCa cells transcription and modulation of metabolism. Interestingly, their results evidenced that PSMA knockdown induces metabolic disorder and abnormal transcription promoting the biosynthesis of arginine and proline in PCa and leading to cell proliferation and migration inhibition (Hong et al. 2022). Despite our study does not assess PSMA<sub>617</sub> – PSMA interaction or internalization of either the protein or the compound or the complex, we were able to observe in the case of PC3-PIP cells a tendency to decrease mitochondrial respiration-related parameters and a slight shift to a more quiescent energetic profile after long-term treatment with 50  $\mu$ M PSMA<sub>617</sub>. This result, although non-significant, suggest that treatment with PSMA<sub>617</sub> in cells expressing PSMA may lead to the internalization of PSMA protein leading to a decrease in cell metabolism which at long-term can lead to cell proliferation and migration inhibition.

In comparison to  $\alpha$ - and  $\beta$ -particles, AE generate low energy with subcellular range (< 100 nm), yielding high LET (4-26 keV) resulting in high radiotoxicity when

located close to radiosensitive targets with limited non-specific radiotoxicity to healthy neighboring cells (Czerwinska et al. 2020; Costa et al. 2021). Therefore, AE-emitting radionuclides are interesting alternative to the  $\alpha$ - and  $\beta$ -emitting radionuclides, and promising appealing tools for the treatment of micro metastasis and circulating tumor cells (Costa et al. 2021). Among therapeutic AE-emitters, several studies evidence  $^{125}\text{I}$  and  $^{111}\text{In}$  as potential radionuclides to consider for clinical translation (Bodei et al. 2003; Unverricht-Yeboah et al. 2020; Costa et al. 2021). So far,  $^{111}\text{In}$  has been evaluated in both breast cancer and neuroendocrine tumors (Othman et al. 2020). Moreover, there is a commercially available  $^{111}\text{In}$  radionuclide TRT ( $^{111}\text{In}$ -Pentetrotide; Phe-D-octreotide) which have an attached octreotide analog for somatostatin receptor specific targeting (Knapp et al. 2016). The  $^{111}\text{In}$ -Pentetrotide internalization by octreotide analog – somatostatin receptor mediation and subsequent therapeutic effectiveness of intracellular AE emission has been demonstrated in both animal tumor models (de Jong et al. 1998) and human tumors *in vivo* (Krenning et al. 1996). Also, AugerTher project aim to develop novel dual-targeting  $^{111}\text{In}$  radionuclides complexes with high-affinity to PCa (ensured by PSMA<sub>617</sub>), and their organelles, namely the nucleus and mitochondria. Therefore, in the present study we performed preliminary work with the  $^{nat}\text{In}$ -DOTAGA-AO. In this cold surrogate the native form of Indium ( $^{nat}\text{In}$ ) was stabilized by DOTAGA chelator and functionalized with AO, a fluorescent and cell-permeable probe commonly used for nuclear cell staining which intercalates DNA and RNA (Baskic et al. 2006; Agorastos et al. 2007). The binding of these probe to double-strand DNA interferes with important biological processes, namely DNA synthesis and gene transcription and translation (Nafisi et al. 2006). We observed a successful internalization of the compound in all the cell lines. Data evidenced a nuclear accumulation of  $^{nat}\text{In}$ -DOTAGA-AO for the four cell lines, and we confirmed the mitochondrial accumulation in PNT2, LNCaP and PC3-PIP cells (PC3-FLU have not been tested). Of note, PCa LNCaP cells presented higher internalization of the compound, and seem to accumulate more compound in the mitochondria than in the nucleus.

When looking at  $^{nat}\text{In}$ -DOTAGA-AO toxicity, data suggested that the compound did not induce cytotoxicity in PNT2, LNCaP, PC3-FLU and PC3-PIP cells. Moreover, data showed that short-term  $^{nat}\text{In}$ -DOTAGA-AO treatment (10  $\mu\text{M}$ ) significantly increased

basal and maximal respiration of PNT2 cells, and although without significance, the respiration associated to ATP production. Curiously, treatment with 50  $\mu\text{M}$  for the same period of exposure, only increased the coupling efficiency of LNCaP. In contrast, long-term treatment with 50  $\mu\text{M}$   $^{nat}\text{In}$ -DOTAGA-AO treatment significantly increased basal and maximal respiration, as well as ATP production-linked and proton leak-linked respiration of PNT2 cells. Treatment with 10  $\mu\text{M}$   $^{nat}\text{In}$ -DOTAGA-AO significantly increased the cellular coupling efficiency. Moreover, data showed that some of the evaluated glycolytic parameters were increased in PNT2 treated cells. In detail, short-term treatment with 10  $\mu\text{M}$   $^{nat}\text{In}$ -DOTAGA-AO increased glycolysis, glycolytic capacity, and glycolytic reserve. Also, although no significant the same parameters seem to be slightly increased in PNT2 cells treated with 50  $\mu\text{M}$   $^{nat}\text{In}$ -DOTAGA-AO for 6 hours. Long-term treatment induced an increased glycolysis and glycolytic capacity of PNT2 cells treated with 10  $\mu\text{M}$   $^{nat}\text{In}$ -DOTAGA-AO. Interestingly, our Mito stress test data suggested a significant reduction in mitochondrial function of PNT2 cells, in a concentration-dependent manner, shifting the cells to a quiescent profile.

Furthermore, data showed that, although short-term  $^{nat}\text{In}$ -DOTAGA-AO treatment (10 and 50  $\mu\text{M}$ ) did not induce alterations in the mitochondrial function of LNCaP cells, increasing the exposure time induced some cellular response of LNCaP. Indeed, long-term treatment with 50  $\mu\text{M}$  markedly decreased basal, maximal, ATP production-linked, and proton leak-linked respiration, as well as the spare respiration capacity of LNCaP cells. In contrast, the evaluated glycolytic parameters were not altered in LNCaP treated cells. Interestingly, taken together, data evidenced a more quiescent profile of LNCaP, in a time- and concentration-dependent manner.

Regarding tumoral PC3 cells, PC3-FLU showed a slight increase in mitochondrial respiration-related parameters (basal and ATP production-linked respiration) after short-term treatment with  $^{nat}\text{In}$ -DOTAGA-AO. Although long-term treatment did not induce significant alterations in PC3-FLU cells, data suggested a slightly decreased in all the assessed mitochondrial parameters in PC3-FLU cells treated with 50  $\mu\text{M}$   $^{nat}\text{In}$ -DOTAGA-AO, similarly to results observed for non-tumoral PNT2 cells, also lacking PSMA protein. In PC3-PIP, which overexpress PSMA, data clearly showed that  $^{nat}\text{In}$ -DOTAGA-AO negatively affects the mitochondrial respiration in a concentration- and time-

dependent manner. In detail, our data suggested that any mitochondrial parameter changed in PC3-PIP treated cells for 6 hours, and in contrast, long-term treatment with 50  $\mu\text{M}$   $^{nat}\text{In}$ -DOTAGA-AO markedly decreased basal, maximal, ATP production-linked, and proton leak-linked respiration, as well as PC3-PIP coupling efficiency. Furthermore, Mito Stress assay evidenced a shift to a more glycolytic profile in treated PC3-PIP, was not proven by our Glycolytic Stress test since we did not find changes to support this hypothesis. Indeed, we only reported an increased glycolytic reserve of PC3-FLU cells treated with 50  $\mu\text{M}$   $^{nat}\text{In}$ -DOTAGA-AO for 72 hours. Curiously, although the  $^{nat}\text{In}$ -DOTAGA-AO compound is not expected to interact with PSMA protein, we reported similar changes in both non-tumoral and tumoral cells not expressing PSMA, suggesting that PSMA expression may affect the cellular response to the compound, but little is known in this regard. Importantly, the comparison of our data evidence that values of basal and maximal respiration, as well as mitochondrial respiration-associated ATP production and proton leak from tumoral cells (LNCaP, PC3-PIP and PC3-Flu) treated with 50  $\mu\text{M}$   $^{nat}\text{In}$ -DOTAGA-AO, decrease to reach values similar to those of untreated non-tumoral PNT2 cells. PNT2 cells, which are predominantly glycolytic have a low mitochondrial function compared to tumoral cells, which undergo a switch to aerobic profile during malignant transformation becoming more aerobic (Costello and Franklin 2016; Bader and McGuire 2020). Thus, data suggest that 50  $\mu\text{M}$   $^{nat}\text{In}$ -DOTAGA-AO treatment induce the tumoral cells to adopt a less aerobic energetic profile, similar to the glycolytic normal prostate cells.

The OXPHOS involves an electron flux that allows the pumping of protons from the mitochondrial matrix to the intermembrane space, producing a proton gradient. These protons return to the mitochondrial matrix through the ATP synthase, leading to ATP formation by ADP phosphorylation (Payen et al. 2020). Indeed, the basal mitochondrial respiration refers to hydrolyzed ATP in order to meet cellular demand. Moreover, maximal mitochondrial respiration is assessed by uncoupling the mitochondria respiration, which means that at this point, respiration is only limited by substrate oxidation (Sotolongo et al. 2020) Our findings, in general, suggested that  $^{nat}\text{In}$ -DOTAGA-AO induced a decreased basal respiration in our cell lines, which means they are demanding less energy. Interestingly, this data agrees with our results that

suggested a shift in the energetic profile, with PNT2, LNCaP and PC3-PIP becoming quiescent (i.e., cells are not very energetic via either OXPHOS or glycolytic pathway). Moreover, our data reported significant decrease in maximal respiration of treated cells, suggesting that the limiting factor of in mitochondrial respiration of treated cells is the substrate oxidation in the ETC. Furthermore, this implies a reduction or even blockage of the pumping of protons from the mitochondrial matrix to the intermembrane space, so that the membrane potential does not favor the return of protons back to the mitochondrial matrix. Therefore, it is expected that consequently, there is a decrease in proton leak. Indeed, our data showed decreased proton leak-linked respiration with treated cells. Concomitantly, and consequently, there is a decreased in ATP production, as we observed measuring the ATP production-linked respiration. Taken together, our findings suggested that <sup>nat</sup>In-DOTAGA-AO may be uncoupling mitochondrial respiration by interfering/inhibiting ETC complexes. Since <sup>nat</sup>In-DOTAGA-AO binds mtDNA interfering with DNA synthesis and gene transcription and translation (Nafisi et al. 2006), it may be affecting the expression of mitochondrial proteins encoded by the mitochondrial genome, with essential function in mitochondrial processes, namely proteins from the ETC complexes.

Although our data are not conclusive, targeting OXPHOS elements, namely complexes or ATP synthase, is not something new. Indeed, several studies propose that inhibition of ETC (Yang Q et al. 2021; Basit et al. 2017) and inhibition of ATP synthase (Fiorillo et al. 2021) are potential strategies for the treatment of cancer. Yang and colleagues showed that the targeting of ETC complexes I and III limits the proliferation of liver cancer cells in cell lines, liver organoids, and xenografts *in vivo*. This restriction is associated to reduced ATP production, increased ROS levels, and induction of apoptosis (Yang Q et al. 2021). Also, using a panel of BRAF<sup>V600E</sup> melanoma cell lines, Basit and colleagues report that ETC complex I inhibition induce a dose-dependently decrease cell viability, and significantly increase the production of ROS, and reduction in cellular ATP levels (Basit et al. 2017). Moreover, Fiorillo and his team, found that Bedaquiline, an FDA-approved antibiotic which binds directly to ATP synthase gamma-subunit (ATP5F1C), induces mitochondrial ATP depletion in a time- and -concentration-

dependent manner, inhibiting spontaneous metastasis *in vivo*, without significant toxicity in MCD10A human cells *in vitro* or chicken embryos *in vivo* (Fiorillo et al. 2021).

Importantly, as we have been seen, a fundamental aspect for the proper functioning of mitochondria and respiration is the balance between in both the flow of electrons and the exchange of protons. Thus, MMP reflects the functional mitochondrial status, and therefore, small changes in MMP values have a significant effect on mitochondrial energetics (DeHart et al. 2018; Distelmaier et al. 2008). Moreover, dysfunctional mitochondria and impaired respiration induce ROS production, namely mitochondrial superoxide, which result from electron leakage of ETC chain and their transfer to molecular oxygen (Fuhrmann et al. 2017). Although low levels of mitochondrial ROS may play a role in essential cell signaling pathways for maintaining cell homeostasis, exacerbated mitochondrial ROS production induce several deleterious effects, leading to mitochondrial dysfunction and ultimately cell death (Amorim et al. 2022). Importantly, mitochondrial membrane depolarization and increased ROS production, among other death signals, induce the release of cytochrome C, and other pro-apoptotic proteins (e.g., AIF, Smac and endonuclease G) as well, activating downstream the effector caspase 9 to carry out the apoptotic pathway (Burke P 2017; Zaib et al. 2022). Taking this in account, and in an attempt to better understand how <sup>nat</sup>In-DOTAGA-AO could be affecting our *in vitro* models, especially in terms of mitochondrial response, we assessed the MMP of PNT2, LNCaP and PC3-PIP treated cells (50  $\mu$ M <sup>nat</sup>In-DOTAGA-AO; 72 hours) using TMRM dye by confocal imaging. Moreover, mitochondrial superoxide levels of PNT2, LNCaP, PC3-FLU, and PC3-PIP cells treated with <sup>nat</sup>In-DOTAGA-AO (10 and 50  $\mu$ M; 72 hours) were assessed using MitoSOX. Our results evidenced that while the MMP of treated PNT2 cells decreased markedly compared to untreated cells (control), the MMP of PC3-PIP cells increases dramatically. Moreover, the MMP of treated LNCaP cells slightly increases although not statistically significant. Furthermore, data indicate that long-term exposure to 50  $\mu$ M <sup>nat</sup>In-DOTAGA induces an increase in non-tumoral and tumoral cell lines mitochondrial ROS, with emphasis on the LNCaP cells for which presented much higher levels of mitochondrial ROS when compared to the other cell lines, in these conditions.

Importantly, data clearly indicated that the MMP of untreated normal prostate PNT2 cells is higher than the MMP of untreated tumoral cells, LNCaP and PC3-PIP. Moreover, 50  $\mu\text{M}$   $^{nat}\text{In-DOTAGA-AO}$  in PC3-PIP and LNCaP cells increases the MMP values to values similar to untreated PNT2 cells. As we have seen with mitochondrial respiration parameters  $^{nat}\text{In-DOTAGA-AO}$  treatment appears to induce a behavioral change in tumoral cells, which seem to adopt a cellular response similar to the non-tumoral counterparts.

Although cell death is associated with membrane depolarization with subsequent release of cytochrome c and activation of the apoptotic pathway (Burke P 2017; Zaib et al. 2022), hyperpolarization, as our data showed for tumoral LNCaP and PC3-PIP cells, can also lead to the same endpoint, cell death. Interestingly, Hsiao et al. 2019 assessed the anti-cancer properties of honokiol, an active component of *Magnolia officinalis*, against bladder cancer; and found that honokiol-induced apoptosis is mediated by ROS accumulation and transient hyperpolarization of the mitochondria membrane (Hsiao et al. 2019). However, our results were not accompanied by decrease cell proliferation. Literature also suggest that mitochondrial hyperpolarization may occur due to a metabolic shift, from an aerobic energetic profile to a predominantly glycolytic metabolism that results in lactate production and subsequent cytosol acidification (Nguyen et al. 2019; Bhat et al. 2015); however, our results do not report evidence significant changes in glycolytic function of LNCaP or PC3-PIP cells. Importantly, the maximum duration of our treatments were 72 hours, and therefore, those events might occur in a different timeline, as the cellular response and adaptation to treatment may take longer.



## 5. Conclusion and future perspectives

The AugerTher project aim to synthesize dual-targeted (PCa and organelle) metal complexes attached to a PSMA ligand (PSMA<sub>617</sub>) to ensure a specific internalization in PCa cells. Moreover, the structure of the compounds would be functionalized with other ligands, a DNA intercalator (AO) or a mitochondriotropic group (TPP<sup>+</sup>) to direct the pharmacophore to the nucleus or mitochondria, respectively.

In the present study, we aim to assess whether PSMA<sub>617</sub> alone and <sup>nat</sup>In-DOTAGA-AO could induce some effects on viability and cellular metabolism of PCa. Our findings suggests that the response of cells to PSMA<sub>617</sub> alone do not induce toxicity to the cells but are accompanied by small alterations in mitochondrial and glycolytic function. Furthermore, results suggest that PSMA<sub>617</sub> treatment is independent of whether cell has a normal or cancerous phenotype. Interestingly, we evidence that PSMA<sub>617</sub> alone induce changes in cells that do not express PSMA. Moreover, results, although non-significant, suggest that treatment with PSMA<sub>617</sub> in cells expressing PSMA may lead to the internalization of PSMA protein leading to a decrease in cell metabolism which at long-term can lead to cell proliferation and migration inhibition. On the other hand, <sup>nat</sup>In-DOTAGA-AO which internalizes within cell nucleus and mitochondria do not induce toxicity in our *in vitro* models. However, <sup>nat</sup>In-DOTAGA-AO induce changes in mitochondrial and glycolytic function, MMP, and mitochondrial ROS levels which tend to revert cancerous phenotype. Thus, our study evidence that <sup>nat</sup>In-DOTAGA-AO, without being fully functionalized have a significant impact on cells, supporting the development of this compound functionalized with the ligands PSMA<sub>617</sub> and TPP<sup>+</sup> to target PCa cells and their mitochondria, respectively; as well as the radioactive isotope of <sup>111</sup>In instead of the native form.

This work is the first steps of a major project and a necessary preliminary work to support the production of an anti-cancer therapy. We expect to further assess whether the PSMA<sub>617</sub> interacts with PSMA protein with subsequent internalization, using for instance a labelled PSMA<sub>617</sub> to assess the distribution and co-localization of the

compound through confocal microscopy. Although the treatment of cells with  $^{nat}\text{In}$ -DOTAGA-AO for 72 hours revealed no toxicity, we reported several effects on cells, namely in terms of remodeled cell bioenergetics. Therefore, it would be important to increase treatment time in cell viability assays. Moreover, it would be interesting to assess the effects reported in this study in more detail. Due to the decreased mitochondrial function and its related parameters, we should assess the mitochondrial content and mitochondrial network morphology through confocal imaging, using Hoechst and TMRM for nuclei and mitochondria labeling, respectively. Additionally, it would be interesting to evaluate the expression levels of proteins related to mitochondrial dynamics and bioenergetic remodeling namely fusion proteins (e.g., MFN1, MFN2 and OPA1) and fission proteins (e.g., Drp1 and Fis1), by western blotting or immunocytochemistry. The process of mitophagy could also be assessed using live imaging and a plasmid construct (mitoKeima). Finally, we could assess the protein expression levels of endogenous ROS/RNS-scavengers such as SOD, Prx, GPxs catalase, by western blotting.

The future perspectives of AugerTher project include synthesizing compounds initially with reactive isotopes, such as  $^{nat}\text{In}$  (in the future with AE-emitting radionuclides as  $^{111}\text{In}$ ), functionalized with PSMA<sub>617</sub> and TPP<sup>+</sup> to ensure targeting to PCa cells and their mitochondria, respectively. Further, it will be necessary to assess the biological effects of these new/re-structured compounds in 2D (e.g., PNT2, LNCaP, PC3, DU145, 22rv1 cell lines) and 3D multicellular spheroids *in vitro* models, and in *in vivo* models such as C57BL/6J-congenic Pten<sup>flox</sup>.

## 6. References

- [1] T. G. Chan, E. O'Neill, C. Habjan, and B. Cornelissen, "Combination Strategies to Improve Targeted Radionuclide Therapy," *J. Nucl. Med.*, vol. 61, no. 11, pp. 1544–1552, Nov. 2020.
- [2] K. Sotolongo, J. Ghiso, and A. Rostagno, "Nrf2 activation through the PI3K/GSK-3 axis protects neuronal cells from A $\beta$ -mediated oxidative and metabolic damage," *Alzheimers. Res. Ther.*, vol. 12, no. 1, p. 13, Dec. 2020.
- [3] W. Yuan et al., "Glycoforms of human prostate-specific membrane antigen (PSMA) in human cells and prostate tissue," *Prostate*, vol. 82, no. 1, pp. 132–144, Jan. 2022.
- [4] T. LIU, D. E. MENDES, and C. E. BERKMAN, "Functional prostate-specific membrane antigen is enriched in exosomes from prostate cancer cells," *Int. J. Oncol.*, vol. 44, no. 3, pp. 918–922, Mar. 2014.
- [5] X. Hong, L. Mao, L. Xu, Q. Hu, and R. Jia, "Prostate-specific membrane antigen modulates the progression of prostate cancer by regulating the synthesis of arginine and proline and the expression of androgen receptors and Fos proto-oncogenes," *Bioengineered*, vol. 13, no. 1, pp. 995–1012, Jan. 2022.
- [6] B. G. Heerdt, M. A. Houston, and L. H. Augenlicht, "Growth Properties of Colonic Tumor Cells Are a Function of the Intrinsic Mitochondrial Membrane Potential," *Cancer Res.*, vol. 66, no. 3, pp. 1591–1596, Feb. 2006.
- [7] T. A. Bhat, S. Kumar, A. K. Chaudhary, N. Yadav, and D. Chandra, "Restoration of mitochondria function as a target for cancer therapy," *Drug Discov. Today*, vol. 20, no. 5, pp. 635–643, May 2015.
- [8] C. Nguyen and S. Pandey, "Exploiting Mitochondrial Vulnerabilities to Trigger Apoptosis Selectively in Cancer Cells," *Cancers (Basel)*, vol. 11, no. 7, p. 916, Jun. 2019.
- [9] C. Hsiao, C. Yao, G. Lai, L. Lee, J. Whang-Peng, and P. Shih, "Honokiol induces apoptotic cell death by oxidative burst and mitochondrial hyperpolarization of bladder cancer cells," *Exp. Ther. Med.*, Mar. 2019.
- [10] X.-Q. Ye et al., "Mitochondrial and energy metabolism-related properties as novel indicators of lung cancer stem cells," *Int. J. Cancer*, vol. 129, no. 4, pp. 820–831, Aug. 2011.

- [11] S. Bonnet et al., "A Mitochondria-K<sup>+</sup> Channel Axis Is Suppressed in Cancer and Its Normalization Promotes Apoptosis and Inhibits Cancer Growth," *Cancer Cell*, vol. 11, no. 1, pp. 37–51, Jan. 2007.
- [12] P. J. Burke, "Mitochondria, Bioenergetics and Apoptosis in Cancer," *Trends in Cancer*, vol. 3, no. 12, pp. 857–870, Dec. 2017.
- [13] M. Onishi, K. Yamano, M. Sato, N. Matsuda, and K. Okamoto, "Molecular mechanisms and physiological functions of mitophagy," *EMBO J.*, vol. 40, no. 3, p. e104705, 2021.
- [14] R. Amorim et al., "Mitochondriotropic antioxidant based on caffeic acid AntiOxClN4 activates Nrf2-dependent antioxidant defenses and quality control mechanisms to antagonize oxidative stress-induced cell damage," *Free Radic. Biol. Med.*, vol. 179, pp. 119–132, Feb. 2022.
- [15] D. C. Fuhrmann and B. Brüne, "Mitochondrial composition and function under the control of hypoxia," *Redox Biol.*, vol. 12, pp. 208–215, Aug. 2017.
- [16] D. N. DeHart, D. Fang, K. Heslop, L. Li, J. J. Lemasters, and E. N. Maldonado, "Opening of voltage dependent anion channels promotes reactive oxygen species generation, mitochondrial dysfunction and cell death in cancer cells," *Biochem. Pharmacol.*, vol. 148, pp. 155–162, Feb. 2018.
- [17] S. Zaib, A. Hayyat, N. Ali, A. Gul, M. Naveed, and I. Khan, "Role of Mitochondrial Membrane Potential and Lactate Dehydrogenase A in Apoptosis," *Anticancer. Agents Med. Chem.*, vol. 22, no. 11, pp. 2048–2062, Jul. 2022.
- [18] M. Fiorillo, C. Scatena, A. G. Naccarato, F. Sotgia, and M. P. Lisanti, "Bedaquiline, an FDA-approved drug, inhibits mitochondrial ATP production and metastasis in vivo, by targeting the gamma subunit (ATP5F1C) of the ATP synthase," *Cell Death Differ.*, vol. 28, no. 9, pp. 2797–2817, Sep. 2021.
- [19] F. Basit et al., "Mitochondrial complex I inhibition triggers a mitophagy-dependent ROS increase leading to necroptosis and ferroptosis in melanoma cells," *Cell Death Dis.*, vol. 8, no. 3, pp. e2716–e2716, Mar. 2017.
- [20] Q. Yang, L. Wang, J. Liu, W. Cao, Q. Pan, and M. Li, "Targeting the complex I and III of mitochondrial electron transport chain as a potentially viable option in liver cancer management," *Cell Death Discov.*, vol. 7, no. 1, p. 293, Dec. 2021.

- [21] C.-H. Liu, S. L. Sahoo, and M.-H. Tsao, "Acridine orange coated magnetic nanoparticles for nucleus labeling and DNA adsorption," *Colloids Surfaces B Biointerfaces*, vol. 115, pp. 150–156, Mar. 2014.
- [22] S. Nafisi, A. A. Saboury, N. Keramat, J.-F. Neault, and H.-A. Tajmir-Riahi, "Stability and structural features of DNA intercalation with ethidium bromide, acridine orange and methylene blue," *J. Mol. Struct.*, vol. 827, no. 1–3, pp. 35–43, Feb. 2007.
- [23] E. P. Krenning et al., "Somatostatin Receptor: Scintigraphy and Radionuclide Therapy," *Digestion*, vol. 57, no. 1, pp. 57–61, 1996.
- [24] M. de Jong et al., "Comparison of (111)In-labeled somatostatin analogues for tumor scintigraphy and radionuclide therapy.," *Cancer Res.*, vol. 58, no. 3, pp. 437–41, Feb. 1998.
- [25] M. F. bin Othman et al., "In vitro cytotoxicity of Auger electron-emitting [67Ga]Ga-trastuzumab," *Nucl. Med. Biol.*, vol. 80–81, pp. 57–64, Jan. 2020.
- [26] M. E. Mycielska et al., "Citrate transport and metabolism in mammalian cells," *BioEssays*, vol. 31, no. 1, pp. 10–20, Jan. 2009.
- [27] N. Putluri et al., "Metabolomic Profiling Reveals a Role for Androgen in Activating Amino Acid Metabolism and Methylation in Prostate Cancer Cells," *PLoS One*, vol. 6, no. 7, p. e21417, Jul. 2011.
- [28] L. C. Costello and R. B. Franklin, "A comprehensive review of the role of zinc in normal prostate function and metabolism; and its implications in prostate cancer," *Arch. Biochem. Biophys.*, vol. 611, pp. 100–112, Dec. 2016.
- [29] "Barron, E. S. G. & Huggins, C. The metabolism of isolated prostatic tissue. *J. Urol.* 51, 630–634 (1944)."
- [30] D. A. Bader and S. E. McGuire, "Tumour metabolism and its unique properties in prostate adenocarcinoma," *Nat. Rev. Urol.*, vol. 17, no. 4, pp. 214–231, Apr. 2020.
- [31] J.-P. Pouget, C. Lozza, E. Deshayes, V. Boudousq, and I. Navarro-Teulon, "Introduction to Radiobiology of Targeted Radionuclide Therapy," *Front. Med.*, vol. 2, Mar. 2015.
- [32] I. Bohovych and O. Khalimonchuk, "Sending Out an SOS: Mitochondria as a Signaling Hub," *Front. Cell Dev. Biol.*, vol. 4, Oct. 2016.

- [33] J. Xiang, C. Wan, R. Guo, and D. Guo, "Is Hydrogen Peroxide a Suitable Apoptosis Inducer for All Cell Types?," *Biomed Res. Int.*, vol. 2016, pp. 1–6, 2016.
- [34] I. M. Costa, J. Cheng, K. M. Osytek, C. Imberti, and S. Y. A. Terry, "Methods and techniques for in vitro subcellular localization of radiopharmaceuticals and radionuclides.," *Nucl. Med. Biol.*, vol. 98–99, pp. 18–29.
- [35] Y.-C. Cheng, I.-L. Hung, Y.-N. Liao, W.-L. Hu, and Y.-C. Hung, "Salvia miltiorrhiza Protects Endothelial Dysfunction against Mitochondrial Oxidative Stress," *Life*, vol. 11, no. 11, p. 1257, Nov. 2021.
- [36] K. E. Verigos, S. Sagredou, K. Orfanakos, P. Dalezis, and D. T. Trafalis, "8-Hydroxy-2'-Deoxyguanosine and 8-Nitroguanine Production and Detection in Blood Serum of Breast Cancer Patients in Response to Postoperative Complementary External Ionizing Irradiation of Normal Tissues.," *Dose. Response.*, vol. 18, no. 4, p. 1559325820982172.
- [37] R. C. Chen et al., "Active Surveillance for the Management of Localized Prostate Cancer (Cancer Care Ontario Guideline): American Society of Clinical Oncology Clinical Practice Guideline Endorsement," *J. Clin. Oncol.*, vol. 34, no. 18, pp. 2182–2190, Jun. 2016.
- [38] J. E. Bekelman et al., "Clinically Localized Prostate Cancer: ASCO Clinical Practice Guideline Endorsement of an American Urological Association/American Society for Radiation Oncology/Society of Urologic Oncology Guideline.," *J. Clin. Oncol.*, vol. 36, no. 32, pp. 3251–3258, Nov. 2018.
- [39] D. F. Gleason and G. T. Mellinger, "Prediction of prognosis for prostatic adenocarcinoma by combined histological grading and clinical staging.," *J. Urol.*, vol. 111, no. 1, pp. 58–64, Jan. 1974.
- [40] T. R. Rebbeck et al., "Global Patterns of Prostate Cancer Incidence, Aggressiveness, and Mortality in Men of African Descent," *Prostate Cancer*, vol. 2013, pp. 1–12, 2013.
- [41] A. Tsodikov et al., "Reconciling the Effects of Screening on Prostate Cancer Mortality in the ERSPC and PLCO Trials," *Ann. Intern. Med.*, vol. 167, no. 7, p. 449, Oct. 2017.
- [42] A. Jemal, M. B. Culp, J. Ma, F. Islami, and S. A. Fedewa, "Prostate Cancer Incidence 5 Years After US Preventive Services Task Force Recommendations Against Screening," *JNCI J. Natl. Cancer Inst.*, vol. 113, no. 1, pp. 64–71, Jan. 2021.

- [43] B. Chazotte, "Labeling mitochondria with MitoTracker dyes.," *Cold Spring Harb. Protoc.*, vol. 2011, no. 8, pp. 990–2, Aug. 2011.
- [44] S. Creed and M. McKenzie, "Measurement of Mitochondrial Membrane Potential with the Fluorescent Dye Tetramethylrhodamine Methyl Ester (TMRM).," *Methods Mol. Biol.*, vol. 1928, pp. 69–76, 2019.
- [45] M. E. Kauffman et al., "MitoSOX-Based Flow Cytometry for Detecting Mitochondrial ROS.," *React. Oxyg. species (Apex, N.C.)*, vol. 2, no. 5, pp. 361–370, 2016.
- [46] B. Kalyanaraman, *Pitfalls of Reactive Oxygen Species (ROS) Measurements by Fluorescent Probes and Mitochondrial Superoxide Determination Using MitoSOX*. 2020.
- [47] M. Adeva-Andany et al., "Comprehensive review on lactate metabolism in human health.," *Mitochondrion*, vol. 17, pp. 76–100, Jul. 2014.
- [48] A. S. Divakaruni, G. W. Rogers, and A. N. Murphy, "Measuring Mitochondrial Function in Permeabilized Cells Using the Seahorse XF Analyzer or a Clark-Type Oxygen Electrode.," *Curr. Protoc. Toxicol.*, vol. 60, pp. 25.2.1–16, May 2014.
- [49] A. van Tonder, A. M. Joubert, and A. D. Cromarty, "Limitations of the 3-(4,5-dimethylthiazol-2-yl)-2,5-diphenyl-2H-tetrazolium bromide (MTT) assay when compared to three commonly used cell enumeration assays.," *BMC Res. Notes*, vol. 8, p. 47, Feb. 2015.
- [50] F. S. G. Silva, I. G. Starostina, V. V Ivanova, A. A. Rizvanov, P. J. Oliveira, and S. P. Pereira, "Determination of Metabolic Viability and Cell Mass Using a Tandem Resazurin/Sulforhodamine B Assay.," *Curr. Protoc. Toxicol.*, vol. 68, pp. 2.24.1-2.24.15, 2016.
- [51] K. Präbst, H. Engelhardt, S. Ringgeler, and H. Hübner, "Basic Colorimetric Proliferation Assays: MTT, WST, and Resazurin.," *Methods Mol. Biol.*, vol. 1601, pp. 1–17, 2017.
- [52] D. Baskić, S. Popović, P. Ristić, and N. N. Arsenijević, "Analysis of cycloheximide-induced apoptosis in human leukocytes: fluorescence microscopy using annexin V/propidium iodide versus acridin orange/ethidium bromide.," *Cell Biol. Int.*, vol. 30, no. 11, pp. 924–32, Nov. 2006.

- [53] N. Agorastos et al., "Cell-specific and nuclear targeting with [M(CO)(3)](+) (M=(99m)Tc, Re)-based complexes conjugated to acridine orange and bombesin.," *Chemistry*, vol. 13, no. 14, pp. 3842–52, 2007.
- [54] P. Sharma and H. Sampath, "Mitochondrial DNA Integrity: Role in Health and Disease.," *Cells*, vol. 8, no. 2, 2019.
- [55] C. Yan, X. Duanmu, L. Zeng, B. Liu, and Z. Song, "Mitochondrial DNA: Distribution, Mutations, and Elimination.," *Cells*, vol. 8, no. 4, 2019.
- [56] D. C. Fuhrmann and B. Brüne, "Mitochondrial composition and function under the control of hypoxia.," *Redox Biol.*, vol. 12, pp. 208–215, 2017.
- [57] L. Guo, "Mitochondria and the permeability transition pore in cancer metabolic reprogramming.," *Biochem. Pharmacol.*, vol. 188, p. 114537, 2021.
- [58] N. Badrinath and S. Y. Yoo, "Mitochondria in cancer: in the aspects of tumorigenesis and targeted therapy.," *Carcinogenesis*, vol. 39, no. 12, pp. 1419–1430, 2018.
- [59] L. P. Poole and K. F. Macleod, "Mitophagy in tumorigenesis and metastasis.," *Cell. Mol. Life Sci.*, vol. 78, no. 8, pp. 3817–3851, Apr. 2021.
- [60] Y. Chen, P. Gao, T. Wu, W. Pan, N. Li, and B. Tang, "Organelle-localized radiosensitizers.," *Chem. Commun. (Camb).*, vol. 56, no. 73, pp. 10621–10630, Sep. 2020.
- [61] E. McCann, J. O'Sullivan, and S. Marcone, "Targeting cancer-cell mitochondria and metabolism to improve radiotherapy response.," *Transl. Oncol.*, vol. 14, no. 1, p. 100905, Jan. 2021.
- [62] I. Heidegger, R. Pichler, A. Heidenreich, W. Horninger, and A. Pircher, "Radium-223 for metastatic castration-resistant prostate cancer: results and remaining open issues after the ALSYMPCA trial.," *Transl. Androl. Urol.*, vol. 7, no. Suppl 1, pp. S132–S134, Mar. 2018.
- [63] C. Parker et al., "Alpha emitter radium-223 and survival in metastatic prostate cancer.," *N. Engl. J. Med.*, vol. 369, no. 3, pp. 213–23, Jul. 2013.
- [64] P. Hoskin et al., "Efficacy and safety of radium-223 dichloride in patients with castration-resistant prostate cancer and symptomatic bone metastases, with or without previous docetaxel use: a prespecified subgroup analysis from the randomised, double-blind, phase 3 ALSYMPCA trial.," *Lancet. Oncol.*, vol. 15, no. 12, pp. 1397–406, Nov. 2014.

- [65] K. Niforou, C. Cheimonidou, and I. P. Trougakos, "Molecular chaperones and proteostasis regulation during redox imbalance.," *Redox Biol.*, vol. 2, pp. 323–32, 2014.
- [66] B. McDonagh, "Detection of ROS Induced Proteomic Signatures by Mass Spectrometry.," *Front. Physiol.*, vol. 8, p. 470, 2017.
- [67] T. Bai et al., "Sigma-1 receptor protects against ferroptosis in hepatocellular carcinoma cells.," *J. Cell. Mol. Med.*, vol. 23, no. 11, pp. 7349–7359, 2019.
- [68] N. Kajarabille and G. O. Latunde-Dada, "Programmed Cell-Death by Ferroptosis: Antioxidants as Mitigators.," *Int. J. Mol. Sci.*, vol. 20, no. 19, Oct. 2019.
- [69] D. Tsikas, "Assessment of lipid peroxidation by measuring malondialdehyde (MDA) and relatives in biological samples: Analytical and biological challenges.," *Anal. Biochem.*, vol. 524, pp. 13–30, May 2017.
- [70] L.-J. Su et al., "Reactive Oxygen Species-Induced Lipid Peroxidation in Apoptosis, Autophagy, and Ferroptosis.," *Oxid. Med. Cell. Longev.*, vol. 2019, p. 5080843, 2019.
- [71] I. B. Slimen, T. Najar, A. Ghram, H. Dabbebi, M. Ben Mrad, and M. Abdrabbah, "Reactive oxygen species, heat stress and oxidative-induced mitochondrial damage. A review.," *Int. J. Hyperthermia*, vol. 30, no. 7, pp. 513–23, Nov. 2014.
- [72] U. S. Srinivas, B. W. Q. Tan, B. A. Vellayappan, and A. D. Jeyasekharan, "ROS and the DNA damage response in cancer.," *Redox Biol.*, vol. 25, p. 101084, 2019.
- [73] R. Zhao, S. Jiang, L. Zhang, and Z. Yu, "Mitochondrial electron transport chain, ROS generation and uncoupling (Review).," *Int. J. Mol. Med.*, May 2019.
- [74] N. Nissanka and C. T. Moraes, "Mitochondrial DNA damage and reactive oxygen species in neurodegenerative disease.," *FEBS Lett.*, vol. 592, no. 5, pp. 728–742, 2018.
- [75] S. Zhao et al., "Recent advances of electrochemical sensors for detecting and monitoring ROS/RNS," *Biosens. Bioelectron.*, vol. 179, p. 113052, May 2021.
- [76] I. Plante, "A review of simulation codes and approaches for radiation chemistry," *Phys. Med. Biol.*, vol. 66, no. 3, p. 03TR02, Feb. 2021.
- [77] Yan, Duanmu, Zeng, Liu, and Song, "Mitochondrial DNA: Distribution, Mutations, and Elimination," *Cells*, vol. 8, no. 4, p. 379, Apr. 2019.
- [78] E. I. Azzam, J.-P. Jay-Gerin, and D. Pain, "Ionizing radiation-induced metabolic oxidative stress and prolonged cell injury," *Cancer Lett.*, vol. 327, no. 1–2, pp. 48–60, Dec. 2012.

- [79] G. Filomeni, D. De Zio, and F. Cecconi, "Oxidative stress and autophagy: the clash between damage and metabolic needs.," *Cell Death Differ.*, vol. 22, no. 3, pp. 377–88, Mar. 2015.
- [80] K. Ragunathan, N. L. E. Upfold, and V. Oksenysh, "Interaction between Fibroblasts and Immune Cells Following DNA Damage Induced by Ionizing Radiation," *Int. J. Mol. Sci.*, vol. 21, no. 22, p. 8635, Nov. 2020.
- [81] D. Einor, A. Bonisoli-Alquati, D. Costantini, T. A. Mousseau, and A. P. Møller, "Ionizing radiation, antioxidant response and oxidative damage: A meta-analysis.," *Sci. Total Environ.*, vol. 548–549, pp. 463–471, Apr. 2016.
- [82] D. S. S. Surasi, B. Chapin, C. Tang, G. Ravizzini, and T. K. Bathala, "Imaging and Management of Prostate Cancer.," *Semin. Ultrasound. CT. MR*, vol. 41, no. 2, pp. 207–221, Apr. 2020.
- [83] H. C. Yoo, Y. C. Yu, Y. Sung, and J. M. Han, "Glutamine reliance in cell metabolism.," *Exp. Mol. Med.*, vol. 52, no. 9, pp. 1496–1516, 2020.
- [84] R. El Ansari, A. McIntyre, M. L. Craze, I. O. Ellis, E. A. Rakha, and A. R. Green, "Altered glutamine metabolism in breast cancer; subtype dependencies and alternative adaptations.," *Histopathology*, vol. 72, no. 2, pp. 183–190, Jan. 2018.
- [85] J. M. Matés, J. A. Campos-Sandoval, J. de L. Santos-Jiménez, and J. Márquez, "Dysregulation of glutaminase and glutamine synthetase in cancer.," *Cancer Lett.*, vol. 467, pp. 29–39, 2019.
- [86] T. Li and A. Le, "Glutamine Metabolism in Cancer.," *Adv. Exp. Med. Biol.*, vol. 1063, pp. 13–32.
- [87] B. J. Altman, Z. E. Stine, and C. V. Dang, "From Krebs to clinic: Glutamine metabolism to cancer therapy," *Nature Reviews Cancer*, vol. 16, no. 10. Nature Publishing Group, pp. 619–634, 23-Sep-2016.
- [88] W. L. Santivasi and F. Xia, "Ionizing Radiation-Induced DNA Damage, Response, and Repair," *Antioxid. Redox Signal.*, vol. 21, no. 2, pp. 251–259, Jul. 2014.
- [89] N. Tang et al., "Assessment of Radio-Induced Damage in Endothelial Cells Irradiated with 40 kVp, 220 kVp, and 4 MV X-rays by Means of Micro and Nanodosimetric Calculations," *Int. J. Mol. Sci.*, vol. 20, no. 24, p. 6204, Dec. 2019.

- [90] M. P. Carante and F. Ballarini, "Radiation Damage in Biomolecules and Cells," *Int. J. Mol. Sci.*, vol. 21, no. 21, p. 8188, Nov. 2020.
- [91] G. Lei et al., "The role of ferroptosis in ionizing radiation-induced cell death and tumor suppression.," *Cell Res.*, vol. 30, no. 2, pp. 146–162, 2020.
- [92] P. Yang et al., "Ionizing Radiation Upregulates Glutamine Metabolism and Induces Cell Death via Accumulation of Reactive Oxygen Species," *Oxid. Med. Cell. Longev.*, vol. 2021, 2021.
- [93] D. Pierre-Victor, H. L. Parnes, G. L. Andriole, and P. F. Pinsky, "Prostate Cancer Incidence and Mortality Following a Negative Biopsy in a Population Undergoing PSA Screening.," *Urology*, vol. 155, pp. 62–69, 2021.
- [94] H. Uno et al., "The accuracy of prostate cancer diagnosis in biopsy-naive patients using combined magnetic resonance imaging and transrectal ultrasound fusion-targeted prostate biopsy.," *Transl. Androl. Urol.*, vol. 10, no. 7, pp. 2982–2989, Jul. 2021.
- [95] M. R. McDevitt et al., "An alpha-particle emitting antibody ([<sup>213</sup>Bi]J591) for radioimmunotherapy of prostate cancer.," *Cancer Res.*, vol. 60, no. 21, pp. 6095–100, Nov. 2000.
- [96] N. Deb et al., "Treatment of hormone-refractory prostate cancer with 90Y-CYT-356 monoclonal antibody.," *Clin. Cancer Res.*, vol. 2, no. 8, pp. 1289–97, Aug. 1996.
- [97] D. Kahn et al., "Radioimmunosintigraphy with <sup>111</sup>Indium Labeled Cyt-356 for the Detection of Occult Prostate Cancer Recurrence," *J. Urol.*, vol. 152, no. 5 Part 1, pp. 1490–1495, Nov. 1994.
- [98] C. do Pazo and R. M. Webster, "The prostate cancer drug market," *Nat. Rev. Drug Discov.*, vol. 20, no. 9, pp. 663–664, Sep. 2021.
- [99] A. K. Miyahira et al., "Meeting report from the Prostate Cancer Foundation PSMA-directed radionuclide scientific working group.," *Prostate*, vol. 78, no. 11, pp. 775–789, 2018.
- [100] N. Lumen, P. Ost, C. Van Praet, G. De Meerleer, G. Villeirs, and V. Fonteyne, "Developments in External Beam Radiotherapy for Prostate Cancer," *Urology*, vol. 82, no. 1, Jul. 2013.
- [101] N. G. Zaorsky et al., "The evolution of brachytherapy for prostate cancer.," *Nat. Rev. Urol.*, vol. 14, no. 7, Jun. 2017.

- [102] J. Crook, M. Marbán, and D. Batchelar, "HDR Prostate Brachytherapy.," *Semin. Radiat. Oncol.*, vol. 30, no. 1, 2020.
- [103] H. A. Gay and J. M. Michalski, "Radiation Therapy for Prostate Cancer.," *Mo. Med.*, vol. 115, no. 2.
- [104] S. W. Dutta, C. E. Alonso, B. Libby, and T. N. Showalter, "Prostate cancer high dose-rate brachytherapy: review of evidence and current perspectives.," *Expert Rev. Med. Devices*, vol. 15, no. 1, 2018.
- [105] S. Brawley, R. Mohan, and C. D. Nein, "Localized Prostate Cancer: Treatment Options.," *Am. Fam. Physician*, vol. 97, no. 12, 2018.
- [106] W. M. Butler and G. S. Merrick, "Focal prostate brachytherapy with 103 Pd seeds," *Phys. Medica*, vol. 32, no. 3, Mar. 2016.
- [107] T. K. Podder, E. T. Fredman, and R. J. Ellis, "Advances in Radiotherapy for Prostate Cancer Treatment.," *Adv. Exp. Med. Biol.*, vol. 1096.
- [108] J.-M. Hannoun-Lévi, "Brachytherapy for prostate cancer: Present and future," *Cancer/Radiothérapie*, vol. 21, no. 6–7, Oct. 2017.
- [109] V. L. Payen, E. Mina, V. F. Van Hée, P. E. Porporato, and P. Sonveaux, "Monocarboxylate transporters in cancer," *Mol. Metab.*, vol. 33, pp. 48–66, 2020.
- [110] W. Dai and L. Jiang, "Dysregulated Mitochondrial Dynamics and Metabolism in Obesity, Diabetes, and Cancer," *Front. Endocrinol. (Lausanne)*, vol. 10, Sep. 2019.
- [111] S. Srinivasan, M. Guha, A. Kashina, and N. G. Avadhani, "Mitochondrial dysfunction and mitochondrial dynamics-The cancer connection," *Biochim. Biophys. Acta - Bioenerg.*, vol. 1858, no. 8, pp. 602–614, Aug. 2017.
- [112] L. D. Popov, "Mitochondrial biogenesis: An update," *J. Cell. Mol. Med.*, vol. 24, no. 9, pp. 4892–4899, May 2020.
- [113] M. Vara-Perez, B. Felipe-Abrio, and P. Agostinis, "Mitophagy in Cancer: A Tale of Adaptation," *Cells*, vol. 8, no. 5, p. 493, May 2019.
- [114] J. P. Bernardini, M. Lazarou, and G. Dewson, "Parkin and mitophagy in cancer," *Oncogene*, vol. 36, no. 10, pp. 1315–1327, Mar. 2017.
- [115] X. S. Hou, H. S. Wang, B. P. Mugaka, G. J. Yang, and Y. Ding, "Mitochondria: Promising organelle targets for cancer diagnosis and treatment," *Biomater. Sci.*, vol. 6, no. 11, pp. 2786–2797, Nov. 2018.

- [116] F. R. Jornayvaz and G. I. Shulman, "Regulation of mitochondrial biogenesis," 2010.
- [117] P. V. Maximchik, A. V. Kulikov, B. D. Zhivotovsky, and V. G. Gogvadze, "Cellular energetics as a target for tumor cell elimination," *Biochem.*, vol. 81, no. 2, pp. 65–79, Feb. 2016.
- [118] I. A. Barbosa, N. G. Machado, A. J. Skildum, P. M. Scott, and P. J. Oliveira, "Mitochondrial remodeling in cancer metabolism and survival: Potential for new therapies," *Biochim. Biophys. Acta - Rev. Cancer*, vol. 1826, no. 1, pp. 238–254, Aug. 2012.
- [119] P. Maycotte, A. Marín-Hernández, M. Goyri-Aguirre, M. Anaya-Ruiz, J. Reyes-Leyva, and P. Cortés-Hernández, "Mitochondrial dynamics and cancer," *Tumor Biol.*, vol. 39, no. 5, May 2017.
- [120] I. Genovese et al., "Mitochondria as the decision makers for cancer cell fate: from signaling pathways to therapeutic strategies," *Cell Calcium*, vol. 92, Dec. 2020.
- [121] J. S. Bhatti, S. Kumar, M. Vijayan, G. K. Bhatti, and P. H. Reddy, "Therapeutic Strategies for Mitochondrial Dysfunction and Oxidative Stress in Age-Related Metabolic Disorders," *Prog. Mol. Biol. Transl. Sci.*, vol. 146, pp. 13–46, 2017.
- [122] U. Maucksch, R. Runge, G. Wunderlich, R. Freudenberg, A. Naumann, and J. Kotzerke, "Comparison of the radiotoxicity of the 99mTc-labeled compounds 99mTc-pertechnetate, 99mTc-HMPAO and 99mTc-MIBI," *Int. J. Radiat. Biol.*, vol. 92, no. 11, pp. 698–706, Nov. 2016.
- [123] B. Ke, M. Tian, J. Li, B. Liu, and G. He, "Targeting Programmed Cell Death Using Small-Molecule Compounds to Improve Potential Cancer Therapy," *Med. Res. Rev.*, vol. 36, no. 6, pp. 983–1035, Nov. 2016.
- [124] S. Goldar, M. S. Khaniani, S. M. Derakhshan, and B. Baradaran, "Molecular mechanisms of apoptosis and roles in cancer development and treatment," *Asian Pacific Journal of Cancer Prevention*, vol. 16, no. 6. Asian Pacific Organization for Cancer Prevention, pp. 2129–2144, 2015.
- [125] F. Ferro, S. Servais, P. Besson, S. Roger, J. F. Dumas, and L. Brisson, "Autophagy and mitophagy in cancer metabolic remodelling," *Semin. Cell Dev. Biol.*, vol. 98, pp. 129–138, Feb. 2020.

- [126] Z. Tan et al., "The role of PGC1 $\alpha$  in cancer metabolism and its therapeutic implications," *Mol. Cancer Ther.*, vol. 15, no. 5, pp. 774–782, May 2016.
- [127] V. S. Lebleu et al., "PGC-1 $\alpha$  mediates mitochondrial biogenesis and oxidative phosphorylation to promote metastasis migratory/invasive cancer cells specifically favor mitochondrial respiration and increased ATP production. Invasive cancer cells use transcription co-activator, PGC-1 $\alpha$  to enhance oxidative HHS Public Access," *Nat Cell Biol*, vol. 16, no. 10, pp. 992–1007, 2014.
- [128] I. San-Millán and G. A. Brooks, "Reexamining cancer metabolism: lactate production for carcinogenesis could be the purpose and explanation of the Warburg Effect," *Carcinogenesis*, vol. 38, no. 2, pp. 119–133, 2017.
- [129] T. M. Ashton, W. Gillies McKenna, L. A. Kunz-Schughart, and G. S. Higgins, "Oxidative phosphorylation as an emerging target in cancer therapy," *Clin. Cancer Res.*, vol. 24, no. 11, pp. 2482–2490, Jun. 2018.
- [130] D. C. Wallace, "Mitochondria and cancer HHS Public Access," *Nat Rev Cancer*, vol. 12, no. 10, pp. 685–698, 2012.
- [131] X. D. Xu et al., "Warburg effect or reverse warburg effect? a review of cancer metabolism," *Oncol. Res. Treat.*, vol. 38, no. 3, pp. 117–122, Mar. 2015.
- [132] D. Hanahan and R. A. Weinberg, "The hallmarks of cancer," *Cell*, vol. 100, no. 1, pp. 57–70, Jan. 2000.
- [133] D. Hanahan and R. A. Weinberg, "Hallmarks of cancer: The next generation," *Cell*, vol. 144, no. 5, pp. 646–674, Mar. 2011.
- [134] G. Russo, M. Mischi, W. Scheepens, J. J. De La Rosette, and H. Wijkstra, "Angiogenesis in prostate cancer: Onset, progression and imaging," *BJU Int.*, vol. 110, no. 11 C, Dec. 2012.
- [135] H. L. Wang et al., "Expression of prostate-specific membrane antigen in lung cancer cells and tumor neovasculature endothelial cells and its clinical significance," *PLoS One*, vol. 10, no. 5, May 2015.
- [136] M. J. M. Uijen et al., "PSMA radioligand therapy for solid tumors other than prostate cancer: background, opportunities, challenges, and first clinical reports," *Eur. J. Nucl. Med. Mol. Imaging*.

- [137] R. E. Conway et al., "Prostate-specific membrane antigen (PSMA)-mediated laminin proteolysis generates a pro-angiogenic peptide," *Angiogenesis*, vol. 19, no. 4, pp. 487–500, Oct. 2016.
- [138] R. E. Conway, N. Petrovic, Z. Li, W. Heston, D. Wu, and L. H. Shapiro, "Prostate-Specific Membrane Antigen Regulates Angiogenesis by Modulating Integrin Signal Transduction †," *Mol. Cell. Biol.*, vol. 26, no. 14, pp. 5310–5324, 2006.
- [139] L. Bodei, A. I. Kassis, S. J. Adelstein, and G. Mariani, "Radionuclide Therapy with Iodine-125 and Other Auger-Electron-Emitting Radionuclides: Experimental Models and Clinical Applications," *Cancer Biother. Radiopharm.*, vol. 18, no. 6, pp. 861–877, 2003.
- [140] T. Das and S. Banerjee, "Theranostic Applications of Lutetium-177 in Radionuclide Therapy," *Curr. Radiopharm.*, vol. 9, no. 1, pp. 94–101, Dec. 2015.
- [141] A. Dash, M. Raghavan, A. Pillai, & Furn, and F. Knapp, "Production of <sup>177</sup>Lu for Targeted Radionuclide Therapy: Available Options."
- [142] M. A. Westcott, D. M. Coldwell, D. M. Liu, and J. F. Zikria, "The development, commercialization, and clinical context of yttrium-90 radiolabeled resin and glass microspheres," 2016.
- [143] A. A. Rosenkranz, T. A. Slastnikova, M. O. Durymanov, G. P. Georgiev, and A. S. Sobolev, "Exploiting active nuclear import for efficient delivery of Auger electron emitters into the cell nucleus," *Int. J. Radiat. Biol.*, 2020.
- [144] Y. Dekempeneer et al., "Targeted alpha therapy using short-lived alpha-particles and the promise of nanobodies as targeting vehicle," *Expert Opin. Biol. Ther.*, vol. 16, 2016.
- [145] C. F. Ramogida and C. Orvig, "Tumour targeting with radiometals for diagnosis and therapy," *Chem. Commun.*, vol. 49, no. 42, pp. 4720–4739, Apr. 2013.
- [146] N. Falzone, J. M. Fernández-Varea, G. Flux, and K. A. Vallis, "Monte Carlo evaluation of Auger electron-emitting theranostic radionuclides," *J. Nucl. Med.*, vol. 56, no. 9, pp. 1441–1446, Sep. 2015.
- [147] J. G. Jurcic, "Targeted Alpha-Particle Therapy for Hematologic Malignancies," *J. Med. Imaging Radiat. Sci.*, vol. 50, no. 4, pp. S53–S57, Dec. 2019.

- [148] L. Marcu, E. Bezak, and B. J. Allen, "Global comparison of targeted alpha vs targeted beta therapy for cancer: In vitro, in vivo and clinical trials," *Crit. Rev. Oncol. Hematol.*, vol. 123, pp. 7–20, Mar. 2018.
- [149] S. C. Vaz, F. Oliveira, K. Herrmann, and P. Veit-Haibach, "Nuclear medicine and molecular imaging advances in the 21st century," *Br. J. Radiol.*, vol. 93, no. 1110, p. 20200095, Jun. 2020.
- [150] A. Sadremomtaz and M. Masoumi, "Comparison between Targeted Radionuclide Therapy of Bone Metastases Based on  $\beta$ -Emitting and  $\alpha$ -Emitting Radionuclides," *J. Med. Imaging Radiat. Sci.*, vol. 50, no. 2, pp. 272–279, Jun. 2019.
- [151] N. Hamada and T. Sato, "Cataractogenesis following high-LET radiation exposure," *Mutat. Res. - Rev. Mutat. Res.*, vol. 770, pp. 262–291, Oct. 2016.
- [152] A. McNamara, H. Willers, and H. Paganetti, "Modelling variable proton relative biological effectiveness for treatment planning," *Br. J. Radiol.*, vol. 93, no. 1107, p. 20190334, Mar. 2020.
- [153] E. Hindie, C. Morgat, P. Zanotti-Fregonara, M. Haissaguerre, L. Bordenave, and A. Tabarin, "Advantages and limits of targeted radionuclide therapy with somatostatin antagonists," *J. Nucl. Med.*, vol. 59, no. 3, pp. 546–547, Mar. 2018.
- [154] L. Filippi, A. Chiaravalloti, O. Schillaci, R. Cianni, and O. Bagni, "Theranostic approaches in nuclear medicine: current status and future prospects," *Expert Rev. Med. Devices*, vol. 17, no. 4, pp. 331–343, Apr. 2020.
- [155] M. R. Gill, N. Falzone, Y. Du, and K. A. Vallis, "Targeted radionuclide therapy in combined-modality regimens," *Lancet Oncol.*, vol. 18, no. 7, pp. e414–e423, Jul. 2017.
- [156] M. Janiczek et al., "Immunotherapy as a Promising Treatment for Prostate Cancer: A Systematic Review," 2017.
- [157] C. Parker et al., "Targeted Alpha Therapy, an Emerging Class of Cancer Agents: A Review," *JAMA Oncology*, vol. 4, no. 12. American Medical Association, pp. 1765–1772, 01-Dec-2018.
- [158] L. Emmett, K. Willowson, J. Violet, J. Shin, A. Blanksby, and J. Lee, "Lutetium 177 PSMA radionuclide therapy for men with prostate cancer: a review of the current literature and discussion of practical aspects of therapy," *J Med Radiat Sci*, vol. 64, pp. 52–60, 2017.

- [159] K. Rahbar, A. Afshar-Oromieh, H. Jadvar, and H. Ahmadzadehfar, "PSMA Theranostics: Current Status and Future Directions."
- [160] M. S. Litwin and H. J. Tan, "The diagnosis and treatment of prostate cancer: A review," *JAMA - Journal of the American Medical Association*, vol. 317, no. 24. American Medical Association, pp. 2532–2542, 27-Jun-2017.
- [161] E. M. Sebesta and C. B. Anderson, "The Surgical Management of Prostate Cancer," *Seminars in Oncology*, vol. 44, no. 5. W.B. Saunders, pp. 347–357, 01-Oct-2017.
- [162] S. V. Carlsson and A. J. Vickers, "Screening for Prostate Cancer," *Medical Clinics of North America*, vol. 104, no. 6. W.B. Saunders, pp. 1051–1062, 01-Nov-2020.
- [163] S. S. Chang, "Overview of Prostate-Specific Membrane Antigen," 2004.
- [164] M. Czerwińska, A. Bilewicz, M. Kruszewski, A. Wegierek-Ciuk, and A. Lankoff, "Targeted radionuclide therapy of prostate cancer-from basic research to clinical perspectives," *Molecules*, vol. 25, no. 7. MDPI AG, 2020.
- [165] C. Müller et al., "Terbium-161 for PSMA-targeted radionuclide therapy of prostate cancer."
- [166] R. Knapp and A. Dash, "Radiopharmaceuticals for Therapy."
- [167] G. Wang, D. Zhao, D. J. Spring, and R. A. Depinho, "Genetics and biology of prostate cancer," 2018.
- [168] S. Vyas, E. Zaganjor, and M. C. Haigis, "Mitochondria and Cancer."
- [169] M. Maddalena Tumedei et al., "Spotlight on PSMA as a new theranostic biomarker for bladder cancer," *Sci. Reports* |, vol. 11, p. 9777, 123AD.
- [170] A. Ku, V. J. Facca, Z. Cai, and R. M. Reilly, "Auger electrons for cancer therapy-a review."
- [171] S. V Gudkov, N. Yu Shilyagina, V. A. Vodeneev, A. V Zvyagin, W. Chi-shing Cho, and A. Lemarié, "Targeted Radionuclide Therapy of Human Tumors."
- [172] K. Bouchelouche and J. Capala, "Prostate Specific Membrane Antigen-A Target for Imaging and Therapy with Radionuclides."
- [173] H. Sung et al., "Global Cancer Statistics 2020: GLOBOCAN Estimates of Incidence and Mortality Worldwide for 36 Cancers in 185 Countries," *CA. Cancer J. Clin.*, vol. 71, no. 3, pp. 209–249, May 2021.
- [174] A. S. Sobolev et al., "Subcellular Targeting of Theranostic Radionuclides," 2018.

- [175] M. Unverricht-Yeboah, K. Holtmann, and R. Kriehuber, "Comet Assay analysis of DNA strand breaks after exposure to the DNA-incorporated Auger Electron Emitter Iodine-125," *Int. J. Radiat. Biol.*, 2020.
- [176] S. Paillas et al., "Localized Irradiation of Cell Membrane by Auger Electrons Is Cytotoxic Through Oxidative Stress-Mediated Nontargeted Effects."
- [177] U. Haberkorn, M. Eder, K. Kopka, J. W. Babich, and M. Eisenhut, "CCR New Strategies New Strategies in Prostate Cancer: Prostate-Specific Membrane Antigen (PSMA) Ligands for Diagnosis and Therapy CME Staff Planners' Disclosures," 2016.
- [178] A. P. Kiess et al., "Auger Radiopharmaceutical Therapy Targeting Prostate-Specific Membrane Antigen," *J Nucl Med*, vol. 56, pp. 1401–1407, 2015.
- [179] C. O'driscoll, J. C. Evans, M. Malhotra, J. F. Cryan, and C. M. O'driscoll, "The therapeutic and diagnostic potential of the prostate specific membrane antigen/glutamate carboxypeptidase II (PSMA/GCPII) in cancer and neurological disease," *Br. J. Pharmacol.*, vol. 173, p. 3041, 2016.
- [180] N. K. Tafreshi et al., "molecules Development of Targeted Alpha Particle Therapy for Solid Tumors," 2019.